FNAL PROPOSAL No. 516

Scientific Spokesperson:

T. Nash
Fermilab
FTS number: 370-3795
Commercial: (312) 840-3795

Proposal to Study Photoproduction of Final States of Mass Above 2.5 GeV with a Magnetic Spectrometer in the Tagged Photon Lab

Submitted by

J. Appel, P. Mantsch and T. Nash
Fermi National Accelerator Laboratory

R. J. Morrison
University of California, Santa Barbara
Santa Barbara, California

G. Luste
University of Toronto
Toronto, Canada

October 1, 1976

Introduction

For some time it has been clear that a wide array of physics opportunities would be opened up by building a magnetic spectrometer at the Tagged Photon Lab. It no longer requires clairvoyance to point out that photons are - along with neutrinos - the ideal probe for studying the new physics. Since photons couple to quark-antiquark pairs, a photon beam carries the highest fraction of charmed quarks (or other new quark flavors) of any "hadronic" beam. In other hadron beams charm appears only in the quark sea, and its manifestation is swamped by the background from the valence - non charmed - quarks. This has become painfully obvious in the Meson Lab. Furthermore, in a photon beam the charmed quark pair carries all of the momentum of the beam,unlike the valence quarks of a hadron beam which carry only a fraction of the momentum. Higher mass states are thus more readily formed by a photon beam.

Fluxes in the Tagged Photon Beam, as will be seen in the later discussions, are more than adequate to study the production and decay of charm and hidden charm states,to find the elusive pseudo-scalar partner of the J/ψ (η_c), and to search for new quantum numbers. Most important is the excellent signal to noise ratios for rare channels like those of interest that will be possible in the Tagged Photon Beam. Backgrounds will be low: $\lesssim 10^4$ muons/m^2 per 10^{12} 400 GeV protons. The beam has $< 10^{-6}$ hadronic contamination which means that final states with K's or Λ^o's will not be

overwhelmed by background initiated by neutrons or kaons in the beam. Additionally, knowledge of the photon energy allows an energy balance constraint, measurement of the forward missing mass with a recoil detector and measurement of production energy dependence. As we will describe later, each of these will be valuable in extracting important final states from the background.

To take advantage of the potential for doing physics at the Tagged Photon Lab we propose to build there a large acceptance, low power magnetic spectrometer with a photon detector and a range - $\frac{dE}{dX}$ missing mass recoil system. With this powerful yet straightforward system we propose to study photoproduced final states with forward masses of 2.5 GeV and higher,using photons in the energy range $70 \lesssim k \lesssim 140$ GeV. This will include, for example, charmed baryon and meson production, the hidden charm states with C = 1, J = 0 (η_c) produced through the Primakoff process, the states reached by radiative transitions from the ψ', as well as states of possible new quarks.

No new magnets or plant construction are contemplated for this proposal, so that we believe the experiment could be ready in two years. As a result,the experiment will be able to make a significant contribution to understanding questions that are relevant today. Furthermore, the reasons for using photoproduction to study physics involving "new" quarks are so fundamental that we believe them not to be a passing fad. In two years we will be able to use this experiment to answer new questions that have grown up since the time of this proposal. In fact, although this

is by no means a proposal for the Energy Doubler, this spectrometer will be ideal - and unique - for studying photoproduction when the Doubler comes into operation. It is probably the only existing P East facility that will be able to operate at 1000 GeV. The extra proton energy will be used either to increase photon intensity in the 70-140 GeV range or to double the photon energy. The latter would involve no modification of the electron beam which already is capable of 300 GeV. The spectrometer can be mounted on the rail system presently installed at the TPL so that it could be scaled for different energy requirements.

The electron beam can also be used to transport pions into the Tagged Photon Lab.[1] R. Rubinstein notes that although spot sizes will be somewhat larger the intensities are potentially only a factor of ~3 below the P West pion beam. Thus, one can imagine a future proposal to use the spectrometer at the TPL for a direct comparison of photoproduction and hadron production with systematic errors caused by using different detectors eliminated. This emphasizes the flexibility and long range benefits to the Proton East program that the spectrometer we propose would bring.

Beam

To a large degree the range of photon physics that will be feasible is determined by the fluxes available in the beam. Before outlining some of the physics we are interested in, we look at the question of how much tagged photon flux can be reliably anticipated in the next generation of experiments based on present experience with the beam. The real limit on flux is the rate at which one can tag photons. Using techniques based on some developed last summer we will be able to tag as many as 6×10^6 γ/second. Modest improvements to the electron beam and reasonable assumptions about 1978 proton beam parameters (6×10^{12}, 450 GeV, 480 seconds/hour) will make it possible for us to obtain this photon flux with 150 GeV e^-. Figure 1 shows the photon spectrum expected. Also shown is the e^- spectrum. Details of how we will obtain these fluxes are given below. Figure 2 is a schematic drawing of the Tagged Photon Beam and may be helpful as a road map in the discussion that follows.

During August of 1975 the beam was operated at $\sim$100 GeV with 3×10^{12} 400 GeV protons on target and produced about 2.2×10^7 electrons. With 450 GeV protons (which should be available routinely by the time of this experiment) and 6×10^{12} p/sec we can expect 6×10^7 electrons/sec at 100 GeV. The electron flux is presently limited by the relatively smaller vertical acceptance. This vertical acceptance can be recovered in one of two ways. In a Technical Memo (TM-633) Morrison and Murphy suggested increasing

the vertical acceptance by installing the lead convertor (that converts photons from the primary target to electrons) inside a dipole. As can be seen in Fig. 3 the lead is at a shallow angle (α) relative to the beam axis. Thus the more positive the photon production angle the more magnetic field will be traversed by the resulting electron. The net effect is a vertical focusing of the electrons plus a small mean bend which is corrected by a following magnet. There is no horizontal defocusing. To get the most significant increase in vertical acceptance using this approach the lead convertor would be placed in the third dumping magnet (M3) inside the target box with the sweeping magnet (M4) acting as the correction magnet. This would increase the vertical acceptance from ~1 mr to ~5 mr with negligible effect on other beam parameters. Using measurements of the electron beam flux as a function of production angle, we estimate this larger vertical acceptance will increase the flux at 100-150 GeV by ~3 1/2. This would give ~2×10^8 100 GeV or 6×10^7 140 GeV electrons (see Fig. 1). Another approach (suggested by B. Cox) is to add a third quadrupole to the first doublet and thereby achieve a more symmetric acceptance. A careful transport study of using a triplet will have to be made before deciding whether to use a Morrison element or a triplet to increase the beam acceptance.

Using a 20% radiator and ignoring tagging for the moment

$$N_\gamma(k)dk \gtrsim N_e \times .2 \times f(k) \times \frac{1}{k}\, dk$$

$$= \begin{cases} \dfrac{2.6\ 10^7}{k}\, dk & 100 \text{ GeV} \\[2ex] \dfrac{8.7\ 10^6}{k}\, dk & 140 \text{ GeV} \end{cases}$$

The factor $f(k) \simeq .65$ comes from thick target and QED corrections to the simple $\frac{dk}{k}$ form. Integrating from 20 GeV to k_{max} we will get 4.2×10^7 photons for the 100 GeV setting and 1.8×10^7 with 150 GeV electrons, untagged. This high rate is useful for physics when one chooses not to take advantage of the energy constraint and missing mass capability allowed by the tagging system.

If tagging is required, the real limit on flux is the rate at which one can tag the photons. With electron fluxes approaching those noted above, a large fraction of RF buckets will be populated with more than one electron. The likelihood of more than one radiated photon of significant energy per electron is also high when using a thick radiator. Thus, it is necessary to cope with more than one electron and more than one photon to tag the energy of the interacting photon. The saving grace is the very low interaction probability of photons which means that it is extremely unlikely ($\lesssim 10^{-3}$) for more than one γ to interact hadronically per bucket. The energy of all non-interacting photons in the beam ($\Sigma\, k_{NI}$) will be measured with a line of shower counters (S_3 in Fig. 5) at the back of the detector. The central counter (C) will measure photons that have not converted. The rest of the S_3 counters will measure e^+e^- pairs with $p > 10$ GeV/c that have been swept out of 0° in the bend plane by the magnets. The S_2 counters located between the magnets extend the pair range down to $P > 1$ or 2 GeV/c. The C counter is lead lucite because lead glass would color rapidly in that location. The S_2 and S_3 counters can be lead lucite or lead glass depending upon economics and inventory.

Extra scintillation counters near the beam in the tagging array will pick up higher energy electrons that radiated lower energy photons. Combined with the shower counters of the tagging system, these will determine the number of electrons (N) in the bucket and their total energy after radiating ($\Sigma E'$). Thus, one can determine the interacted photon's energy:

$$k_I = NE_{beam} - \Sigma E' - \Sigma k_{NI}.$$

A specific scheme has been worked out along these lines which allows tagging radiated photons with a resolution of $\frac{\delta k_I}{k_I} \simeq 5\%$ from up to 6×10^7 100 GeV e^- in a 20% radiator (6×10^6 tagged photons). The only changes to the tagging system are eleven scintillation counters which would be added to the present tagging hodoscopes on the high e^- energy end. The tagging magnets would be run at maximum current (the present 300 GeV setting) in order a) to spread out the electrons so that there is sufficient spatial resolution to measure E' of the higher energy electron well enough to get $\delta k_I \simeq 5.5$ GeV; and b) to keep the counting rate $\lesssim$ 2MHz in the hodoscopes and $\lesssim$ 0.3 MHz in the shower tagging counters.

The C counter will require special consideration. The pulse height of this counter, like the tagging counters, will be digitized for any RF bucket with an interaction that satisfies the experimental trigger. The problem is to get the pulse height information from only the relevant bucket without contamination from the preceding or following buckets. The pulse can be clipped to 15 ns and the ADC gate set short enough to ignore the following

bucket. The energy at the preceding bucket can also be digitized (with appropriate delaying). Using calibration data one will then be able to subtract the energy that leaked from the previous bucket. The problem is by no means trivial,but techniques like these are similar to those used in correcting for shower leakage from a neighboring shower counter. Therefore,we believe we will be able to deal with the problem.

We have described above what might be called a second generation tagging system which, with minor modifications based on previous experience, will push the tagging rate a factor of ~6 beyond that already attained. When 1000 GeV protons are available in P East,the choice will be whether to use the extra energy to do physics in the 200-300 GeV range or to continue in the 100-150 GeV range with substantially increased intensity. If the latter choice is made,the tagging system will have to be modified to cope with the higher rates. Perhaps this will be done by adding more magnets which will spread the electrons and photons out vertically and horizontally to keep rates manageable in each of a greater number of counters.

Comparison with the Broad Band Beam

The question will inevitably be asked how the Tagged Photon Beam compares with the Broad Band Beam for doing the type of physics we propose. For a comparison of fluxes see Fig. 1 The broad band fluxes are for a collimator hole twice as large as the largest used to date and using 5×10^{12} protons. Up to

~150 GeV tagged photons are ~5 x lower and untagged photons in the TPB ~2x lower than these broad band fluxes. At higher energies the broad band fluxes are even more favorable.

Muon backgrounds are $\sim 10^4$ μ/m^2 per 10^{12} p @ 400 GeV in the TPB compared to ~ 2 x 10^5 μ/m^2 in the BBB. More importantly the hadronic contamination is $<10^{-6}$ in the TPB compared to neutron/photon ratios in the BBB which are of the order of a few percent depending on energy. This means that in the TPB final states with Λ^o,Σ etc. will be just as clean of background as $\bar{\Lambda}^o$,$\bar{\Sigma}$ etc. Since so much of the "new" physics we are interested in investigating involves such final states,this is an important advantage.

Knowledge of the photon energy allows energy balance constrained triggers and measurement of the forward missing mass with a recoil detector. The production energy in the BBB is known by summing final state energies,which is done with accuracy only for simple all charged states. Production energy dependence and missing mass information is very important input for understanding the production of charmed hadron pairs, for discovering thresholds of newly flavored quarks in complicated final states, and for separating Primakoff produced (even C) states from the odd C background, just to name three examples.

The broad band and Tagged Photon beams are very complementary. One allows searches at the highest possible energies and masses. The other provides energy information, a background-free environment, and a potentially higher signal to noise ratio in many channels. Photons, along with neutrinos, are now so obviously

the beams of choice for advancing physics that even in the most austere economic environment both photon programs should be pursued for as long as they remain productive.

Targets and Luminosity

We would in most cases use a 2m hydrogen target which at 0.22 radiation lengths is about the maximum tolerable in a photon beam. With 6×10^6 γ/sec, 480 sec/hr the luminosity will be 25 events/nb-hr. For reference the table below gives luminosities on other targets, all 0.22 X_o:

H_2	25 events/nb-hr
D_2 (2 meters=.26X_o)	28
Be	2.8
C	1.4
Al	.34
Cu	.077
Pb	.0117

Heavier nuclei targets would be useful, for example, in proving that a Primakoff signal has an electromagnetic Z^2 dependence. Also, when the energy is doubled and higher intensities are available heavy lepton searches/studies will be possible and enhanced on heavy nuclei.

Physics: Event Rates for Photoproduced Final States

We will outline here estimates for the event rates for some states typical of those we are interested in. The estimates are listed in Table I. We assume a luminosity of 25 events/nb-hr as described in the discussion of the beam. This corresponds to a total hadronic interaction rate of 2.8 x 10^6 per hour or 5800 per beam second. For reference Table I gives the event rate for ω^o and ψ. These rates demonstrate the potential sensitivity of the system.

One hundred percent acceptance is assumed in Table I. The actual acceptance will, of course, be lower and will depend on the mass and multiplicity of a particular state. As we will discuss later, the acceptance of the spectrometer is designed to include virtually all (~98%) of the inclusive distribution down to a few GeV. A Monte Carlo calculation will be carried out to estimate the spectrometer's acceptance for different states.

The ability of the system to measure accurately the momentum or energy of all final state particles except K_L^o's and neutrons is an important feature that means that we will be sensitive to the majority of decay states. This is true even for charmed baryons which will often have strange baryons in the final state.[2] Table II shows what fraction of the decays of Λ^o, Σ and Ξ do not have neutrons. With the exception of Σ^- we see that we will lose good mass resolution on only ~ 40% of these states. These events are not completely lost as the hadrometer will make about a 25% measurement on the energy of neutrons and K_L^o's.

Unitarity arguments based on the measurement of $\sigma_{\psi N}$ require that the total photoproduction of charm is $\gtrsim$ 300 nb.[3] In fact, the charmed baryon found by Experiment 87 apparently has a cross section that is in the ball park of 1 μb.[4] In Table I we assume the total charm cross section is 1 μb. Even if the acceptance is only 1% we would accumulate ~ 300 K charm events after 1000 hours.

The evidence for a C = 1 state at 2.8 GeV found at DESY has not been confirmed at SPEAR. This state couples to 2γ not 1γ as most e^+e^- collisions do. A very promising way to produce it is via the 2γ Primakoff process (see diagram in Fig. 5) in photoproduction.[2] The cross section is[12]

$$\frac{d\sigma}{d\theta} = .14 \text{ mb } \frac{Z^2 \Gamma\gamma\gamma}{m^3} \frac{\theta^3 k^4}{t^2} F_c^{\,2}(t)$$

where F_c is the Coulomb form factor. The rates shown in Fig. 5 were found by integrating this cross section for $\Gamma\gamma\gamma$ = 20 keV. Two theoretical estimates have been made of $\Gamma\gamma\gamma$: one based on scaling from π^o gives 100 keV, the other a Charmonium calculation gives ~ 10 keV.[5] An unimpeachable theoretical source of ours says he would be suprised if $\Gamma\gamma\gamma$ was outside the range 5 keV to 200 keV.[6] Hydrogen turns out to be the most effective target. This is convenient because it makes the study of this state compatible with using a missing mass measurement in studying other states. The reason hydrogen has the highest event rate is that the target thickness in radiation lengths cannot be much larger than $.22X_o$ no matter what target nucleus is used.

Since $X_o \sim \frac{1}{Z^2}$ this requirement cancels the Z^2 in the cross section and the effect of t_{min} in the form factor makes the event rate lowest for high Z. The Primakoff signal will have a very distinctive energy dependence (caused by the form factor) as may be seen in Fig. 4. If such a signal is observed it may be confirmed by checking for the Z^2 dependence with other nuclei. We would aim to detect all the final states of η_c (including $p\bar{p}$, $\gamma\gamma$, 4π etc.) and given the relatively low mass the detection efficiency should be high. If the efficiency is as bad as 30% we would still see more than 1 event/hour at m = 3 GeV. At worst with $\Gamma\gamma\gamma$ = 5 keV after 1000 hours there would be over 200 events.

The total rate for ψ' is estimated using the Fermilab measurements of ψ and $\psi' \to e^+e^-$[7] and SPEAR branching ratio numbers.[8] The estimates of $\psi' \to \chi$ or P_c use preliminary results from SPEAR.[9] A total of ~ 5% of ψ' is observed at SPEAR going through 2γ and one of the χ states to ψ. A total of ~ 1% goes through χ states that decay into hadronic channels like 4 $\pi^\pm$ and $2\pi^\pm$ $2K^\pm$ Even if we are pessimistic about acceptance we can expect several hundred $\chi \to$ hadronic states after 1000 hours.

These examples indicate the potential sensitivity of the spectrometer and beam we propose to use.

Physics: Requirements on the Detection System

As a guide to the acceptance requirements for our forward detector we Lorentz transformed to the lab the x dependence of e^+e^- colliding beam data at 4 GeV as measured in the SPEAR magnetic detector.[10] Table III shows the results of integrating these distributions. The table gives angles that include 95%, 98% and 99% of all secondaries above a given momentum. From these numbers we see that magnet acceptance of ± 120 mrad will include almost all secondaries down to 5 GeV and most of those below 5 GeV. Above 10-15 GeV ± 75 mrad is required.

The mass resolution for an n particle system with mass M is

$$\frac{\delta M}{M} = \frac{1}{M^2} \quad \Sigma\Sigma^{\text{Quadrature}} \frac{1}{2} P_i P_j \theta_{ij}^2 \left[\left(\frac{\delta P_j}{P_j}\right)^2 + \left(\frac{\delta \theta_{ij}}{\theta_{ij}}\right)^2 \right]^{1/2}$$

$$\approx \left[\left(\frac{\delta P_j}{P_j}\right)^2 + \left(\frac{\delta \theta_{ij}}{\theta_{ij}}\right)^2 \right]^{1/2}$$

in the approximation that each $\frac{1}{2}P_i P_j \theta_{ij}^2 = \langle \frac{1}{2} P_i P_j \theta_{ij}^2 \rangle = \frac{M^2}{n(n-1)}$.
Since $\langle \theta_{ij} \rangle \simeq \sqrt{2}\,\frac{M}{K}$ and $\delta\theta_i \approx \frac{1}{\sqrt{2}}\,\delta\theta_{ij}$

$$\frac{\delta M}{M} \approx \left[\left(\frac{\delta P_i}{P_j}\right)^2 + \left(\frac{K}{M} \frac{\delta \theta_i}{\theta_i}\right)^2 \right]^{1/2}$$

where K is the incident photon momentum. It is easy to make $\delta\theta$ small enough so δP dominates the mass resolution. The δP requirement on the spectrometer is now clear: if we aim for $\delta M \simeq$ 50 MeV for M = 4 GeV then $\frac{\delta P}{P} \simeq 1\%$ for average momenta.

If the system cannot measure photon and π^o energy the acceptance for good mass resolution will suffer drastically since typically 40% of final state particles are neutral. Accordingly we require a neutral detector with energy resolution approaching that called for in the magnetic spectrometer. Discrimination between π^o and γ will be important in distinguishing radiative states (of the ψ', for example).

Particle identification is also needed to separate the many final states we will be studying. Separation of π, K, and protons below 20 GeV is particularly important since most particles will have low momentum because of the large multiplicities involved. Also,the multiplicities will require that the Cerenkov counters be segmented into enough sectors so that the probability of two tracks in one sector is low.

A recoil system should be able to distinguish events with proton recoils from those in which the target fragments. This will be of importance in understanding production mechanisms. Missing mass of the forward going particles is valuable information that the tagged photon energy makes possible and the recoil detector should provide. The missing mass will be used as an important constraint in studying the radiative decay states of the ψ' as well as in understanding how charm hadron pairs are produced. The missing mass is, in effect, the mass of the virtual photon that is producing the state observed in the magnetic spectrometer. The missing mass will be particularly useful at high mass where the mass resolution is best.

The Detection Apparatus: Forward Spectrometer

We have designed a spectrometer that meets the requirements outlined above in a straightforward and comparatively inexpensive way. The detector as we presently conceive it is shown in Fig. 5 . Parameters of this design may be found in Table IV and detector sizes, locations, etc. in Table V . The magnets are SCM105's from Argonne which are presently or soon to be idle. There are several reasons for using two magnets: it a) increases vertical acceptance and b) reduces detector size since one can divide the spectrometer into a low and a high momentum system by installing detectors between the magnets; c) lowers power consumption; d) allows for a potentially higher beam energy in the future since more bending power is available than is used; e) makes it possible to install the first drift chamber (D1) in the fringe field of the first magnet, thereby protecting it from the problem causing low energy electron soup that spills out of the target.

The magnets are opened to 28" and are each run at 5KG-M. The total power consumption will be $\lesssim$ 400 kW. With the tagging magnets running flat out (see Beam discussion) the total cooling load at the Tagged Photon Lab will be 670 kW. This would at most require an increase in pumping capacity (maximum cost $20K)[13] and probably would not even require that. Cooling towers, electric substations, etc. are all sized for $1\frac{1}{2}$ MW.

The drift chambers, D1-D4 have .15 mm resolution and cell sizes that vary from 1 cm or less at the center of D1 to 4 cm or more in the outer cells of D4. The cell sizes will be

determined after a Monte Carlo study with the aim of keeping low the probability of more than 1 track in a cell. The chambers will be deadened in the regions where there are electron pairs. The drift chambers will be used for good momentum resolution. We are considering adding some large "previously owned" MWPC planes to add redundancy for the analysis of complicated states.

The resolution of the low momentum system for P > 10 GeV will be $\frac{\delta P}{P} = .0029P$. For the high momentum system $\frac{\delta P}{P} = .00047P$.

The two large Čerenkov counters ($\check{C}_2$ and $\check{C}_3$) will be operated at atmospheric pressure with the mixture ratio of nitrogen and helium (and other gasses) adjusted to give appropriate indices of refraction. They will be very similar in concept and design to those presently being used by E-260 in the Meson Lab. In addition, a third smaller Čerenkov counter capable of operating at > 1 atmosphere will be located between the magnets to extend the identification to lower momenta. Separation of $\pi^{\pm}$, $K^{\pm}$, and protons from ~ 6 GeV to ~ 20 GeV will be possible at one setting. Because of the high multiplicities the Čerenkov counters will each have 16 mirrors and phototubes. The mirrors will be in two horizontal rows with a gap between them to allow the e^+e^- pairs to pass through without giving a signal. Table VI gives examples of three different settings and the particle separation possible with each. Detailed Monte Carlo calculations will be used to choose appropriate settings.

The physics imposes tough requirements. Particle identification forces the photon detector a good distance from the target. Yet neutral energy and position resolution must not be much larger

than for charged. Our solution for this problem (S4) will not be inordinately expensive. We will build a liquid scintillator tank with about 20 immersed lead plates each 1 X_o thick. Between the plates will be honey comb structures with cells alternately running horizontally and vertically. Light pipes will connect the cells to phototubes so that each tube sees 10 samples along one strip in x or y. Teflon will coat all surfaces to give total internal reflection. A cell size of ~2-4 cm will give good π^o vs γ discrimination for $E \gtrsim 5$ GeV and a resolution of $\delta x \lesssim .4$cm from shower sharing information. We expect $\frac{\delta E}{E} \simeq 2\ 1/2\ \%$ at 100 GeV will be readily obtainable based on experience with lead lucite counters. Because P is measured in the magnets excellent e/π identification will be possible. The inspiration for this detector comes from two sources: the Tollestrup-Walker detector used in the Meson Lab charge exchange experiment and the large liquid scintillation γ-catcher of Experiment 1A. Two banks of short lead glass (S1) counters will be located between the magnets and detect γ's and π^o's outside the vertical acceptance of the second magnet. The pair and beam counters (S1 and S2) are discussed in the tagging system section.

Behind the whole experiment will be a typical steel scintillator hadrometer/μ identifier. This will be useful in triggering schemes and will catch the energy of neutrons and K_L^o's which is otherwise lost.

The mass resolution of this spectrometer will of course depend on the final state. As a typical example:

$k = 100$, $m = 4$, $n = 6$

$\delta M = 33$ MeV	all charged
$\delta M = 66$ MeV	neutral/all = .4
$\delta M = 100$ MeV	all neutral

Other examples may be found in Table VII.

The spectrometer can be built at reasonable cost and in a reasonable time (see later discussion) and has the resolution, acceptance and particle identification to do the job we are asking for. Exact locations of the magnets and detectors of the system will be determined after careful Monte Carlo calculations. The rails presently installed in the TPL will be used to facilitate rearrangement of the geometry for future experiments.

The Detection Apparatus: Recoil System

As with much of the rest of the detector we have by no means settled on a final design of the recoil system. A preliminary cross sectional drawing is shown in Fig. 6. Missing mass requires a measurement of θ and momentum or kinetic energy. Recoil kinematics are shown in Fig. 7. The system must also be able to separate π^+ from p in order to distinguish diffractive single proton recoils from $N^* \rightarrow n\pi^+$ or $p\pi^-$ with the proton stopping in the target. To do this both kinetic energy and momentum must be measured. The two cylindrical wire chambers (SC_1 and SC_2) will measure θ. Surrounding the outer chambers is a box with steel plates and liquid scintillator. Once again liquid scintillator is used so that acceptance is not sacrificed to cost. Figure 8 shows a cross section of one quadrant of the

liquid scintillator box in a scheme in which there are 12 segments each viewed with a phototube. The range measurement would give $\frac{\delta P}{P} \sim 5\%$ up to 1000 MeV/c. Pulse height measurement of individual segments would give enough $\frac{dE}{dX}$ information to separate pions from protons. A total of ~ 12 tons of steel would be required. (Another scheme we are considering would use no steel, only liquid scintillator to range the protons.) Figure 9 gives an idea of the mass resolution for a system like that described here.

Trigger

One of the advantages of a photon beam is that despite the sensitivity to rare physics the rate of hadronic interactions is small. Even with the high beam intensity there will be only ~ 5800 hadronic interactions per second. We do not wish to write all these events on tape. The decision on which events to write can be made in as long as 10-15 μsec and the dead time will remain below 10%. We expect, therefore, to run the experiment with a fast and a slow trigger.

The fast trigger will fire on a tagging signal in which energy is lost outside of the pair and photon counters (S_2 and S_3). The additional requirement that there is a hadronic signal in the recoil, the hadrometer or the S_4 detectors may prove useful.

Once the fast trigger has fired and started latches, ADC's etc., the electronics will have 10-15 μsec, which is a long time, to decide whether to record the event or not. The following is

an example of a slow trigger we are considering:

a) (Recoil has one track) and (M_x > 2 GeV). M_x is determined by matrix logic on latches set in the recoil system. These tell which level of the range system was hit and the Z position in each of two circles of hodoscopes.

b) (Recoil has more or less than one track) and (K or proton signal from Čerenkov counters) or $P_\perp$ measured in S_4 and hadrometer greater than some value).

A trigger like this will reduce the data rate on tape to a comfortable and unbiased 100-200 per second.

Business Matters: Running Time, Costs and Time Scale

We estimate the cost of the detectors to be of the order of $250K broken down approximately as follows:

Drift chambers	$50K
Recoil system	50K
Čerenkov counters	70K
Liquid scintillator γ ctr	50K
Hadrometer	20K
Shower counters	20K

The experiment can, with reasonable priority, be mounted and ready for data in two years' time.

Two runs of five weeks each (1000 hours) should satisfy the goals outlined in this proposal.

Acknowledgements

We would like to acknowledge valuable discussions with B. Brown, B. Lee, U. Nauenberg, C. Quigg, K. Stanfield, and R. Thun. K. Stanfield provided us with calculations regarding the Čerenkov counters, for which we are grateful.

Table I

Some Estimates of Event Rates

(Beam assumptions noted in text: Luminosity = 25 events/nb-hr
100% Acceptance)

Physics			Events/hr
$\gamma p \to \omega^{o} p$			70K
$\gamma p \to J/\psi p$			940
$\gamma p \to \psi'$			325
$\psi' \to \chi \to$ hadrons			>3
$\chi \to \psi$			15
$\gamma p \to$ all charm			25K
$\gamma p \to \eta_c p$	$m = 2.8$	$\Gamma\gamma\gamma = 20$ keV	4.2
	$m = 3.0$		3.1
	$m = 3.5$	$k = 100$ GeV	1.5

Table II

Strange Particle Branching Ratios to States without Neutrons[11]

Λ^o	.64
Σ^+	.52
Σ^o	.64
Σ^-	0
Ξ^o	.64
Ξ^-	.64
K_s^o	1.00

Table III

Typical Angular Acceptance Requirements
for Multi Hadron Final States

(Lorentz transformed from SPEAR inclusive data.)

$M_x = 4$ $n_{ch} \simeq 4$ $n = 6$

		Angles that include 95%, 98% and 99% of secondaries		
k GeV	p_{GeV}	θ(95%) rad	θ(98%) rad	θ(99%) rad
100	1	.262	.300	.326
	5	.110	.127	.139
	10	.076	.088	.096
	15	.062	.072	.079
	20	.054	.062	.068
	30	.045	.053	.058
	40	.040	.046	.051
75	1	.300	.345	.377
	5	.126	.145	.160
	10	.088	.101	.111
	15	.072	.083	.091
	20	.064	.074	.080
	30	.053	.062	.067
	40	.047	.054	.059

Table IV

Forward Detector Parameters

Low Momentum System		
Charged:		
1 GeV < P < 10 GeV	$\frac{\delta P}{P} = .0029P$	$\delta\theta = .0003$*
$\theta_H < \pm 120$ mr		
$\theta_V < \pm 140$ mr		
Neutral:		
$\theta < \pm 120$ mr	$\frac{\delta E}{} = \frac{1}{\sqrt{E}} + .01$	$\delta\theta = .009$*
$\pm 66 < \theta < \pm 140$ mr		$\frac{\delta\theta}{\theta} \lesssim .013$*
High Momentum System		
Charged:		
10 GeV < P < 120 GeV	$\frac{\delta P}{P} = .00047P$	$\delta\theta = .0001$*
$\theta_H < \pm 100$ mr		
$\theta_V < \pm 66$ mr		
Neutral:		
$\theta_H < \pm 120$ mr	$\frac{\delta E}{E} \simeq \frac{.1}{\sqrt{E}} + .015$	$\delta\theta = .00033$*
$\theta_V < \pm 66$ mr		

*Not including vertex information.

Table V

Detector Sizes and Locations

	Z m	Size Horiz. m	Vert. m	Length m	Detector Description
D_1	1.2	.60	.40		Drift chamber x,y,u. δx = .15 mm
D_2	1.8	.70	.50		
D_3	3.3	1.20	1.00		
D_4	7.5	1.75	1.00		
$\check{C}_1$ upstr	1.9	.70	.50		> 1 Atm. C counter
$\check{C}_1$ dnstr	3.2	1.2	1.0		
$\check{C}_2$ upstr	3.4	.84	.50	4	1 Atm. $\check{C}$ counters- segmented He-air mix to adjust n
dnstr	7.4	1.75	1.00		
$\check{C}_3$ upstr	7.6	1.75	1.00	4	
dnstr	11.6	2.80	1.55		
S_1x2	3.4	.75	.50	.35	Lead glass or lead lucite ~$15X_o$, $\delta x \simeq .3$cm
S_2x2	3.4	.08	.065	.35	Lead glass or lead lucite ~$15X_o$, $\delta x \simeq .3$cm
S_3	11.7	2.85	.065	.40	~$24X_o$
S_4	12.1	2.90	1.60	.30	Liquid scintillator/ lead ~$20X_o$; segmented 10 x samples, 10 y samples $\delta X \simeq .4$cm $\delta E = .025E$
Hadr	13.1	3.15	1.75	1.00	Steel/scintillator $\frac{\delta E}{E}$ ~25%

Table VI

Examples of Cerenkov Counter Settings

Setting	Range (GeV) π/K/P Separation	Counter	Gas	Pressure (Atm)	n-1	Thresholds (GeV) π	K	P
1	11-39	C_1	Fr12	1	1.06×10^{-3}	4	11	21
		C_2	N_2	1	2.75×10^{-4}	6	21	41
		C_3	N_2-He	1	0.8×10^{-4}	11	39	-
2	6-20	C_1	Fr12	3.55	3.45×10^{-3}	1.5	6	11
		C_2	N_2	1	2.9×10^{-4}	6	20	38
		C_3	Propane	1	9.3×10^{-4}	3	11	21.5
3	17.5-61	C_1	CO_2	1	4.15×10^{-4}	5	17.5	32.5
		C_2	Fr12	1	1.06×10^{-4}	9.5	32.5	64
		C_3	He	1	3.25×10^{-5}	17.5	61	-

Table VII

Approximate Spectrometer Mass Resolution

M (GeV)	E (GeV)	n	δM (MeV) all charged	all neutral	charged/all = .6
2	50	6	8	50	32
	100	4	25		37
		6	17		34
		8	13		33
3	50	6	13	75	48
	100	4	37		56
		6	25		51
		8	19		50
4	50	6	17	100	65
	100	4	50		74
		6	33		68
		8	25		66
5	50	6	21	125	81
	100	4	62		93
		6	42		85
		8	31		83
6	50	6	25	150	97
	100	4	75		111
		6	50		102
		8	38		99

References

[1] R. Rubinstein, "Use of the NAL Electron Beam for Pion Experiments", NAL TM-476.

[2] M. K. Gaillard, B. W. Lee, and J. L. Rosner, Rev. Mod. Phys. 47, 277 (1975).

[3] D. Sivers, J. Townsend and G. West, Phys. Rev. D 13, 1234 (1976).

[4] John Peoples (Private Communication); Irwin Gaines (Private Communication).

[5] R. F. Dashen, I. J. Muzinich, B. W. Lee, and C. Quigg, FERMILAB-PUB/75/18-THY.

[6] C. Quigg (Private Communication).

[7] W. Lee, Proc. 1975 International Symp. on Lepton and Photon Interactions at High Energy, Stanford (1975).

[8] G. S. Abrams, Proc. 1975 International Symp. on Lepton and Photon Interactions at High Energy, Stanford (1975).

[9] G. Goldhaber, Proc. International Conference on Production of Particles with New Quantum Numbers, Madison (1976).

[10] R. F. Schwitters, Proc. 1975 Intern. Symp. on Lepton and Photon Interactions at High Energy, Stanford (1975).

[11] Particle Data Group, Rev. Mod. Phys. 48, II (1976).

[12] G. Morpurgo, Nuovo cimento XXXI, N.3 (1964).

[13] E. Tilles (Private Communication).

Figure 1

Anticipated Fluxes

Electron, Tagged γ, Broad Band γ

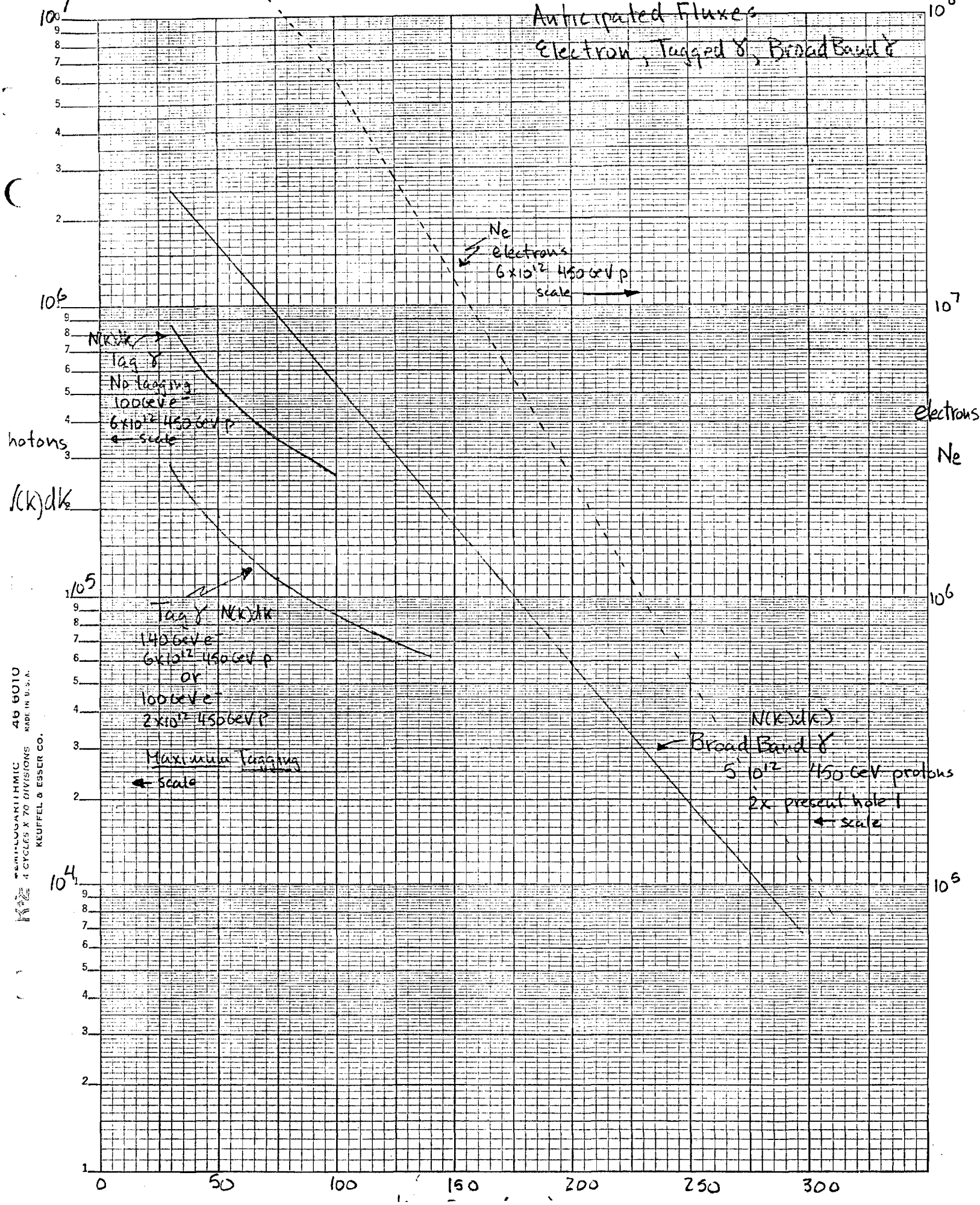

Figure 2
Schematic Drawing of Tagged Photon Beam

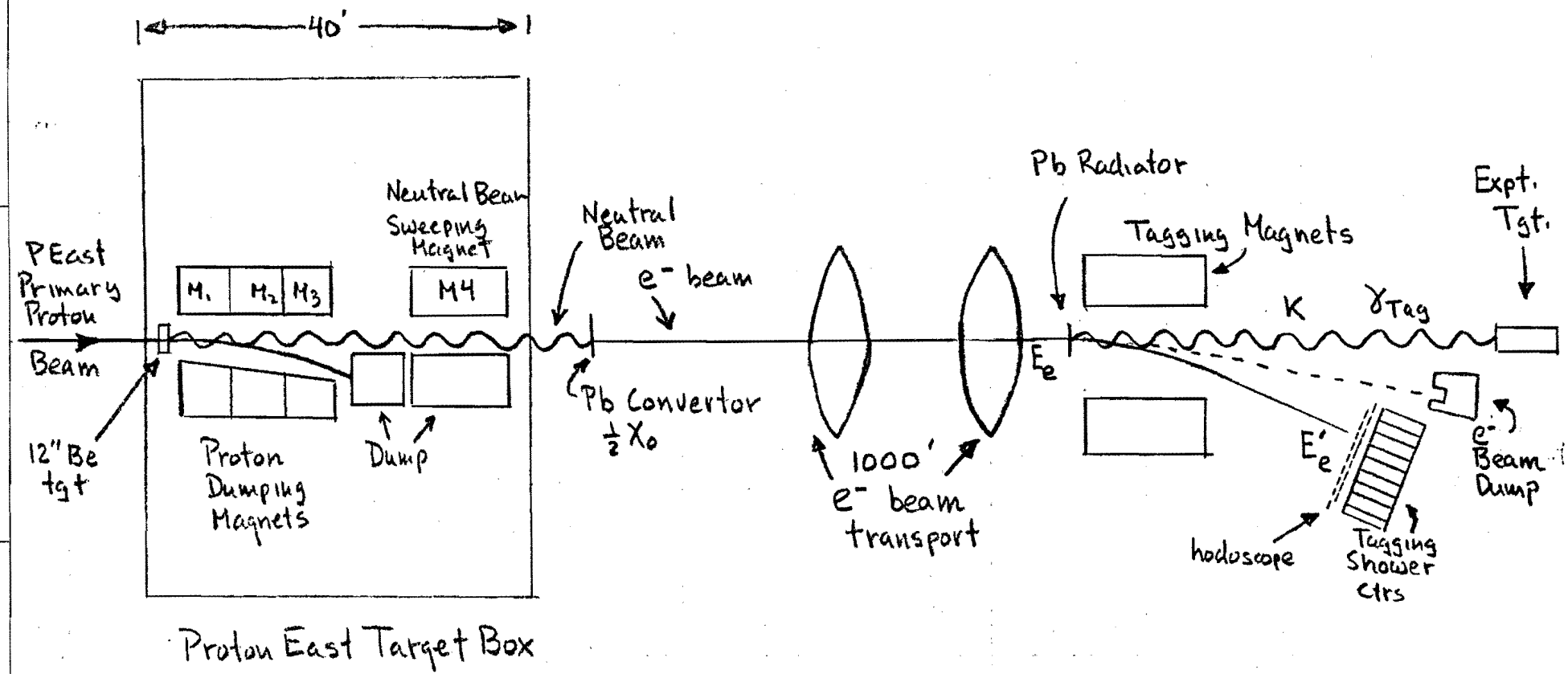

Proton East Target Box

Figure 3

Schematic Drawing of Vertical Focusing of Electron Beam in Target Box

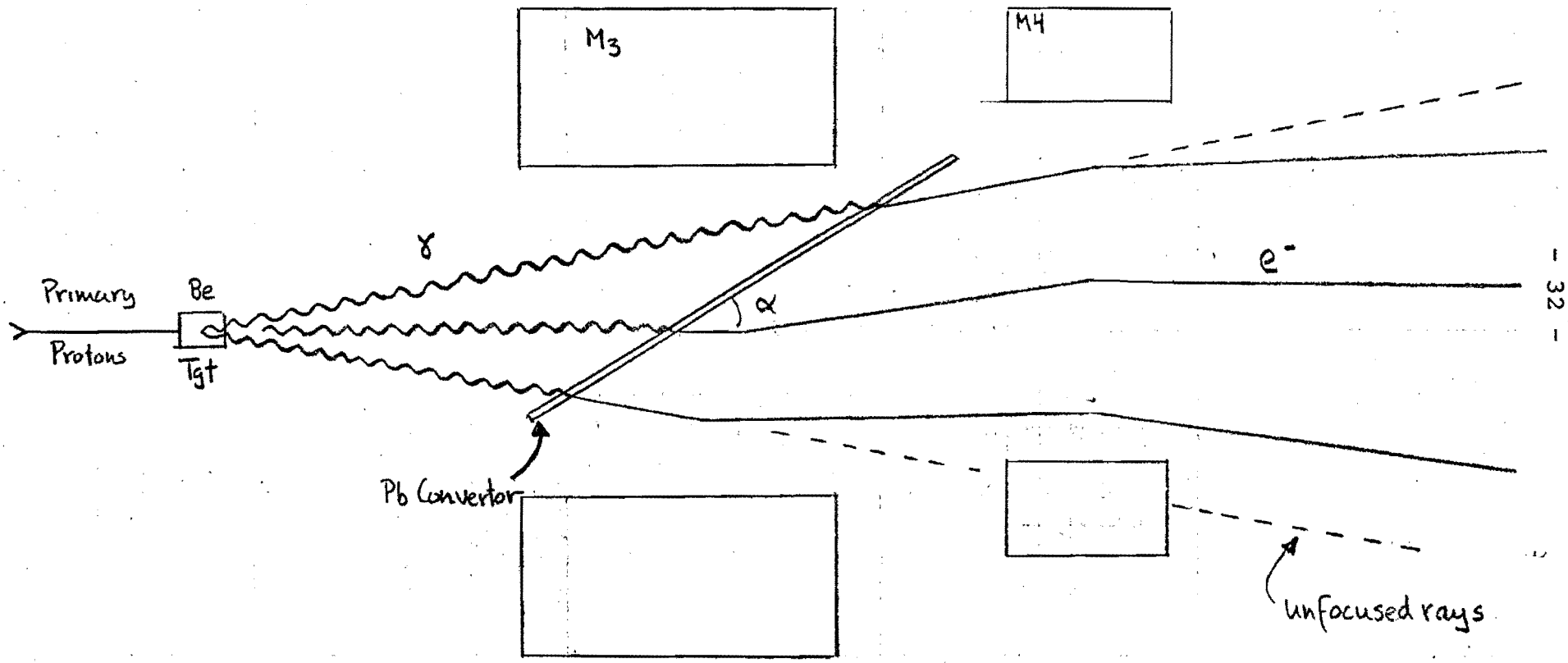

Figure 4

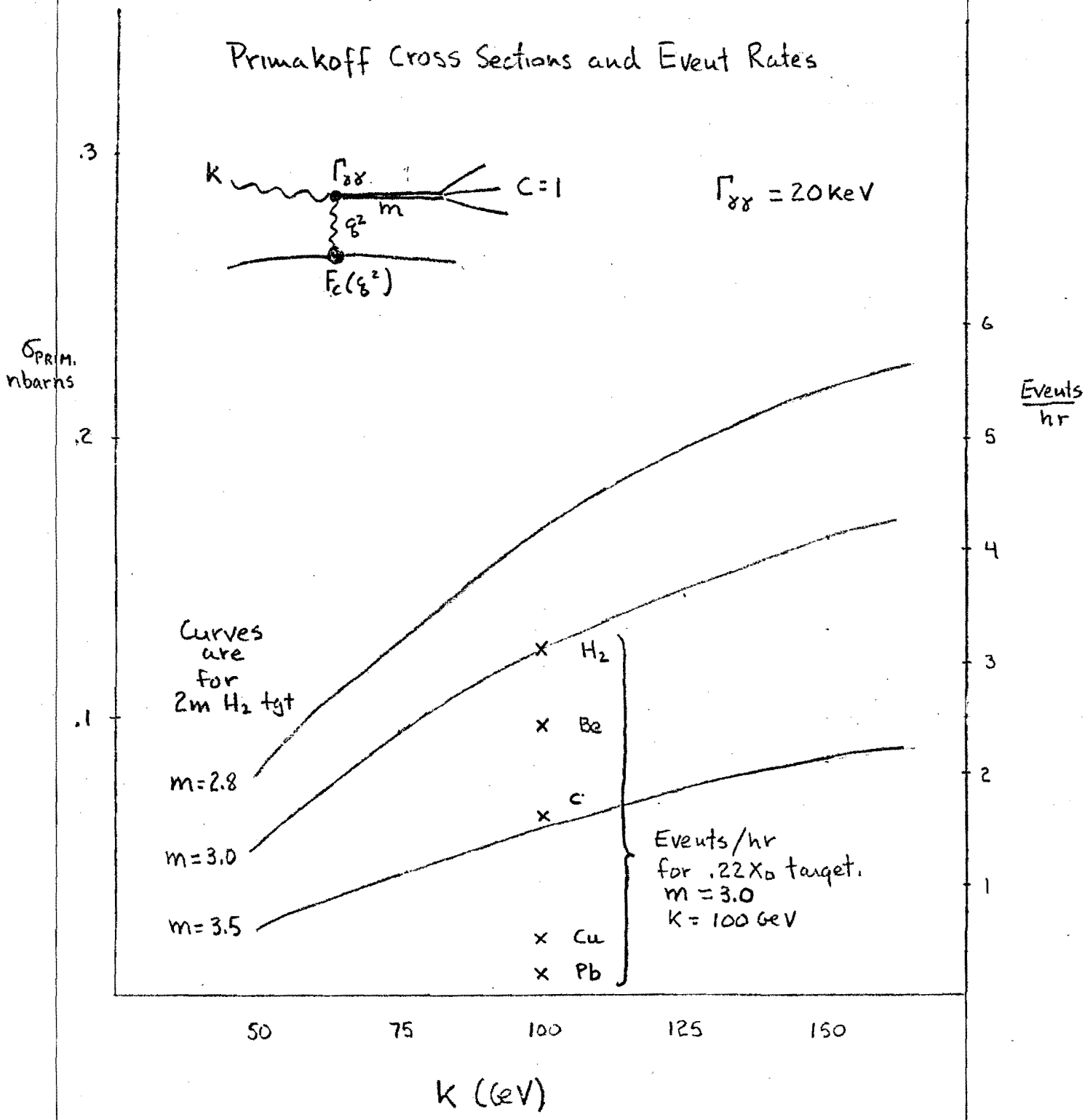
Primakoff Cross Sections and Event Rates
K
$\Gamma_{\gamma\gamma}$
m
q^2
$F_c(q^2)$
C=1
$\Gamma_{\gamma\gamma}$ = 20 keV
$\sigma_{PRIM.}$ nbarns
.3
.2
.1
Events/hr
6
5
4
3
2
1
Curves are for 2m H_2 tgt
m=2.8
m=3.0
m=3.5
H_2
Be
C
Cu
Pb
Events/hr for .22 X_0 target.
m = 3.0
K = 100 GeV
50
75
100
125
150
K (GeV)

Figure 5

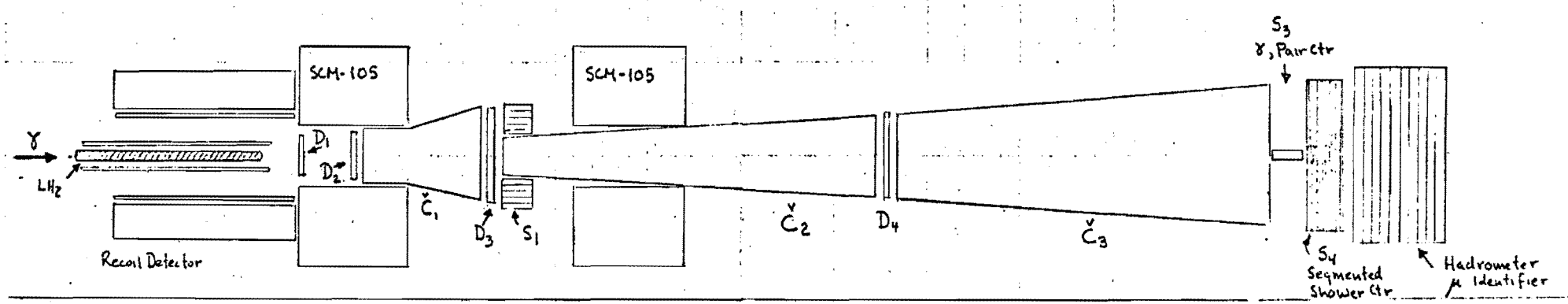

Floor

Elevation View

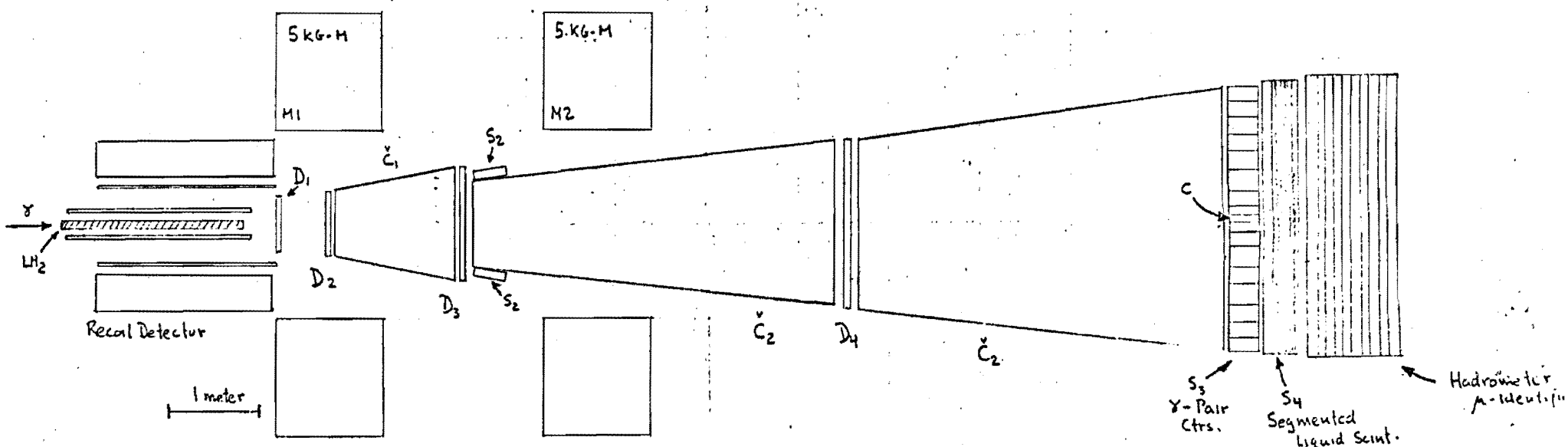

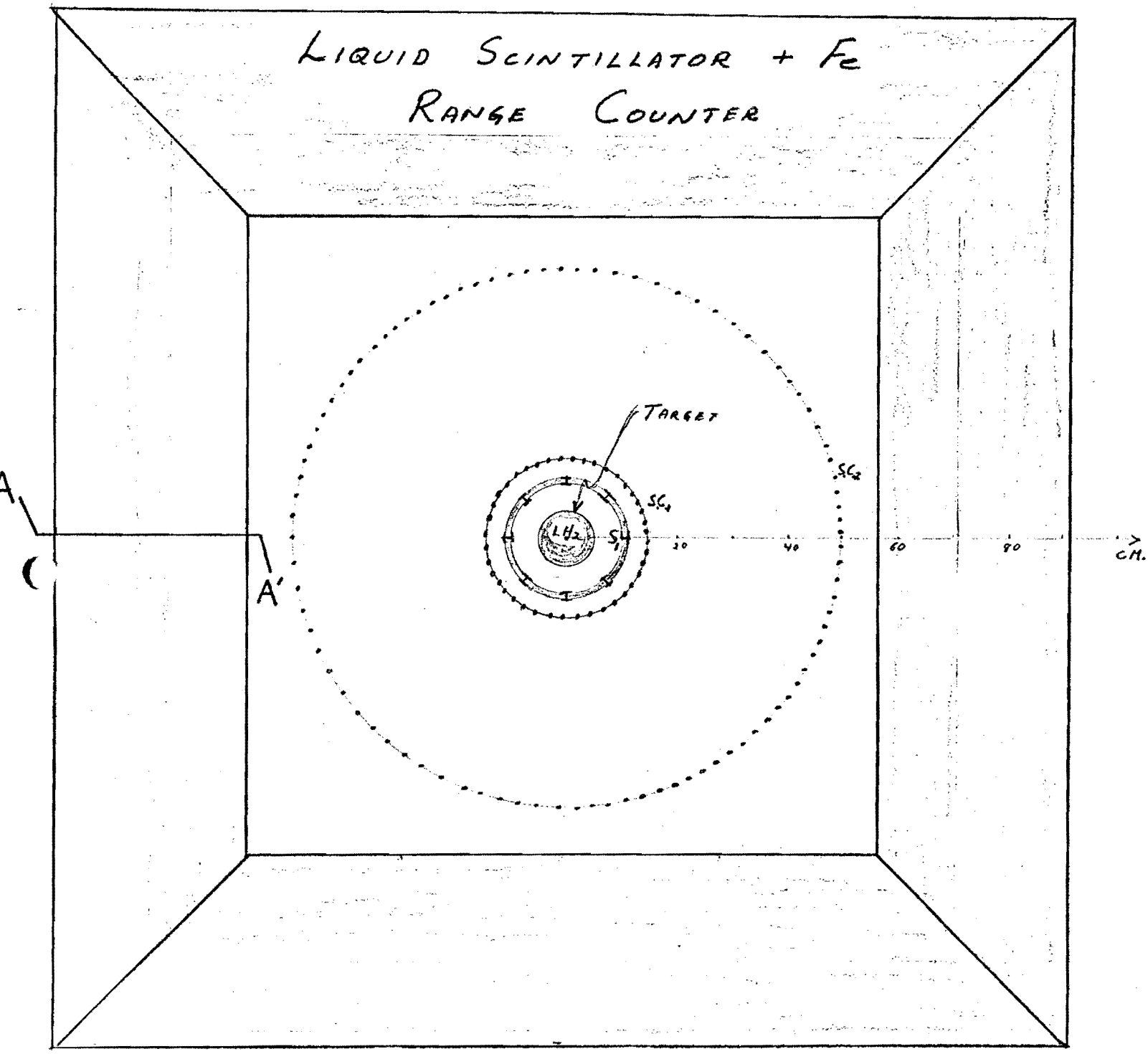

RECOIL DETECTOR

Figure 6

K+E 5 X 5 TO THE CENTIMETER 18 X 24 CM.
KEUFFEL & ESSER CO. MADE IN U.S.A.
46 1610

Figure 7

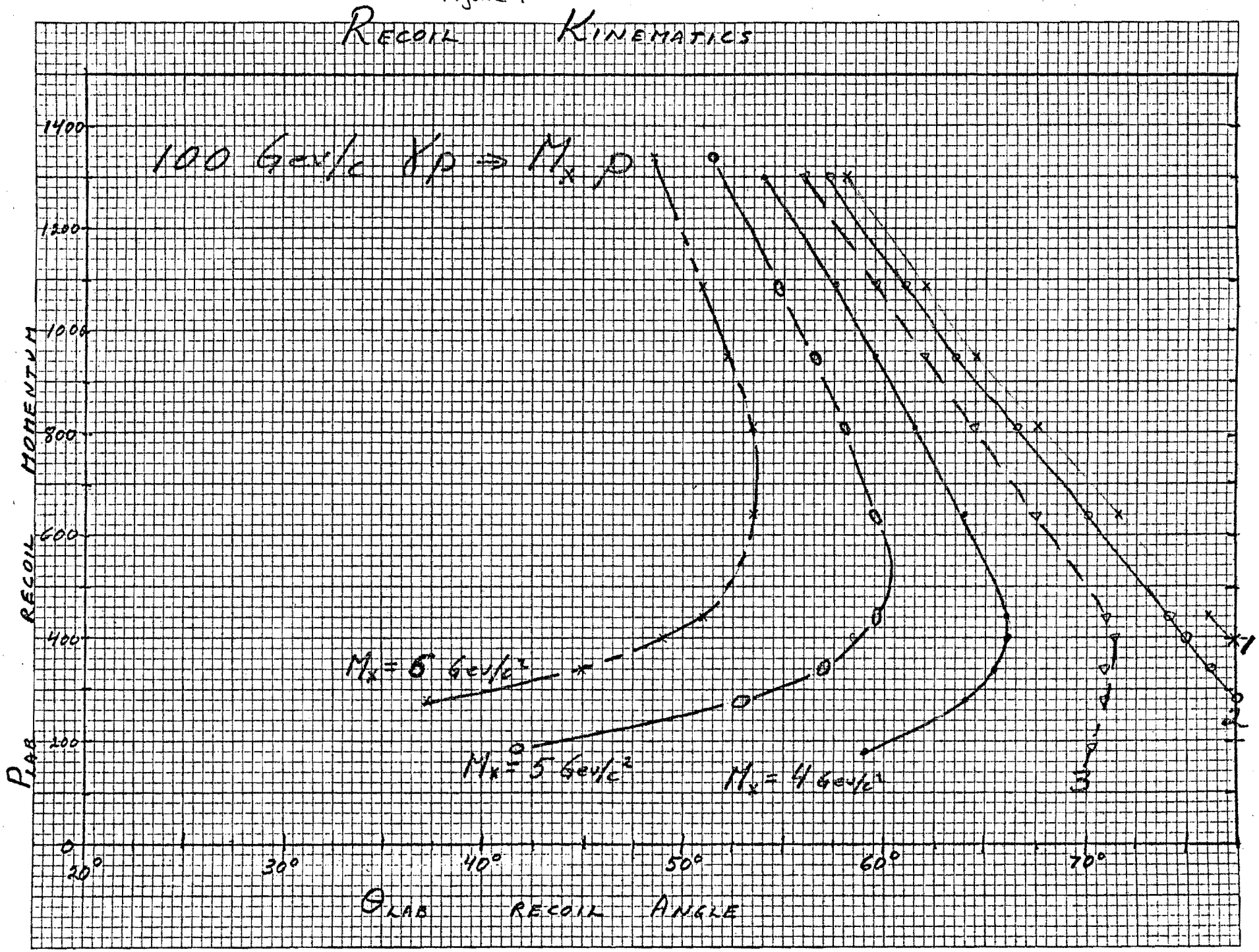

Figure 8 - Cross Sectional View of One Quadrant of Liquid Scintillator Range-dE/dx Detector (Section A-A', Fig 7)

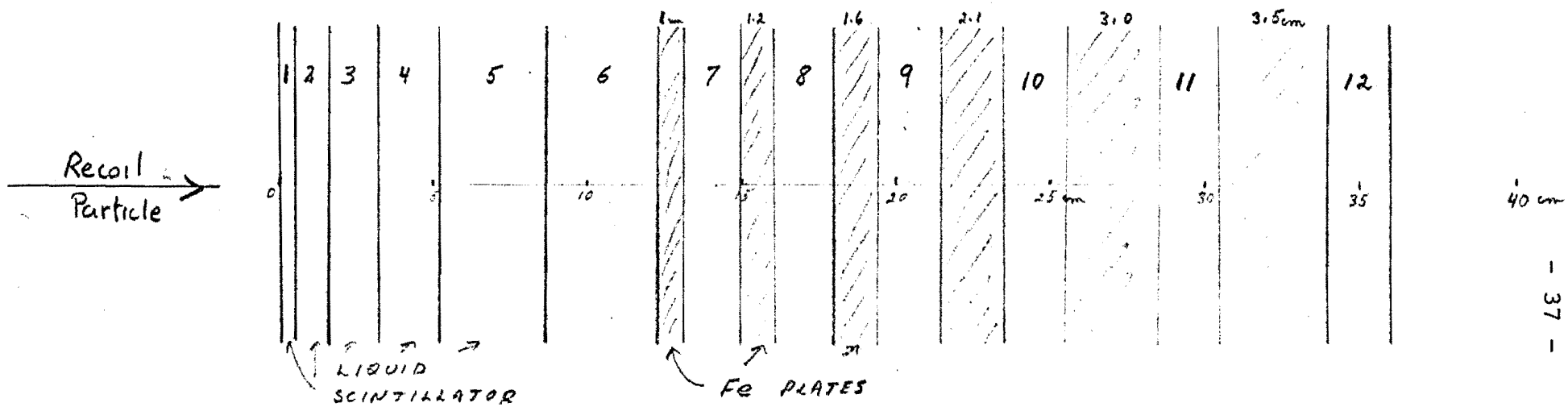

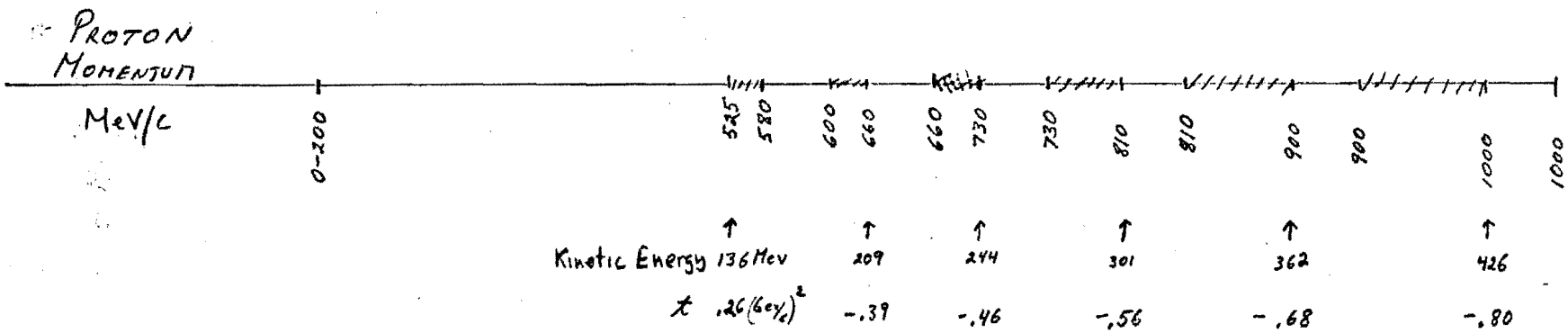

Figure 9

Missing Mass Resolution

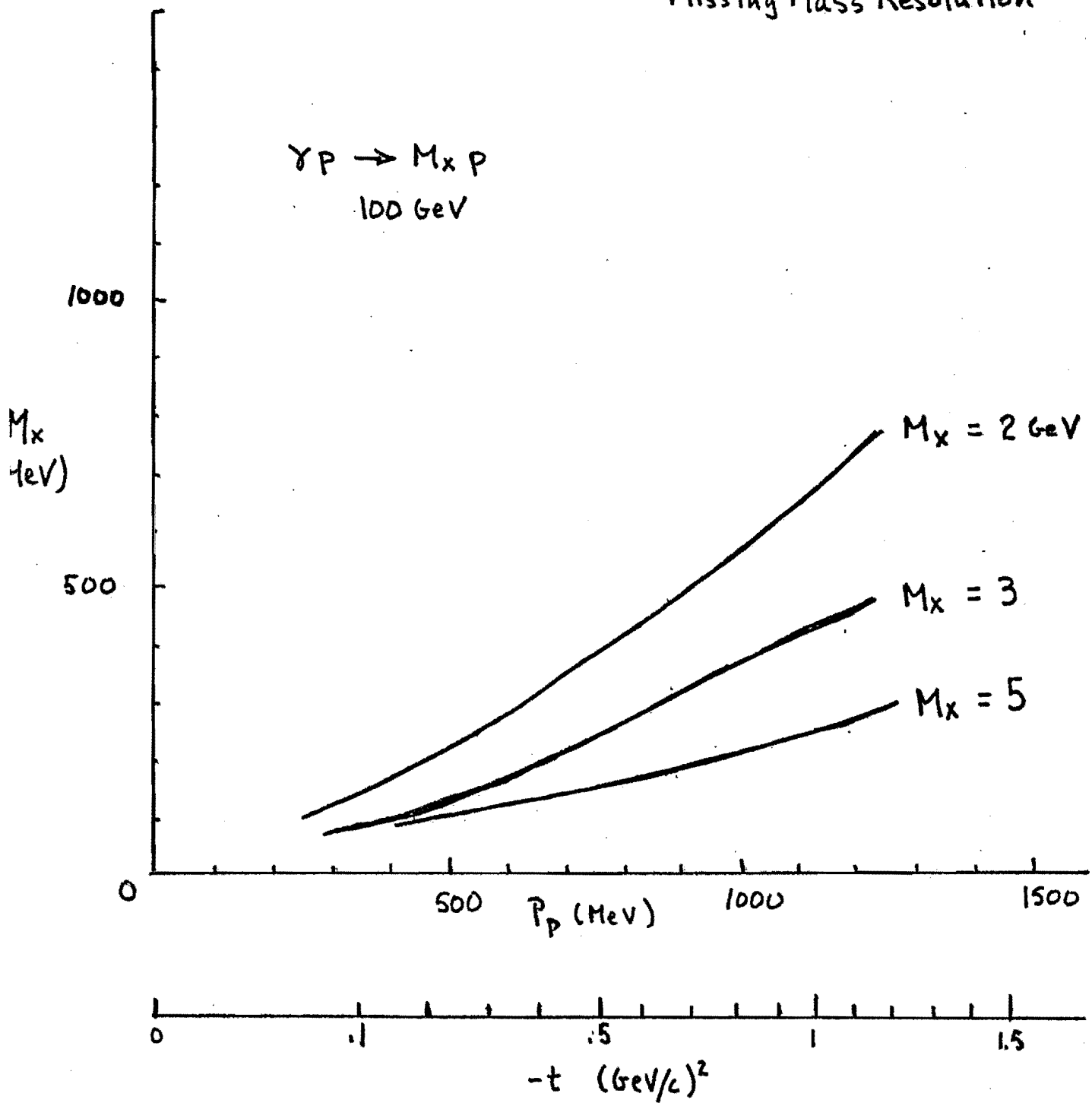

516 addendum

Scientific Spokesperson:

T. Nash
Fermilab

FTS number: 370-3795
Commercial: (312) 840-3795

The Tagged Photon Magnetic Spectrometer: Facility Design Report

May 1, 1977

J. Appel, D. Bartlett, S. Bracker, G. Hartner, G. Kalbfleisch, G. Luste, P. Mantsch, J. Martin, R. Morrison, T. Nash, U. Nauenberg, D. Ritchie, K. Stanfield, and S. Yellin

Fermi National Accelerator Laboratory, Batavia, Il.*
University of California at Santa Barbara*
University of Colorado, Boulder*
University of Toronto†

*Supported by the U.S. Energy Research and Development Administration

†Supported by the Institute for Particle Physics and the National Research Council, Canada

Table of Contents

I. Introduction 2

Table I Detector Locations and sizes 4

Table II Spectrometer Capabilities 5

Figure 1 Spectrometer Layout. 6

II. Design Considerations of the Recoil System 7

A. Acceptance 7

Figure 2 Missing Mass Kinematics 8

Figure 3 Recoil Detector: End View. 9

Figure 4 Recoil Detector: Top View. 10

Figure 5 Recoil Acceptance 12

B. Resolution 13

Figure 6 Missing Mass Resolution 14

C. π, P Identification. 15

Figure 7 π, p Energy Loss in Detector. 16

III. Design Considerations for the Forward Spectrometer . . 17

A. Acceptance 17

Table III Angular Acceptance Requirements . . . 18

Figure 8 Typical Angle vs Momentum Requirement 20

Table IV Monte Carlo Calculation of Spectrometer Acceptance 22

B. Resolution 21

Table V Mass Resolution 25

C. Particle Identification and the Overall Length of the Spectrometer 24

D. Spectrometer Layout. 26

Table VI Charged Particle Momentum and Angle Resolution. 29

E. Magnet Requirements 30

Table VII Magnet Requirements 31

F. Track Reconstruction Considerations and Location of Drift Chambers. 32

G. Cell Sizes. 36

Table VIII Drift Chamber Orientations and Cell Structure 39

Figure 9 Average Number of Particles giving Cerenkov Light. 42

Figure 10 Particle Position Distributions: C1. 43

Figure 11 Particle Position Distributions: C2. 44

IV. Triggers. 45

A. Fast Trigger. 45

B. High Level Triggers 46

V. Trigger Processor 54

Table IX Fast Memory Organization for Lookup Functions 56

Table X Neutral Recoil Veto Patterns. 59

VI. Recoil System 65

A. Cylindrical Wire Chambers 65

B. Liquid Scintillator Range Detector. 71

Table XI Range Detector Parameters 74

Figure 13 Range Detector Light Collection . . . 79

Table XII Dynamic Range Requirements. 80

VII. Liquid Hydrogen Target 81

Figure 14 Hydrogen Target Flask. 83

VIII. Forward Detectors. 84

A. Drift Chambers 84

Figure 15 Cell Structure 85

Figure 16 Cross Section of a Drift Plane 86

B. Cerenkov Counter 91

Table XIII Cerenkov Counter Specifications. . . . 92

Figure 17 Excitation Curves: C1 93

Figure 18 Excitation Curves: C2 94

Figure 19 Winston Cones. 95

Figure 20 Cerenkov Counter Gas System. 97

C. SLIC 99

Figure 21 SLIC 100

D. Hadrometer 105

Table XIV Hadrometer Specifications. 106

Figure 22a Hadrometer 107

Figure 22b Typical Hadrometer Scintillator Module 108

IX. Online Computer Configuration. 110

A. Hardware Requirements 110

Table XV Online Computer Requirements 114

B. Online Software 115

X. Track Reconstruction 117

Figure 23 Track Reconstruction in Forward System . 118

XI. Beam 122

Figure 24 Photon and Electron Fluxes 123

Figure 25 Tagged Photon Beam Schematic Drawing . . 124

Figure 26 Radiator Focussing Element 126

XII. Schedule 130

Table XVI Time Schedule. 132, 133

XIII. Cost Estimates 134

Table XVII Cost Estimates 135, 136

XIV. Acknowledgements 134

I. Introduction

This report describes the design of a magnetic spectrometer facility to be built in the Tagged Photon Lab. The design has been developed by a collaboration of physicists from Fermilab, The University of California at Santa Barbara, The University of Colorado and The University of Toronto. This group was formed to build the facility and to carry out the experiment described in Proposal 516,[1] which is a study of photoproduced states (including charm and hidden charm) with a forward mass > 2.5 GeV. Although the design of the facility is developed from that outlined in P-516, much thought has gone into making the facility versatile enough to be used for a continuing program of physics by different groups. In addition to the 100 GeV photon physics of P-516, this facility is designed to be useful for experiments like the following: pion production experiments, hadron jet experiments, $\gtrsim$ 300 GeV and very high intensity photon physics with the energy doubler including searches for and studies of heavy leptons.

A detailed layout of the spectrometer is shown in Fig. 1. In Table I may be found the sizes and locations of the detectors. These are the locations expected for the startup of the facility with photon energies in the range $70 < k < 140$ GeV. However, much of the spectrometer will be mounted on a rail system. This will allow, for example, the spectrometer to be stretched out for future use at higher energies.

The following is a brief overview of the system prior to the

detailed discussions in the remainder of the report. The recoil system surrounding the target identifies recoil protons and measures their angles and kinetic energy (see Fig. 3 & 4 in Section II). This information can be used to determine the missing mass of the forward going system of particles that recoiled off the proton. Angles are measured by three cylindrical wire chambers (PWC1, PWC2, PWC3). Energy is measured by total absorption and range in a four-tiered cylindrical liquid scintillator detector (A_i, B_i, C_i, D_i). Pions and protons are distinguished by the dE/dX information. The forward spectrometer is a two magnet system (M_1, M_2) consisting of a low momentum, high acceptance spectrometer combined with a lower acceptance spectrometer for higher momentum particles. There are five banks of drift chambers (D_1, D_2, D_3, D_4, D_5) to measure momenta and angles of charged tracks. Two atmosphere pressure Cerenkov counters ($\check{C}_1$, $\check{C}_2$) will be used for K, π, p particle identification. A segmented liquid scintillator shower counter (SLIC) will measure energy and angles of electromagnetic particles ($e^{\pm}$, π^{o}, γ). A segmented hadrometer will be used to detect neutral hadrons (K_L^o, n) and will be used in triggers. It will also be essential to possible hadron jet experiments. Table II summarizes broadly the capabilities of the facility, including acceptances, resolutions, etc.

In the following sections of this report we will first discuss the design considerations and constraints that have lead to the present design of the recoil system and the forward spectrometer. We will describe the approach to triggering that we are planning and the reconstruction of multitrack events. This will

Table I

Locations, Sizes and Acceptance of Detectors

	Location (m) on beam line	Size (m)(2) Hor.	Vert.	Acceptance(1) P_{min} (GeV)	$\Delta\theta_x$ (mrad)	$\Delta\theta_y$ (mrad)
tgt center	0	-	-	-	-	-
D1XUV	1.68	.67	.56	1	±199	±167
D2XUV1	2.18	.85	.65	1	±182	±149
D2XUV2	2.21	.85	.65	1	±180	±147
D2XUV3	2.24	.85	.65	1	±178	±145
M1	2.2±.6	~2	.76	-	~±350	±136
D3XUV1	3.41	1.75	1.20	1	±176	±176
D3XUV2	3.71	1.75	1.20	1	±162	±162
D3XUV3	4.01	1.75	1.20	1	±150	±150
M2	4.7±.6	~2	.76	-	~±170	± 72
C1 upstr	4.2	1.40	.64	5	±148	± 74
C1 dnstr	7.45	2.51	1.14	5	±135	± 77
D4XUV1	7.51	2.10	1.25	10	±120	± 79
D4XUV2	7.97	2.10	1.25	10	±120	± 78
D4XUV3	8.12	2.10	1.25	10	±120	± 77
C2 upstr	8.2	2.1	1.25	10	±120	± 77
C2 dnstr	15.1	4.33	2.50	10	±120	± 82
D5X12	15.2	4.33	2.50	10	±120	± 82
Control Shower Ctr (C) upstr	15.3	.064	.064	accepts γ beam only		
SLIC dnstr	16.4	4.14	2.64	neutrals	±127	± 82
Hadrom. dnstr	18.15	4.90	2.95	10	±110	± 81

Notes:

1) Acceptance for rays from target center. Magnet bends at 5 kG-m, same polarity

2) Sizes specified as follows: Only magnet apertures to limit vertical rays from either end of target. Horizontal acceptance ± 120 mrad for P_{min} rays from upstream end of target for low P system and from target center for high P system (± 110 mr for hadrometer).

Table II

Overview of Spectrometer Capabilities
(for electron beam energy = 140 GeV)

Recoil:

$.1 < |t| < .6 \ \text{GeV}^2$ $\qquad \frac{\delta T}{T} \simeq \pm .1 \qquad \delta\theta = \pm 6$ mr

$30^\circ \lesssim \theta \lesssim 90^\circ$

acceptance $\simeq$ 50% for $e^{-\lambda|t|}$, $\qquad \delta M_x < \pm 350$ MeV for $M_x > 2$ GeV

$2 < \lambda < 15 \ \text{GeV}^{-2}$

$\pi\pm$ vs p identification range $|t| \lesssim .6 \ \text{GeV}^2$

π^0 identification efficiency~.72

n identification efficiency ~ .45

Forward charged spectrometer:

Low momentum system

$1 < P < 10$ GeV $\qquad \frac{\delta P}{P} = \pm 8.6 \ 10^{-4} P \qquad \delta\theta = \pm .1$ mr

$\theta_{horiz} < \pm 150$ mr

$\theta_{vert} < \pm 135$ mr

High momentum system

$10 < P < 120$ GeV $\qquad \frac{\delta P}{P} = \pm 2.2 \ 10^{-4} P \qquad \delta\theta = \pm .05$ mr

$\theta_{horiz} < \pm 120$ mr

$\theta_{vert} < \pm 72$ mr

Particle Identification - π vs (K or p): $5.5 < P \lesssim 50$ GeV

π vs K vs p: $21 < P \lesssim 50$ GeV

Neutrals:

$\theta_{horiz} < \pm 120$ mr

$\theta_{vert} < \pm 82$ mr* $\qquad \frac{\delta E}{E} \lesssim \pm .1 \ E^{-\frac{1}{2}} \qquad \delta\theta = \pm .3$ mr

---

Luminosity: ~ 1 event/nb/10^{15} protons

*(±120 mr with upstream shower counters)

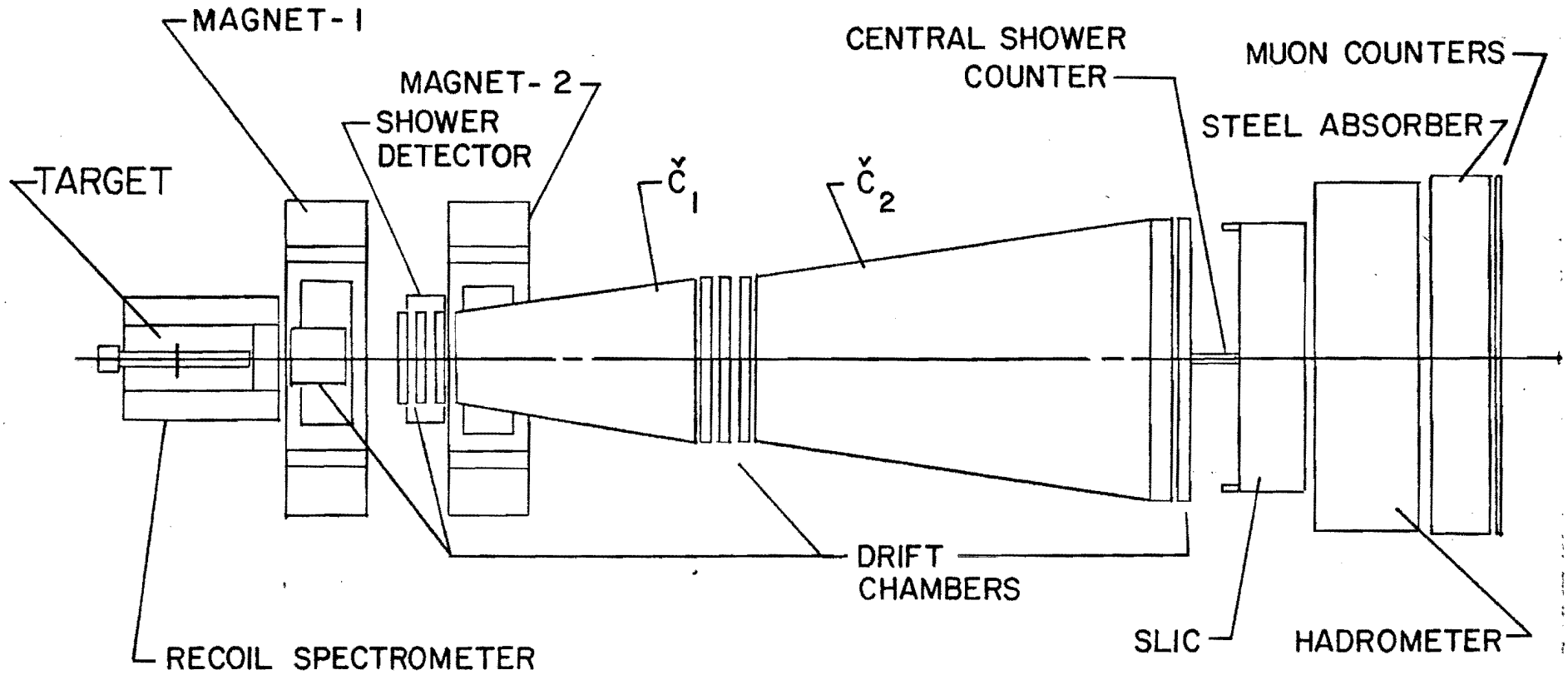

PLAN VIEW

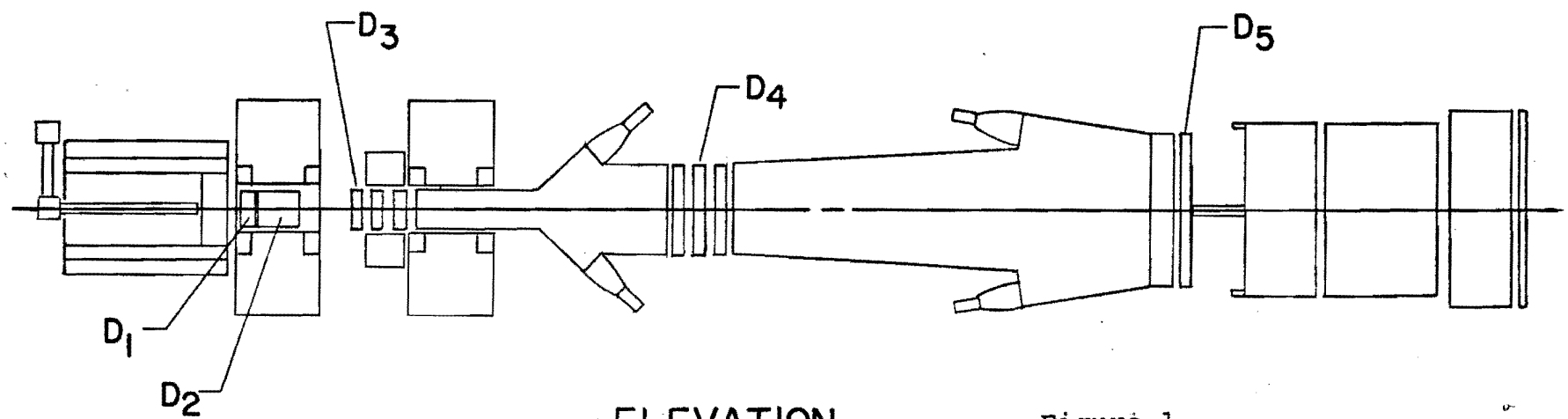

ELEVATION

Figure 1

be followed by a detailed description of the various detectors and experimental equipment that will be built. We will leave to the last, appropriately next to the acknowledgements, an outline of costs and scheduling.

II. Design Considerations of the Recoil System

The purpose of the recoil system is to measure the four vectors of particles recoiling from the 2m long hydrogen target. It must do this in less than ~ 1μsec so that a missing mass can be calculated and used in the trigger. Since the associated photoproduction of charmed states will require missing mass in excess of 2 times 1.80 GeV, the missing mass threshold can be safely set at 2.5 GeV in the trigger. As discussed in Section IV, this will reject most of the γp cross section including all the low mass neutral vector mesons (ρ^o, ω^o, ϕ^o, $\rho^{o'}$, etc.) and will enrich the data with charm events.

A. Acceptance

We consider the reaction

$$\gamma p \rightarrow M_x\, p'$$

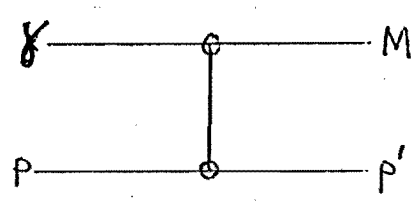

where particle M_x is the forward going system predominately detected in the two magnet spectometer. Figure 2 shows the simple two body kinematics curves for this reaction at several energies. It is clear that the polar angle θ for the

Fig. 2

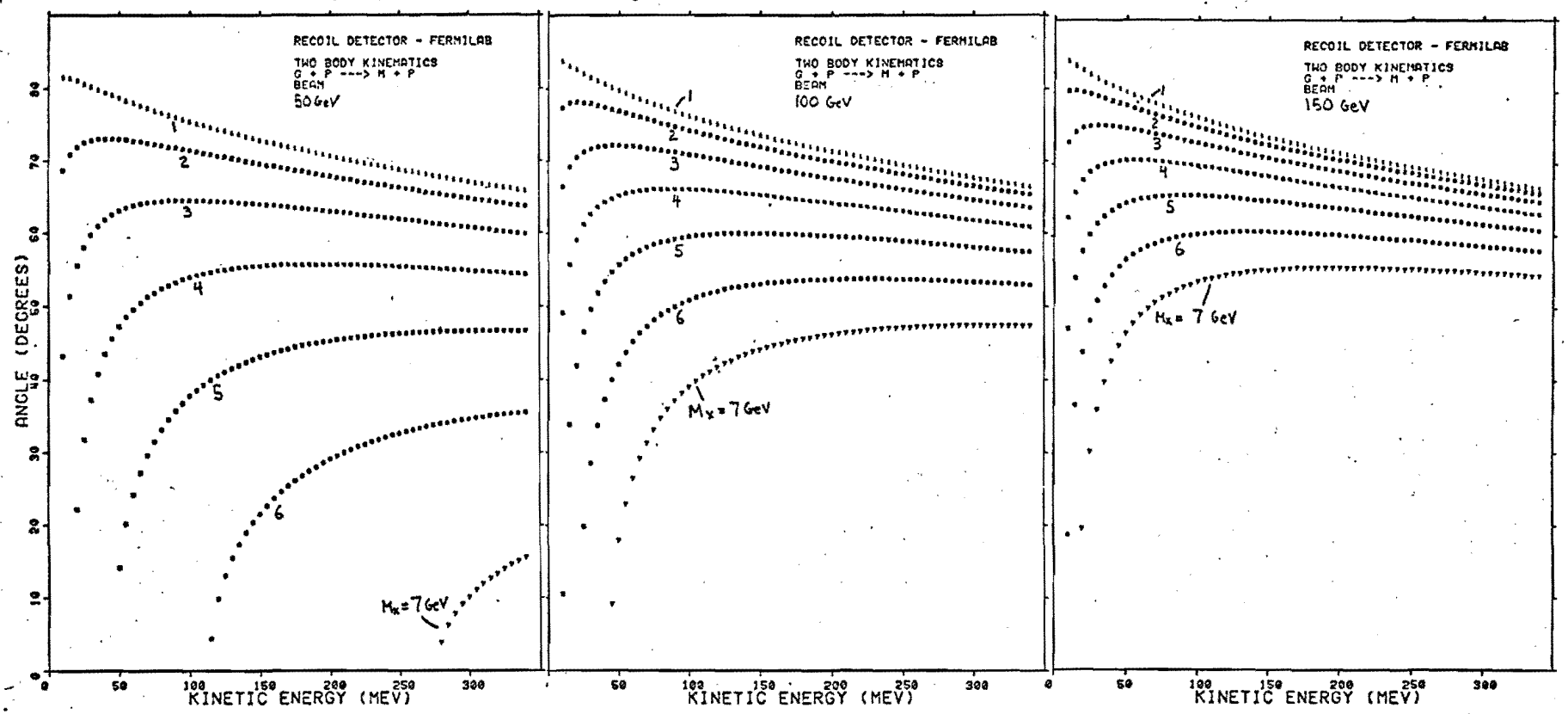
RECOIL DETECTOR - FERMILAB
TWO BODY KINEMATICS
G + P ---> M + P
BEAM
50 GeV
100 GeV
150 GeV
ANGLE (DEGREES)
KINETIC ENERGY (MEV)
Mx = 7 GeV
1
2
3
4
5
6

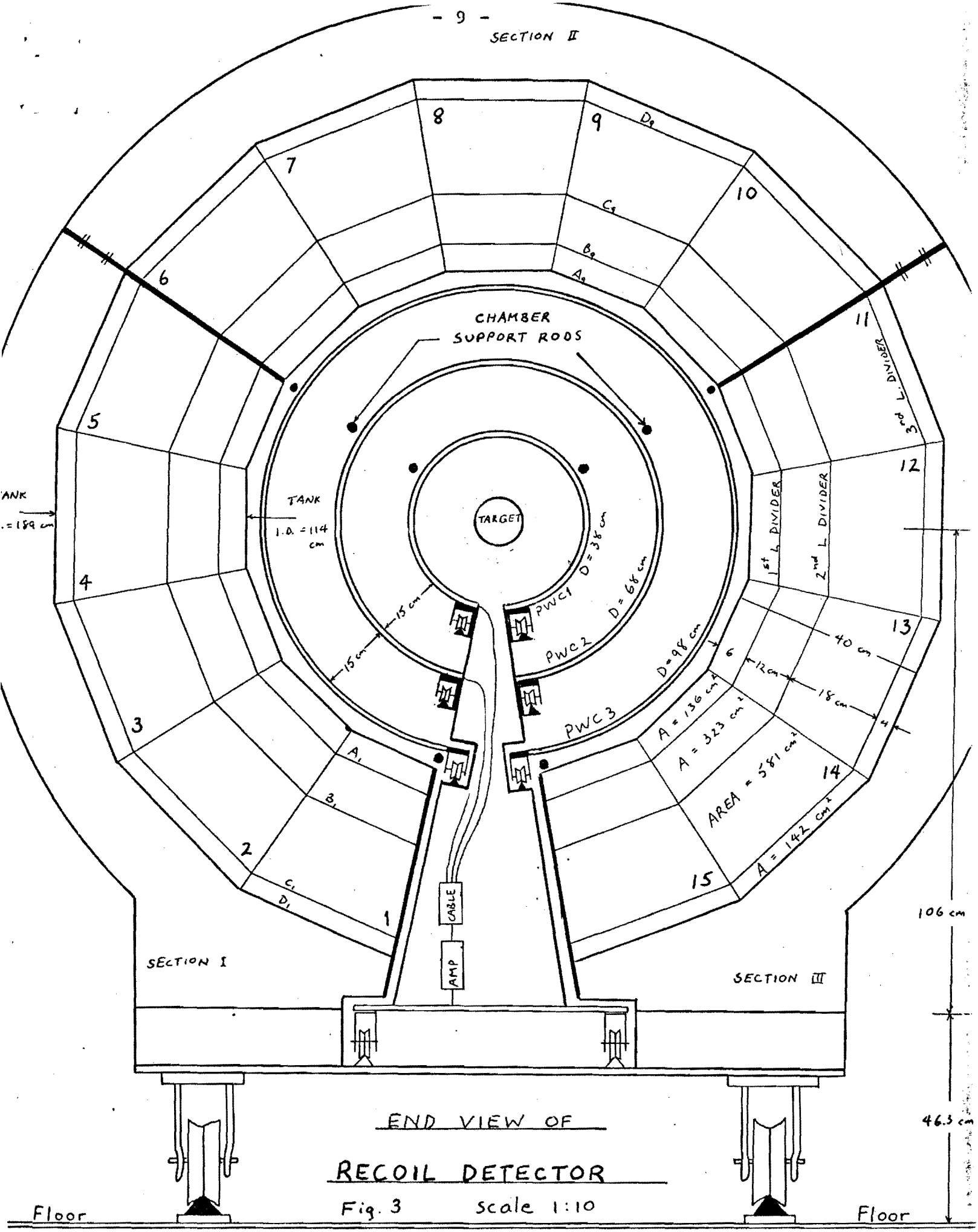

END VIEW OF

RECOIL DETECTOR

Fig. 3 Scale 1:10

RECOIL DETECTOR

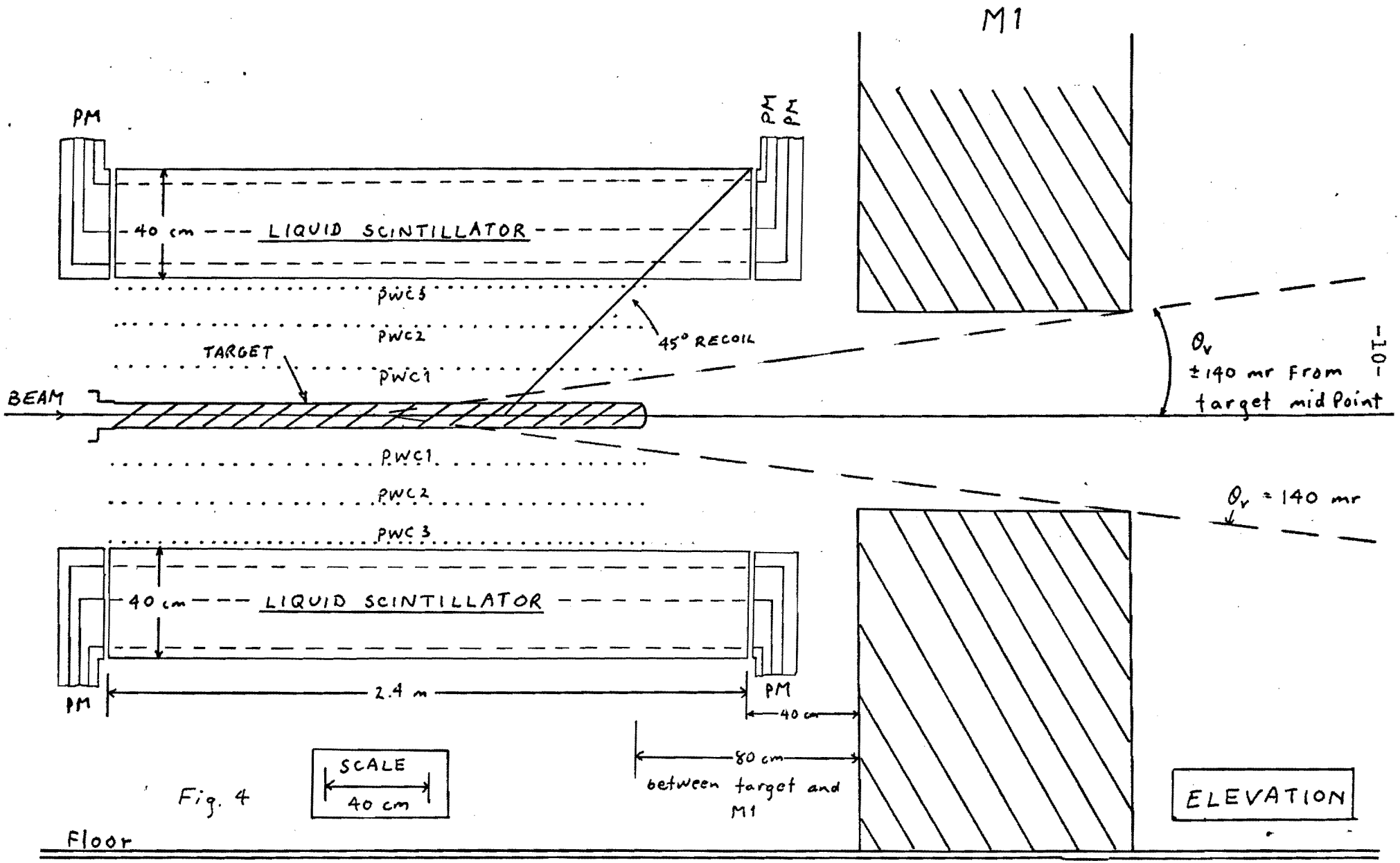

Fig. 4

p' recoil mainly lies between 30° and 80° for the M_x range of 2 to 6 GeV. Only near values of $|t|_{min}$ is the angle less than 30°. Thus the recoil system is designed to have high acceptance for $\theta \gtrsim 45^{\circ}$. Only in the downstream one-half meter of a 2.0 m long hydrogen target is there any acceptance loss for $\theta \lesssim 45^{\circ}$. Figures 3 and 4 show a side and frontal view of the recoil system and illustrate how the detector encloses the target.

The azimuthal angle acceptance is almost 337.5°. This is 94% of the full 2π. As shown in Fig. 3, a segment in θ is removed to provide structural support for the access to the three cylindrical PWC's.

We define momentum acceptance of the recoil proton as that percentage which stop inside the liquid scintillator range detector. This of course depends on the t distribution of the recoil particle, and its recoil angle θ. The recoil angle θ determines how much material the proton must traverse (in the target and PWC's) before it reaches the scintillator. It defines a minimum momentum. The effective scintillator thickness increases as θ decreases and defines a maximum momentum. A reasonable estimate is that the acceptance will be in the range of 45% to 55%. This assumes a recoil slope of $\lambda \simeq 4$ GeV^{-2}, which is the value suggested by the high energy ψ photoproduction experiments. Figure 5 shows how the proton recoil acceptance varies with the $e^{\lambda t}$ recoil slope λ and for three different ranges of t measurement. The expected range is $0.1 < |t| < 0.6$ GeV^2. It is clear that

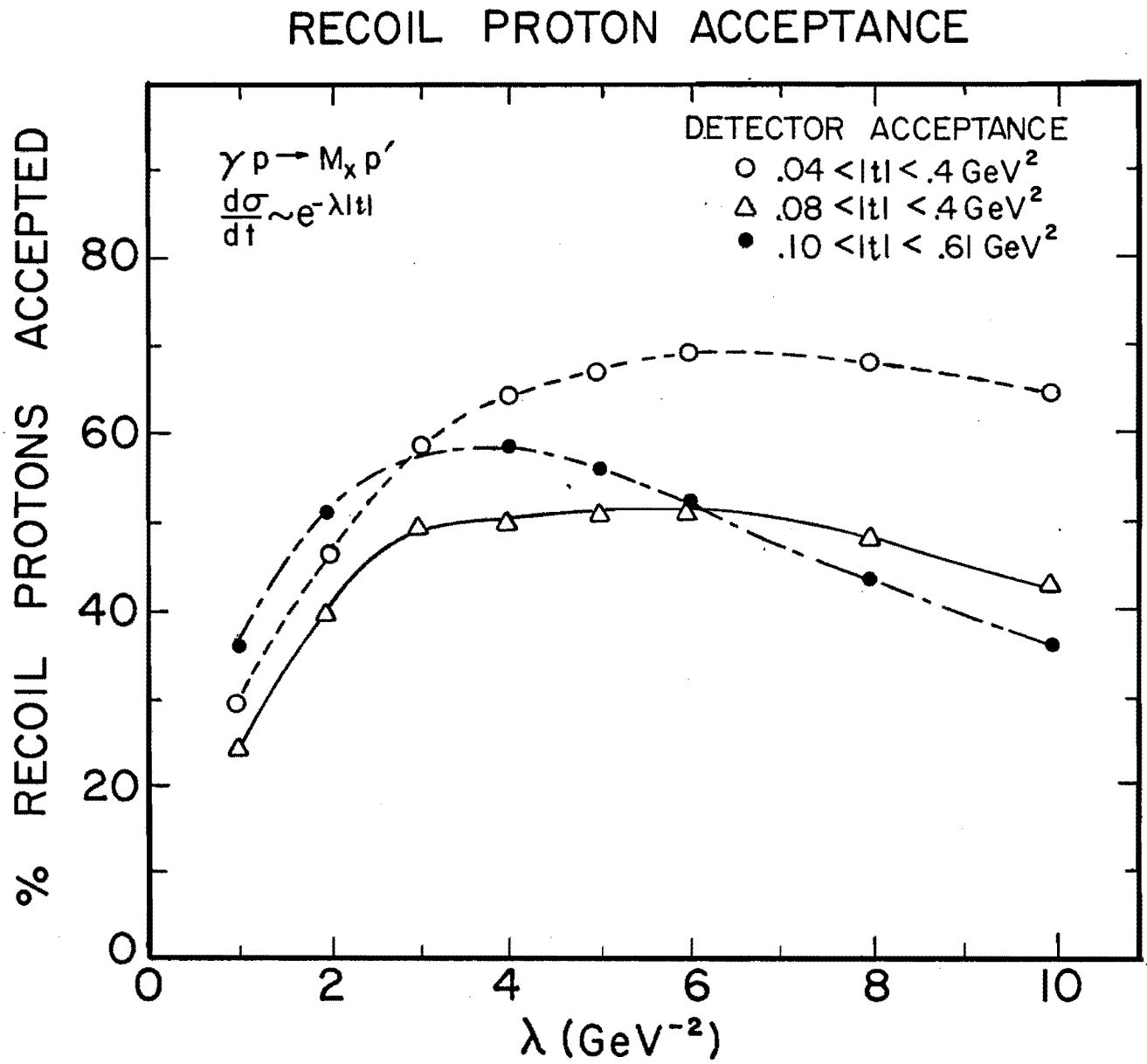
RECOIL PROTON ACCEPTANCE
DETECTOR ACCEPTANCE
○ .04 < |t| < .4 GeV²
△ .08 < |t| < .4 GeV²
● .10 < |t| < .61 GeV²
γ p → M_x p′
dσ/dt ~ e^{-λ|t|}
% RECOIL PROTONS ACCEPTED
0
20
40
60
80
0
2
4
6
8
10
λ (GeV⁻²)

Figure 5

building a detector to measure much lower and/or higher t, which would greatly increase the complexity and expense, would not provide a commensurate gain in acceptance.

B. Resolution

The equation for missing mass is $M_x^2 = 2kp'\cos\theta - 2kT - 2mT$ where k is the beam energy, T and p' are the recoil proton kinetic energy and momentum, θ is the recoil proton angle relative to the beam and m is the proton mass. The error contributions then vary as

$$\delta M_k = \frac{1}{M}(p' \cos\theta - T)\delta k$$

$$\delta M_T = \frac{1}{M}\left(\frac{k \cos\theta}{\beta} - (k+m)\right)\delta T$$

$$\delta M_\theta \doteq \frac{1}{M} k\, p' \sin\theta\, \delta\theta$$

and the total missing mass resolution is

$$\delta M_x = \sqrt{\delta M_k^2 + \delta M_T^2 + \delta M_\theta^2}$$

The variation of the δM_i curves with T and different values for M, k, δk, δT, and $\delta\theta$, representing extremes, are shown in Figs. 6a-d. The T interval from about 30 to 300 MeV represents the typical acceptance of the liquid scintillator. At very low T, multiple scattering dominates $\delta\theta$ which, in turn, dominates δM. These low T protons are also the recoils which will not make it through the hydrogen, the target walls

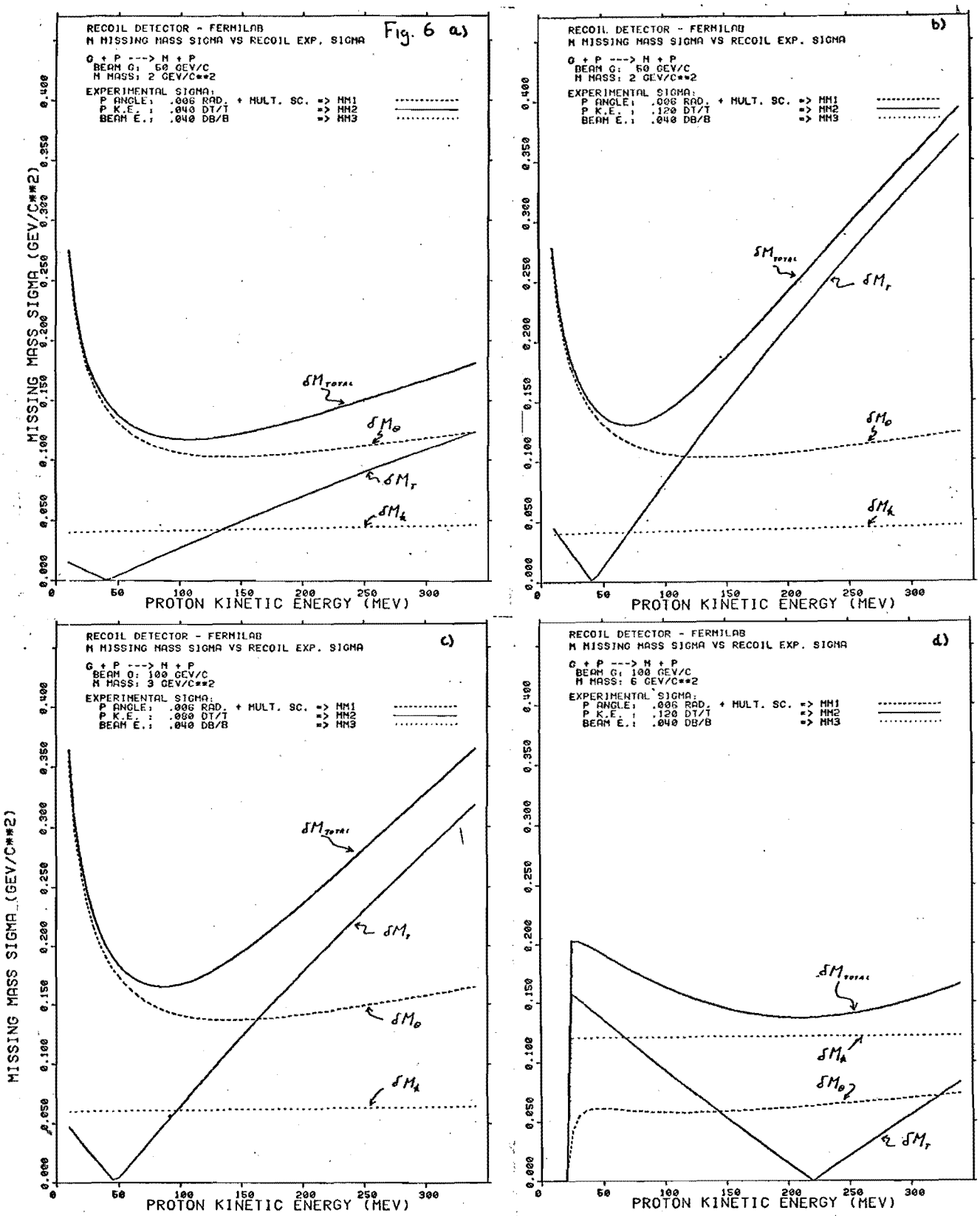
Fig. 6 a)
RECOIL DETECTOR - FERMILAB
M MISSING MASS SIGMA VS RECOIL EXP. SIGMA
G + P ---> M + P
BEAM G: 60 GEV/C
M MASS: 2 GEV/C**2
EXPERIMENTAL SIGMA:
P ANGLE: .006 RAD. + MULT. SC. => MM1
P K.E. : .040 DT/T => MM2
BEAM E.: .040 DB/B => MM3
δM_TOTAL
δM_θ
δM_T
δM_k
MISSING MASS SIGMA (GEV/C**2)
PROTON KINETIC ENERGY (MEV)
b)
RECOIL DETECTOR - FERMILAB
M MISSING MASS SIGMA VS RECOIL EXP. SIGMA
G + P ---> M + P
BEAM G: 60 GEV/C
M MASS: 2 GEV/C**2
EXPERIMENTAL SIGMA:
P ANGLE: .006 RAD. + MULT. SC. => MM1
P K.E. : .120 DT/T => MM2
BEAM E.: .040 DB/B => MM3
δM_TOTAL
δM_T
δM_θ
δM_k
PROTON KINETIC ENERGY (MEV)
c)
RECOIL DETECTOR - FERMILAB
M MISSING MASS SIGMA VS RECOIL EXP. SIGMA
G + P ---> M + P
BEAM G: 100 GEV/C
M MASS: 3 GEV/C**2
EXPERIMENTAL SIGMA:
P ANGLE: .006 RAD. + MULT. SC. => MM1
P K.E. : .080 DT/T => MM2
BEAM E.: .040 DB/B => MM3
δM_TOTAL
δM_T
δM_θ
δM_k
MISSING MASS SIGMA (GEV/C**2)
PROTON KINETIC ENERGY (MEV)
d)
RECOIL DETECTOR - FERMILAB
M MISSING MASS SIGMA VS RECOIL EXP. SIGMA
G + P ---> M + P
BEAM G: 100 GEV/C
M MASS: 6 GEV/C**2
EXPERIMENTAL SIGMA:
P ANGLE: .006 RAD. + MULT. SC. => MM1
P K.E. : .120 DT/T => MM2
BEAM E.: .040 DB/B => MM3
δM_TOTAL
δM_k
δM_θ
δM_T
PROTON KINETIC ENERGY (MEV)

and the chambers into the liquid scintillator.

In Fig. 6a, at T = 300 MeV the error contributions from δM_T and δM_θ are equal when $\delta T/T = \pm 4\%$ and $\delta\theta = \pm 6$ milliradians. The resulting $\delta M_{total} = \pm 175$ MeV at M = 2 GeV, k = 50 GeV. This guides our choice of wire spacing in the cylindrical PWC's to measure $\delta\theta$ to $\pm$ 6 mrad. A pessimistic case of $\delta T/T = \pm 12\%$ gives $\delta M_{total} = \pm 350$ MeV for the difficult case of low mass (2 GeV) and γ energy (50 GeV), as shown in Fig. 6b. Even here the missing mass resolution is acceptable. For very high missing mass the resolution is dominated by the beam momentum uncertainty $\delta k/k \simeq \pm 4\%$. This is illustrated in Fig. 6d.

In conclusion, the recoil system is designed to measure recoil protons in the t range 0.1 to 0.6 GeV^2 and to calculate the missing mass to within $\pm$ 350 MeV/c^2 i[illegible] $M_x > 2$ GeV.

C. <u>π, P Identification</u>

Pions and protons (T < 300 MeV) can be separated by relative dE/dx signals in liquid scintillator compartments A_i, B_i, C_i, and D_i. The relative pulse heights in each compartment are shown in Fig. 7a for recoil angle $\theta = 90^\circ$ and in Fig. 7b for recoil angle $\theta = 30^\circ$. For example, in Fig. 7b, a 230 MeV proton could not be mistaken for a pion of any energy because of its large pulse height in segment B and zero pulse height in segment C. A more ambiguous case is a ~ 470 MeV proton, which perhaps could be interpreted as a 200 MeV pion.

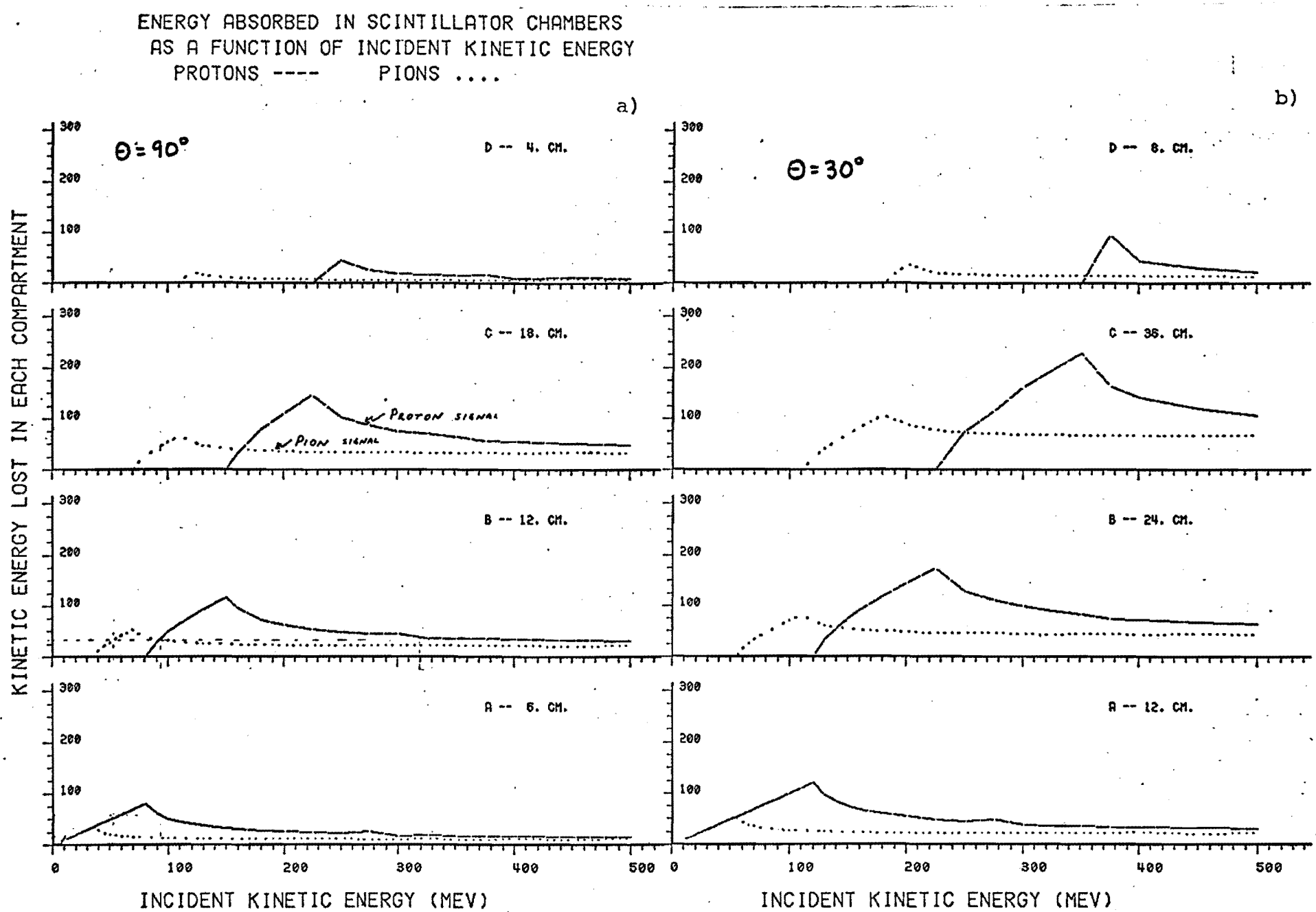
ENERGY ABSORBED IN SCINTILLATOR CHAMBERS
AS A FUNCTION OF INCIDENT KINETIC ENERGY
PROTONS ---- PIONS ....
a)
b)
Θ=90°
Θ=30°
D -- 4. CM.
C -- 18. CM.
B -- 12. CM.
A -- 6. CM.
D -- 8. CM.
C -- 36. CM.
B -- 24. CM.
A -- 12. CM.
PROTON SIGNAL
PION SIGNAL
KINETIC ENERGY LOST IN EACH COMPARTMENT
INCIDENT KINETIC ENERGY (MEV)
INCIDENT KINETIC ENERGY (MEV)
0
100
200
300
400
500

Figure 7

The exact energy range over which this particle identification is useful will depend upon the precise energy loss dependence and the resolution of the energy measurement in each compartment. If no special mapping or correction calculations are required, it may be possible to have this information on-line. Otherwise it will be available off-line, after the resolution has been fine tuned.

III. Design Considerations for the Forward Spectrometer System

A. Acceptance

High mass states tend to decay into a high multiplicity of particles. In order to be able to reconstruct the masses and decays of these states it is essential to have very good single particle acceptance. For experiments involving electromagnetic production of η_c or heavy leptons, cross sections are extremely low and one cannot afford to lose any acceptance. Nature has apparently been more generous with charm photoproduction cross sections, but not so generous as to allow experiments that skimp on acceptance. For these reasons we have studied carefully the acceptance requirements and have designed the spectrometer to meet these requirements.

A first guide to the acceptance requirements for the forward detector comes from Lorentz transforming to the lab the x dependence of e^+e^- colliding beam data at 4 GeV as measured in the SPEAR magnetic detector.[2] Table III shows the results of integrating these distributions. The Table

Table III

Typical Angular Acceptance Requirements
for Multi Hadron Final States

(Lorentz transformed from SPEAR inclusive data.)

$M_x = 4$ $n_{ch} \simeq 4$ $n = 6$

k GeV	p_{GeV}	Angles that include 95%, 98% and 99% of secondaries θ(95%) rad	θ(98%) rad	θ(99%) rad
100	1	.262	.300	.326
	5	.110	.127	.139
	10	.076	.088	.096
	15	.062	.072	.079
	20	.054	.062	.068
	30	.045	.053	.058
	40	.040	.046	.051
75	1	.300	.345	.377
	5	.126	.145	.160
	10	.088	.101	.111
	15	.072	.083	.091
	20	.064	.074	.080
	30	.053	.062	.067
	40	.047	.054	.059

gives angles that include 95%, 98% and 99% of all secondaries above a given momentum. From these numbers we see that magnet acceptance of ± 120 mrad will include almost all secondaries down to 5 GeV and most of those below 5 GeV. Above 10-15 GeV only about ± 75 mrad is required. The two magnet system matches these requirements by providing more bending power at smaller angles for the higher momentum particles and large acceptance at low momentum. A more graphic approach which also demonstrates the reason for a two magnet system is shown in Fig. 8. Here, as an example, the solid curve shows the dependence of angle on momentum for a pair of 500 MeV particles decaying from a 3 GeV state produced at 100 GeV. These in turn decay into a pair of 140 MeV particles for which θ and p are allowed to fall within the dashed curves. The spectrometer acceptance is roughly shown on the figure. For this particular case $\theta_{max} \simeq 170$ mrad. As another example, the cascade

$$(M = 4.4) \rightarrow (M = 1.85) + (M = 1.85)$$
$$\hookrightarrow (M = .5) + (M = .5)$$
$$\hookrightarrow (M = .139) + (M = .139)$$

has $\theta_{max} \simeq 150$ mrad and will also have good acceptance. For M = 6 GeV instead of M = 4.4 the same cascade will have $\theta_{max} \simeq 300$ mrad indicating a beginning of the fall-off in acceptance at 6 GeV for k = 100 GeV.

Considerations like those outlined above have been used as a guide in designing the acceptance of the spectrometer.

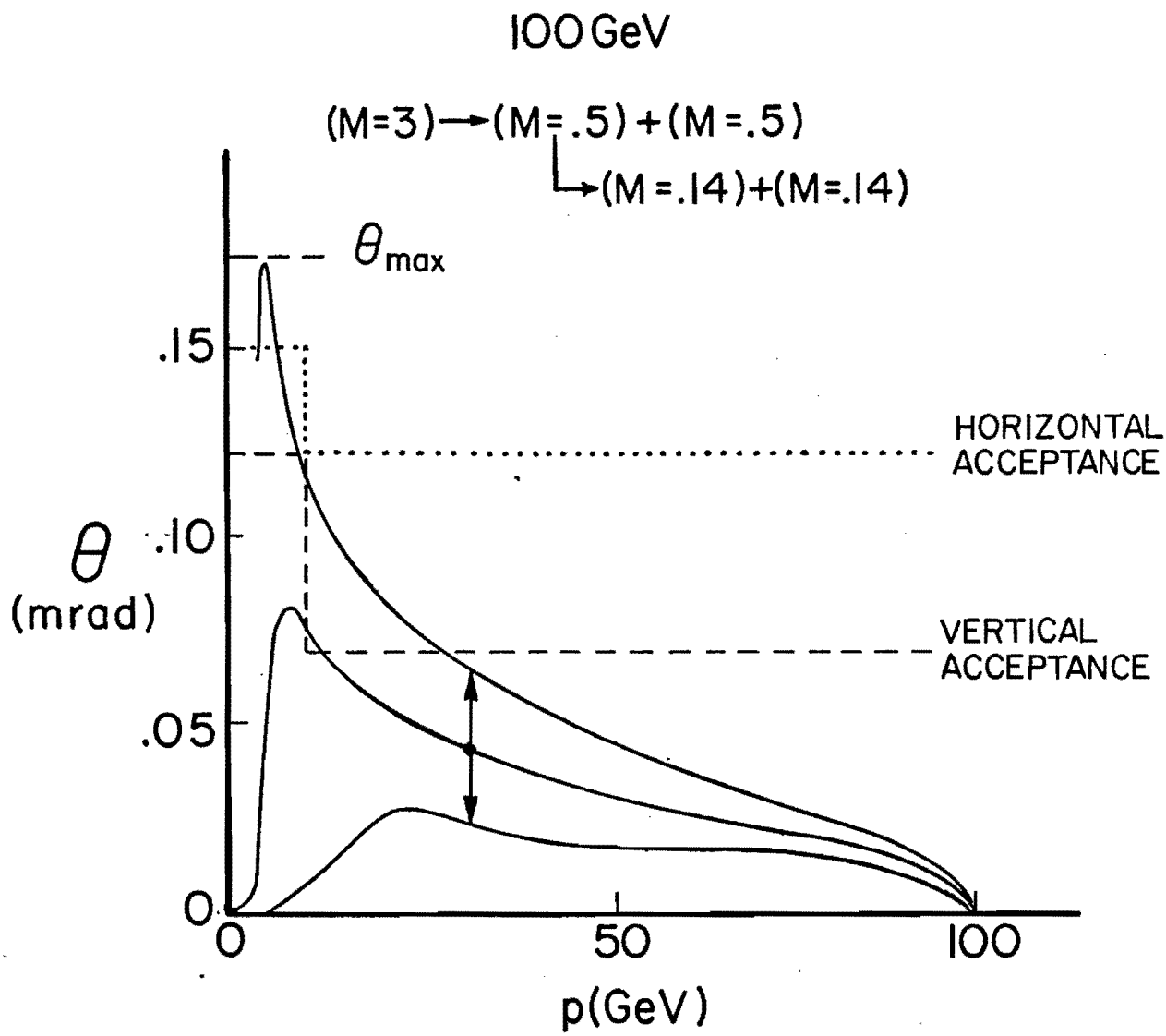
100 GeV
(M=3)→(M=.5)+(M=.5)
→(M=.14)+(M=.14)
θmax
.15
.10
.05
0
θ
(mrad)
HORIZONTAL
ACCEPTANCE
VERTICAL
ACCEPTANCE
0
50
100
p(GeV)

Figure 8

We have also checked the acceptance of the design in detail using a Monte Carlo program. Several different production models were used including

1) Assuming the photon to be excited to a 4 GeV intermediate state and then decaying with the characteristic multiplicity and spectrum measured in e^+e^- interactions at SPEAR as described above.
2) Assuming the photon to be a hadron, interacting with a proton, and producing hadrons with the characteristic spectrum measured in πp and pp interactions:

$$\frac{d\sigma}{dP_\perp dX} = P_\perp \, e^{-6P_\perp} \, (1 - x)^4$$

3) Assuming the photon is diffractively excited into a $D\bar{D}$ state with each charm particle decaying into a $K\pi\pi$ final state.

As can be seen from Table IV, the results are similar for the different models with the acceptance falling below 98% of secondaries only for pairs of particles with masses over 6 GeV.

B. Resolution

Given realistic limitations on drift chamber resolution and magnet power consumption, there is a tradeoff between mass resolution (derived from angle and momentum resolution) and acceptance. From the standpoint of charm spectroscopy one can get an idea of mass resolution requirements by noting that theoretical predictions[3] for meson and baryon states of

Table IV

Monte Carlo Calculation of Spectrometer Acceptance

Model (see text)	n_{ch}	K (GeV)	Mass (GeV)	Acceptance Per Particle	Acceptance Per Event
1. Lorentz transformed SPEAR e^+e^- data	~4	75	4	.988	.95
		100		.998	.99
		140		.999	.997
2. Hadronic	6	75	-	.995	.97
	7	100		.999	.992
	7	140		.999	.999
3. Charm Pair	6	75	4 (2+2)	.984	.90
			5 (2½+2½)	.96	.80
			6 (3+3)	.93	.73
			7 (3½+3½)	.91	.57
	6	100	4	.995	.964
			5	.984	.90
			6	.97	.83
			7	.95	.73
			9	.90	.52
	6	140	4	.999	.994
			5	.995	.97
			6	.982	.93
			7	.975	.865

2-3 GeV suggest level spacing of 40-90 MeV and higher. Widths are either extremely narrow (low lying mesons) or when cascades are involved (baryons) widths are expected to be at least 30 MeV and usually over 100 MeV.[4] Taking into consideration these numbers and the good signal to noise we expect for these channels we feel that it will be appropriate to start with $\delta M \lesssim$ 25-50 MeV and maximum acceptance. If at some point it becomes desirable to improve resolution (at higher mass, for example) to study a particular channel at a cost of reduced acceptance, it will be a straightforward matter to increase magnet current or to stretch out the spectrometer. There is plenty of space at the back of the experiment in the Tagged Photon Lab.

The mass resolution for an n particle system with mass M is

$$\frac{\delta M}{M} = \frac{1}{M^2} \quad \Sigma\Sigma^{\text{Quadrature}} \frac{1}{2} P_i P_j \theta_{ij}^{\ 2} \left[\left(\frac{\delta P_j}{P_j}\right)^2 + \left(\frac{\delta \theta_{ij}}{\theta_{ij}}\right)^2 \right]^{1/2}$$

$$\approx \left[\left(\frac{\delta P_j}{P_j}\right)^2 + \left(\frac{\delta \theta_{ij}}{\theta_{ij}}\right)^2 \right]^{1/2}$$

in the approximation that each $\frac{1}{2}P_i P_j \theta_{ij}^2 = \langle \frac{1}{2} P_i P_j \theta_{ij}^2 \rangle = \frac{M^2}{n(n-1)}$. Since $\langle \theta_{ij} \rangle \approx \sqrt{2}\,\frac{M}{k}$ and $\delta\theta_i \approx \frac{1}{\sqrt{2}}\,\delta\theta_{ij}$

$$\frac{\delta M}{M} \approx \left[\left(\frac{\delta P_i}{P_j}\right)^2 + \left(\frac{k}{M} \ \frac{\delta \theta_i}{\theta_i}\right)^2 \right]^{1/2}$$

where k is the photon energy. Generally it is easy to have $\delta\theta$ make a smaller contribution to δM than does δP. It is clear then that the requirement on δP is $\frac{\delta P}{P} \lesssim \frac{\delta M}{M}$. So for 25 MeV resolution at 2 GeV, $\frac{\delta\theta}{\theta}$ and $\frac{\delta P}{P}$ should be $\lesssim$ 1% for average momenta. It may be noted in Table VI which will be discussed later that the ~1% requirement has been met for charged particles in this spectrometer. For photons detected by the SLIC, one will not be able to reach the 1% level particularly at low energies since at best, $\frac{\delta E}{E} \simeq \frac{8}{\sqrt{E}} \simeq 1.7\%$ at 22 GeV. Thus, final states with π^0's will have somewhat worse mass resolution. Table V gives examples of δM for a variety of conditions. The resolutions in the Table are given for the case where there is either a recoil particle or one can project several forward particles to a vertex and substantially improve δP, $\delta\theta$ and therefore δM. When no vertex is available δM is a factor of 1.5 to 2 times worse.

C. Particle Identification and the Overall Length of the Spectrometer

The length of the forward spectrometer is primarily determined by the need to measure the momenta and identify the masses of the secondaries. For momenta of interest the only known technique for mass identification is to use gas Cerenkov counters in conjunction with the magnetic spectrometer. Ideally we would like full particle (π,K,p) identification from the lowest energies to the highest. Below about 5.5 GeV it is impossible at the present time to do this without using gas pressures over 1 atmosphere. In photoproduction experiments

Table V

Monte Carlo Calculation of Forward Mass Resolution

Model (see text)	n_{ch}	K (GeV)	Mass (GeV)	$\frac{\delta M}{M}$ $\times 10^{-4}$	δM (MeV)
1. Lorentz transformed SPEAR e^+e^- data	~4	75	4	50	20 (34)*
		100		59	24 (39)*
		140		71	28 (47)*
2. Hadronic	6	75	-	56	-
	7	100		64	-
	7	140		80	-
3. Charm Pair	6	75	4 (2+2)	46	9 + 9
			5 (2½+2½)	46	12 + 12
			6 (3+3)	46	14 + 14
			7 (3½+3½)	45	16 + 16
	6	100	4 (2+2)	52	10 + 10
			5 (2½+2½)	52	13 + 13
			6 (3+3)	52	16 + 16
			7 (3½+3½)	52	18 + 18
			9 (4½+4½)	50	23 + 23
	6	140	4 (2+2)	67	13 + 13
			5 (2½+2½)	66	17 + 17
			6 (3+3)	65	20 + 20
			7 (3½+3½)	64	22 + 22

*Examples of resolution for states of 60% charged, 40% neutral are given in parenthesis. This fraction of neutrals causes ~ 70% increase in δM.

it is necessary to keep material in the path of the beam at a minimum. This prohibits use of a pressure vessel. To achieve full π, K, p separation above 5.5 GeV would require three Cerenkov counters. In order to keep the overall spectrometer length under control we have limited to two Cerenkov counters so that K,p separation is in effect only above ~20 GeV.

The number of photoelectrons/cm $\simeq \alpha \sin^2\theta_c$ where α is, in practice, a figure of merit including phototube, window, reflection and gas effects. As described later, α may be as high as 170 for the counters, not including reflections. Since this assumes ideal conditions we have chosen the lengths assuming a more conservative $\alpha = 120$ and have required at least 12 photoelectrons for an ultra-relativisitic particle. The resulting lengths are 3.25 meters and 7 meters for C1 and C2, respectively. This design yields sufficient numbers of photoelectrons that it may be possible to differentiate particles near threshold from those having higher momenta. The counters will be built in a modular fashion so that the lengths may be extended for higher energy (low index of refraction gasses) or shortened if the designed lengths prove to be more conservative than necessary.

D. Spectrometer Layout

The last three subsections of this report have described the requirements that acceptance, resolution and particle identification make on the spectrometer. One of the strongest

motivations for the two magnet design comes from the typical secondary particle distribution shown in Fig. 8. Low momentum secondaries, tending to come out at large angles, require a large acceptance. This forces the location of the first magnet to be as close to the target and recoil system as possible. It also requires that the length of this first magnet be kept as short as possible in order to keep the vertical acceptance high without opening the magnet gap prohibitively wide. The second magnet adds the additional bending power necessary to get good momentum resolution for higher momentum particles that do not require as much acceptance. The position of the second magnet is chosen to optimize the momentum resolution of high momentum tracks without compromising their acceptance. Low momentum particles need not be detected following the full magnetic bend required for the high momentum particles. As a result, detector sizes are reduced in the two magnet design. In addition the two magnet approach lowers power consumption and makes it possible to install the first drift chamber (D1) in the fringe field of the first magnet, thereby protecting it from the problem causing low energy electron soup that spills out of the target.

The first Cerenkov counter (C1) is located as far upstream as possible so it will accept particles down to 5 GeV. Since there is not enough room for C1 between the magnets, it is located in and following M2. Sufficient space is left

for reflectors and phototubes between the end of M2 and the end of C1. The upstream part of C1 protudes through M2 to meet the length requirement outlined earlier. C2 immediately follows a small gap for drift chambers after C1.

Drift chambers are used to measure track positions because their good resolution allows the use of relatively low magnet bending power. This in turn permits us to use the large acceptance magnets we require without making unreasonable electrical power demands. As will be discussed in a separate section below, the drift chamber locations are motivated primarily by requirements on tracking multiparticle states.

With the magnet and chamber location of this design (Table I) the momentum resolution requirements described earlier can be met with bends of +5kG-m in each magnet. Table VI lists $\frac{\delta P}{P^2}$ and $\delta\theta$ for this and several other magnet conditions. The calculations of resolution assume δx = .0015 m except for D5, the largest chamber, where δx = .0003 m. Table V gives estimates of the forward mass resolution for various final state masses, energies and multiplicities. Both magnets are assumed to have a bend of +5kG-m and the resolution for photons is assumed to be $\delta E = \pm \frac{8}{\sqrt{E}}$ %, $\delta x \simeq .5$ cm ($\delta\theta \simeq .3$ mrad) as discussed in the later section on the SLIC. Shown in Table VI are resolutions both for the case where no vertex information is available and for the case where there is at least one other high momentum charged track so that a vertex fit can be made. The latter

Table VI

Momentum and Angular Resolution for Charged Tracks

Magnet Settings (kG-m) M1	M2	$\frac{\delta P}{P^2}$ ($\times 10^{-4}$ GeV^{-1}) Hi P	Lo P	$\delta\theta_x$ (mrad) Hi P	LoP	$\delta\theta_y$ (mrad) Hi P	Lo P
		No vertex used in Fit					
5	5	2.8	20.8	.064	.26	.059	.21
	-5	3.7		.024			
	+10	1.5		.048			
		Vertex used in Fit					
5	5	2.2	8.6	.051	.098	.046	.10
	-5	3.7		.024			
	+10	1.3		.041			

has significantly improved resolution.

As can be seen from Table VI, there is a good deal of flexibility in the choice of magnet conditions. In particular, one can choose between operating the magnets at the same or opposite polarities. Magnets at the same polarity give better momentum resolution. When the magnets are set at opposite polarity, trajectories following the second magnet preserve the original production angle. This reduces ray crossing in the Cerenkov counters and the resulting confusion (see below). It also means that for a fixed hadrometer size the acceptance is larger. Another option is to run M2 at 10 kG-m for improved resolution at a cost of a factor 2½ more power and a loss of some acceptance particularly in the hadrometer. This will be a useful option when experiments require the ultimate in mass resolution. The magnet setting options demonstrate the flexibility of this facility.

E. Magnet Requirements

In order to be specific in this design report, we have assumed except in this subsection, that SCM105 magnets will be used for M1 and M2. In Table VII we outline the minimum dimensional and field requirements for magnets in this spectrometer. These specifications will be used in selecting the magnets to be built or obtained for actual use in the facility. The specifications follow from the resolution and acceptance requirements described in the previous sections

Table VII

Magnet Requirements

	M1	M2
Bending Power	$\gtrsim$ 12 kG-m	$\gtrsim$ 12 kG-m
Gap - vertical	$\geq$ 30"	$\gtrsim$ 30"
Gap - length (including coils)	$\leq$ 48"	$\lesssim$ 60"
Gap - width	$\geq$ 40" (good field)	$\geq$ 75" (aperture) $\gtrsim$ 40" (good field)

and do not require further explanation except for the following points. The bending power requirement is ~ 12 kG-m per magnet in order to accommodate higher energy experiments although we anticipate needing only 5 kG-m bends at first. The maximum gap length of M1 is determined by the vertical acceptance requirement. Thus, if the gap height is > 30", the length could be correspondingly > 48". Finally, the large horizontal acceptance requirement for M2 allows 5 GeV particles to be detected in the first Cerenkov counter. If new magnets are fabricated, the field should be as uniform as reasonable cost will allow. This would premit possible simple on-line track reconstruction.

F. Track Reconstruction Considerations and Location of Drift Chambers

The location and orientation of the drift chambers must meet certain goals and at the same time satisfy a number of constraints. First, let us consider some of the constraints.

In order to take advantage of the large solid angle provided by the two magnet system, it is necessary that the liquid hydrogen target be placed immediately upstream of the first magnet. Therefore, little or no field free region is available in which to place a drift chamber. At the same time, it is necessary to shield the first set of chambers from the large number of highly ionizing low energy charged particles produced in the target. These chambers must therefore be placed in the magnetic field of the first magnet. On the other hand, the best momentum resolution is obtained

by placing the chambers as far upstream as possible. The position of this set of chambers must, as a result, be a compromise between chamber HV, current, magnetic field uniformity, and momentum resolution. They will be located far enough into the gap of the first magnet so that a charged particle will have to traverse .25 kG-m before the first chamber. Hence, no particle with $p \lesssim 5$ MeV will penetrate to the chambers.

An additional constraint is imposed by the Cerenkov counters. Particle identification requires that most of the available drift space behind the second magnet be dedicated to Cerenkov counters. Only a short distance along the beam between C1 and C2 may be occupied.

It must be possible to make a complete measurement, including momentum determination, on low momentum tracks before the second magnet. To this end we place a second set of chambers at the middle of M1. A third set is located in the drift space between M1 and M2. In order to complete the measurement with good resolution for high momentum tracks, two sets of chambers are added after M2. The first is placed between C1 and C2; the second follows C2. We have thus arrived at a system containing five sets of chambers as indicated in Fig. 1.

When specifying the number of planes and their wire orientation in each set, it is necessary to keep in mind that the system must have good multitrack capability and must therefore have a high level of redundancy. Track coordinates

must be measured more often than geometry or resolution would require with the understanding that background tracks and coordinate degeneracies will cause the loss of some measurements. In addition, the left-right ambiguity inherent in drift chambers must be resolved. Finally, the chamber locations and wire orientations must be chosen so as to minimize computing time. This is especially pertinent to the track matching problem from one chamber module to another when it is necessary to trace rays through inhomogeneous magnetic fields.

In order to achieve the goals outlined above we have adopted the philosophy that each chamber module should simultaneously measure position as well as angles while at the same time resolving multitrack and left-right ambiguities. This philosophy allows tracking each module independently and reduces the overall spectrometer tracking problem to that of matching track segments between modules. This approach will minimize computing time and the problems of track matching in a multitrack event.

We consider now the question of left-right ambiguity resolution. For a multitrack spectrometer the best way to solve this problem is to stagger successive chambers by one-half cell. Good multitrack efficiency requires that many chambers be placed along the track to achieve a high level of redundancy. In addition the measurement of angle at each drift chamber location requires extra chambers. These three requirements are compatible and can be met by

the same set of planes. In the simplest case, that of straight tracks at normal incidence, only two chambers offset by one-half cell are required for left-right ambiguity resolution. However, when large angles of incidence are encountered, at least three chambers (four in a magnetic field) are required to establish the correct solution. Outside the magnets there will therefore be three chambers with each wire orientation in each module. These three chambers are spaced along z sufficiently far so that the angle is also determined at each module.

The chambers in the first magnet must deal with circular tracks in the horizontal plane. For tracking purposes, these circles must be over-determined. Since any three points determine a circle, we must therefore have at least four chambers with each wire orientation. It is then possible in a single view to uniquely assign hits to tracks. We consider all the chambers in M1 (D1 and D2) as a single set of chambers which are tracked together. D1 will have one chamber at each wire orientation and D2 will have three at each orientation.

There are several considerations in choosing wire orientations: 1) It must be possible to build reliable chambers. For this reason we have decided not to build chambers with horizontal wires (Y readout) which would be excessively long. The longest sense wire is therefore 2.25 m at D5 and only 1.12 m elsewhere. 2) The tracking algorithm

should be relatively simple and the chambers should allow some flexibility in choosing the tracking philosophy.

3) Wire orientation should optimize those position measurements that most affect mass resolution.

These requirements taken together lead us to three wire orientations which provide small angle stereo in the bend plane. These are vertical wires (x coordinate), wires rotated clockwise about the beam by 14.04° (u), and wires rotated counter-clockwise by 14.04° (v). The small angle stereo gives the best possible determination of the angle in the bend plane. The projected resolution in the non-bend plane is worse by only a factor of ~ 4. The measurement of θ_y is still sufficiently good so that momentum resolution dominates the mass resolution.

D2 and D3 therefore have three x chambers, three u chambers and three v chambers. D1 and D2 together have four chambers at each orientation as discussed above. D5 is used for additional tracking information in the bend plane and to improve momentum resolution. Multitrack ambiguities and the measurement of θ_y can be resolved with D4 so that u and v chambers are not necessary. Therefore at D5 there are two x planes and no u or v chambers.

G. Cell Sizes

When there is more than one track in a given cell or strip of the drift chambers, Cerenkov counters or SLIC, there will be some confusion in reconstructing the event. Simply

adding more cells to deal with this problem can be a very expensive matter. In order to be able to optimize cell locations and make efficient decisions on the total number of cells required per detector, we have studied predictions of particle distributions in these detectors. Two techniques were used. The $\frac{dN}{d\cos\theta\ dp}$ distribution obtained by Lorentz transforming SPEAR x dependence data at 4 GeV was used to calculate the cell sizes at different locations in each detector that correspond to a given probability (f) per event that more than one track goes into any cell. As a cross check, a Monte Carlo program was run for the three different production models described earlier. There was agreement between all calculations in direct comparisons. The Monte Carlo was used mainly to study distributions and cell boundary effects in the Cerenkov counters.

For the drift chambers we have chosen cell sizes that correspond to $f \lesssim 10\%$ except within 1" of the beam in D1 and D2 where $f \simeq 20\%$. This means that no more than 10% of events will have some confusion in each bank of drift chambers. This will result in a total of $\lesssim 2000$ wires which is a financially reasonable number. The confusion for two tracks in a drift cell of a single plane results from the fact that only the track nearest the sense wire will register the proper location. However, in the forward direction one can use information from the offset twin to the drift plane to resolve this problem and determine the position of the

second track. In such cases one loses the fast timing information for the particular cell that can normally be obtained by summing the times from the offset planes ($t_L + t_R$). The cell size calculations indicate, as one would expect, that cell sizes can be larger further away from the beam. We have chosen four standard cell sizes (6 mm, 1.8, 4.8, 10 cm). The distribution of these cell sizes for each chamber location is listed in Table VIII.

The SLIC is located so far from the target that confusion is not a serious problem. Cell sizes of 1.25" (3.18 cm) near the beam and 2.5" further out (as shown in Fig. 22, Sec. VIII C) will result in $f \lesssim 1\%$ everywhere. The smaller cells near the beam are motivated by the need for better θ resolution for small angles. As will be described later, the shower distribution in neighboring cells is normally used to obtain position resolution far more precise than the cell size. The maximum cell size is chosen so that it will not contain a whole shower. Otherwise, there would not be shower sharing information available to get good position resolution. Confusion results when there are two tracks in a cell because it then becomes impossible to determine more than the precise location of the energy weighted average of the two tracks. The photon pair from π^o decay will go into different cells and not be confused. Even at an energy as high as 60 GeV the γ opening angle ($\theta > 2\frac{m_\pi}{E}$) leads to a separation of $\gtrsim 9$ cm.

Table VIII

Module	Dimensions Hor.	Vert.	Coordinate	No. Planes	No. Wires Per Plane	Distribution 6mm	1.8cm	4.8cm	10cm	Total Wires Per Module
D1	70.8 x	56cm^2	X	1	42	24	10	8	-	126
			U	1	42	24	10	8	-	
			V	1	42	24	10	8	-	
D2	90 x	65cm^2	X	3	46	24	10	12	-	414
			U	3	46	24	10	12	-	
			V	3	46	24	10	12	-	
D3	177.2 x	120cm^2	X	3	76	30	14	28	-	672
			U	3	76	30	14	28	-	
			V	3	76	30	14	28	-	
D4	229.2 x	125cm^2	X	3	64	-	26	38	-	576
			U	3	64	-	26	38	-	
			V	3	64	-	26	38	-	
D5	420 x	250cm^2	X	2	42	-	-	-	42	84
				32						1,872

The size of the Cerenkov light cone is an approximate lower limit on the size of Cerenkov counter cells in the central region. For this reason (as well as considerations of cost) the Cerenkov counters cannot have quite the small cell sizes of the SLIC or drift chambers. On the other hand only a fraction of charged tracks give Cerenkov signals. Furthermore, the Cerenkov cells are rectangular rather than strips. As a result, the fraction of confused events is comparable to the other detectors.

The two Cerenkov counters will each have 20 mirrors. The size of these mirrors increases with distance from the beam so that each mirror has approximately the same probability (1/20) of being hit by a secondary particle. With this design the probability of an event having two hits in the same mirror is

$$f = \sum_{i=1}^{n-1} i/20 = \frac{(n)(n-1)}{40} ,$$

where n is the number of particles which are fast enough to give Cerenkov light. For the processes simulated in our Monte Carlo studies we find $n \simeq 2-4$, so $f \simeq 0.05 - 0.30$.

A particle which is directed to one mirror may give Cerenkov light which hits another mirror. This "cross-talk" increases f, but only slightly. (See later discussion in this section.)

The particular arrangement of Cerenkov counters and magnets shown in Fig. 1 has been analyzed with a Monte Carlo

program using various particle production models which were described in subsection A. The results for the various models are similar to each other. Here we discuss in detail results from only the model which assumes a 100-GeV γ ray is diffractively excited into a $(c\bar{c})$ state. Each charmed particle decays into $K\pi\pi$ yielding a multiplicity of 6 charged particles. In Fig. 9 we present the average multiplicity (where the generated multiplicity is 6 particles) of particles that give Cerenkov light. On the average 1 of the 2 kaons and 3 of the 4 pions triggers C1 while 2.5 of the 4 pions and hardly any of the kaons triggers C2. This allows for a very clean separation of pions and kaons.

In Fig. 10 and 11 we show the x-y distribution of the particles that are above threshold for Cerenkov light for two Monte Carlo models. Superimposed are the dimensions of the individual mirrors of the Cerenkov counters C_1 and C_2.

The sizes of the individual mirrors are chosen so that the probability of any one mirror being penetrated by a particle above threshold is approximately 1/20. Thus the mirrors closest to the beam are the smallest. With the indicated mirror segmentation, the correct particle identification can be made in 90% of the events. In the remaining 10%, light from a pion going to or near a Cerenkov cell in which there is a kaon leads to the kaon being misidentified.

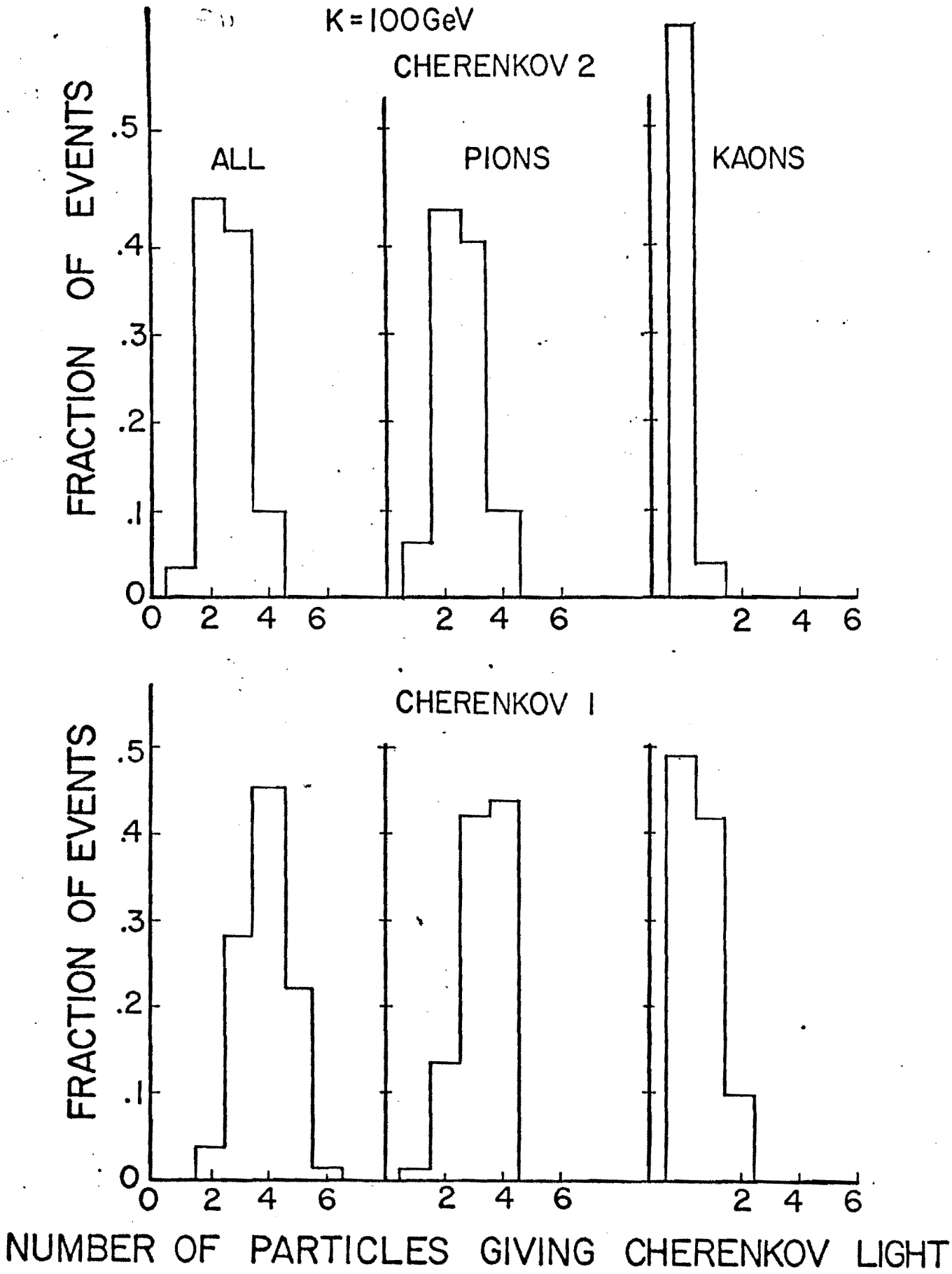
K = 100GeV
CHERENKOV 2
ALL
PIONS
KAONS
FRACTION OF EVENTS
.5
.4
.3
.2
.1
0
0 2 4 6
2 4 6
2 4 6
CHERENKOV I
FRACTION OF EVENTS
.5
.4
.3
.2
.1
0
0 2 4 6
2 4 6
2 4 6
NUMBER OF PARTICLES GIVING CHERENKOV LIGHT

Figure 9

Fig. 10

C_1 Mirror Segmentation and Monte Carlo x-y Distribution

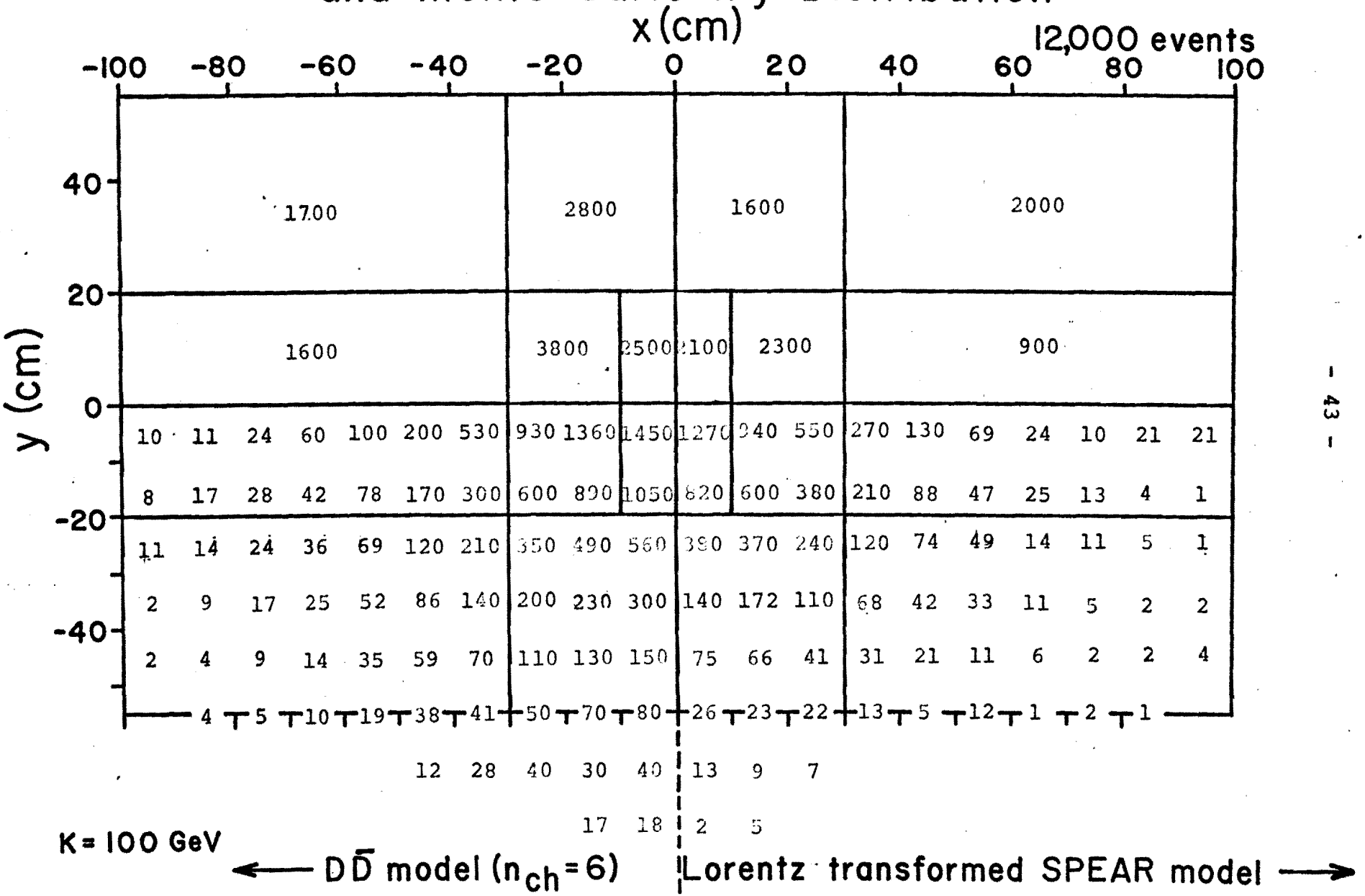

Fig. 11

C_2 Mirror Segmentation and Monte Carlo x-y Distribution

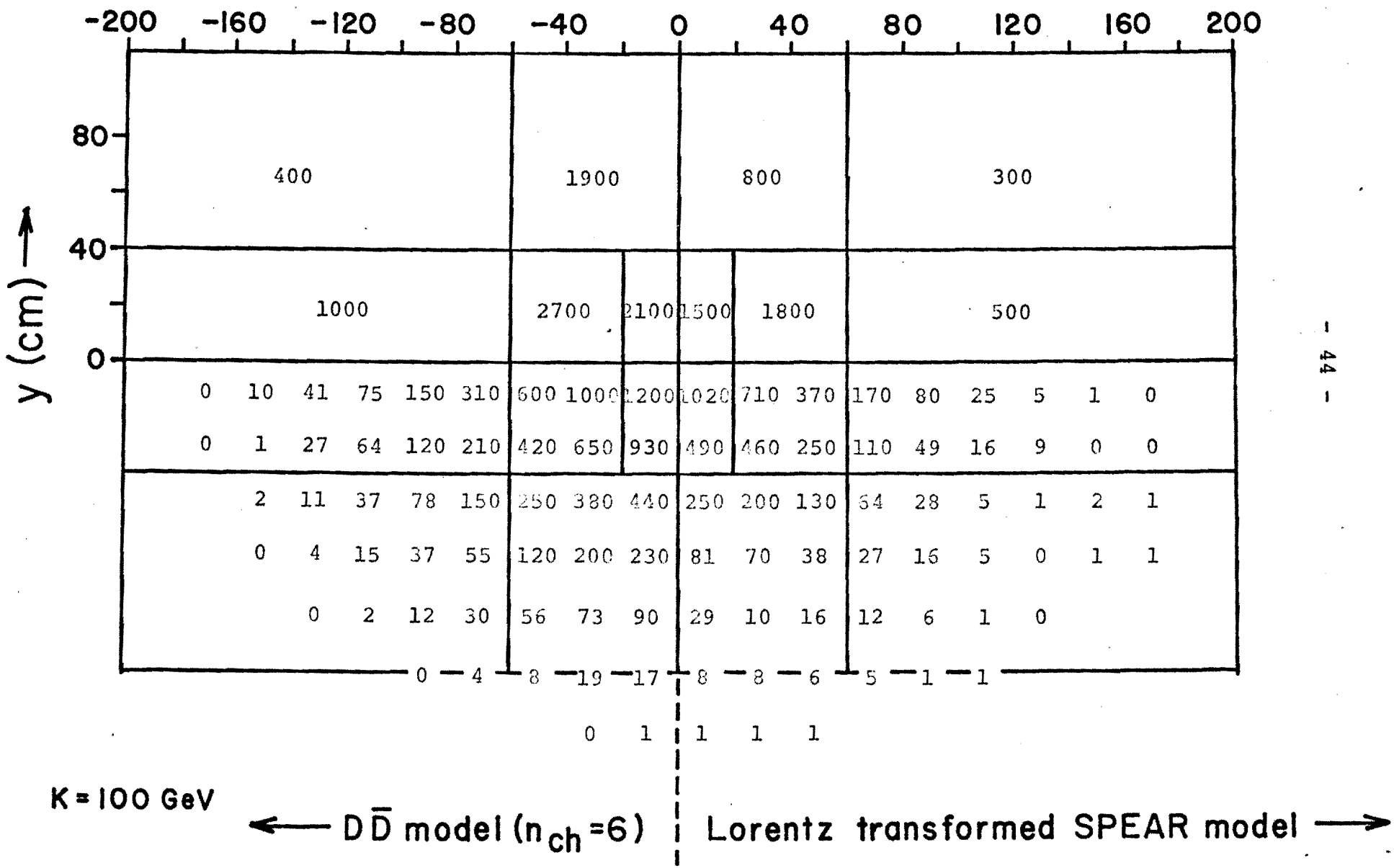

IV. Triggers

Triggering of photoproduction experiments can be done in a two step process that allows very sophisticated selection. A fast trigger using conventional logic will trigger on every hadronic interaction and reject pair production. At the highest luminosities being considered in this report the rate of hadronic triggers will be ~ 6000/sec. That means that an average processing time as long as about 10 μsec can be used to define a higher level sophisticated trigger without causing deadtime greater than 6%. Several higher level triggers will be described below. They will be used initially to reduce the data taking rate from a few thousand/second events containing all of photoproduction to 100-200 events. The reduced data sample will be significantly enriched with charm and hidden charm particles. This will mean that off-line computer analysis will be simplified, thereby reducing computer time and, most important, reducing the delay between data taking and preliminary analysis results. The latter, we feel, is crucial to being able to run experiments on this facility with the flexibility and feedback of a small experiment. It is this kind of closeness to the physics that is required to make this a powerful facility. A two step trigger can also be used for experiments with a hadron beam by defining a simple ~ 5K/sec fast trigger and using a trigger processor like that discussed below to define a selective higher level trigger.

A. Fast Trigger

The fast trigger is a coincidence of a "Tag" signal

from the tagging system and a signal indicating the presence of a hadronic event in the spectrometer. A hadronic event is identified by requiring a signal above threshold in either the SLIC or hadrometer and no large signal in the pair portion of the SLIC (horizontal strips in the beam plane) or in the central shower counter (C) in the beam. To increase the acceptance for this trigger (and for all γ measurements) in the vertical direction, two lead scintillator shower counters, above and below the beam, will be located just in front of the downstream magnet. A large signal or a coincidence indicating a minimum ionizing particle in these counters would also give a hadronic trigger.

B. High Level Triggers

As will be seen from the discussion in the next section on the trigger processor, the potential capability of processors based on available electronic technology is extremely powerful. However, we feel it necessary to be cautious at implementing this technology so that we can be sure that the total facility system will turn on in an organized fashion as early as summer 1978. To this end we have given clearly defined priorities - an order of attack - to the high level triggers we plan. The recoil system will be used in the first high level triggers. We will select out events with a single proton recoil and then compute the missing mass, triggering when the mass is in a prespecified range. A first look at a detailed processor algorithm to accomplish

this is outlined in the next section. For example, the mass range $2.5 < M_x < 9$ GeV could be selected by the processor. We can make an estimate of what fraction of the total cross section this trigger will be by comparing the relevant photoproduction channels with those measured in the $pp \rightarrow pX$ inclusive scattering experiment of P. and J. Franzini et al.[5] The fraction of events with a single recoil proton will be about .35. Of these about .37 will fall in the mass range selected and about .78 will have $|t| \gtrsim .04$ GeV^2. This trigger, therefore, will take about 10% of all hadronic events. Similar estimates suggest that charm states will appear in as many as 20% of the triggered events.

Pair production of charmed particles will lead to multiparticle final states. The combination of the fast hadronic trigger plus the recoil proton missing mass processor yields a reasonably unbiased trigger for enriching pair production of charmed particles. However, at the highest luminosities to be expected after the spectrometer has been brought into routine operation, the trigger rate will be several times higher than the high data handling capability of this facility. Thus, after exploratory studies using the recoil trigger have been made, additional higher level triggers must be implemented. These will probably be biased towards some aspect of charmed particle production, which is expected either on theoretical grounds, or empirically determined from the exploratory runs or from other

experimental results then available. In the following, we outline considerations on various high level triggers that involve the various forward detectors.

The purely two body decay modes of charmed states will generally be small. Therefore, a high multiplicity of charged and neutral particles is expected. However, the average multiplicity of 100 GeV/c hadronic photon interactions is also large, around six. Thus, multiplicity selection will only be useful in special cases such as for the η_c discussed below. Charmed particle decays will, it is believed, often lead to a final state involving strange particles, such as $K\pm$, K_S^o, K_L^o, Λ, $\bar{\Lambda}$, etc. A unique signature not yet exploited is that of a hadronic final state which does not conserve strangeness. However, the identification of the strangeness of all of the final state particles is difficult, and can be made only in some small fraction of the events. This does not lend itself, per se, to an on-line trigger, although it might be an interesting one to pursue off-line.

Pair production of charmed baryons will lead to final states involving a baryon-antibaryon pair. Any other process which leads to such a pair will also be unusual and physically interesting. Thus identification of <u>one</u> or more strange particles or of a baryon (or antibaryon) in the forward spectrometer will lead to useful, specific, although biased

triggers. These can be built into one or more trigger processors, although in some cases they may be simple enough to be easily implemented in standard fast logic.

The above considerations suggest that the following particle pattern identification should be implemented in the first high level triggers involving the forward detectors.

1. Charged particles: $K^{\pm}$ and $p^{\pm}$. Some of these are identifiable by the Cerenkov counters. A "not-a-pion" trigger in general requires some knowledge of the momentum of the particle.
2. Neutral particles, mostly K_L^o and n. These will interact in the hadrometer and be useful directly in the trigger.
3. "Vees", i.e., $K_S^o \rightarrow \pi^+\pi^-$ and Λ, $\bar{\Lambda} \rightarrow p^{\pm}\pi^{\pm}$, where the decays occur in the drift space of the spectrometer. (Neutral decays of vees will be seen in the SLIC and the hadrometer, as in 2. above.) Detection of vees on-line in the trigger can in principle be detected by a change in the multiplicity of particles, as seen in the various downstream detectors. In this spectrometer, the drift chamber modules are, of necessity, widely spaced out. The effective solid angles subtended by each module differ because of this spacing and because of the magnetic field

regions. Thus apparent multiplicity changes occur when none is present. However, with careful consideration, a useful change of multiplicity trigger may be realized. A 15-50 GeV K_S or $\Lambda(\bar{\Lambda})$ has mean decay length ranging from one to three meters. At 15 GeV, about 20 percent of such vees will decay in the region of the D1, D2, D3 modules, while at $\gtrsim$ 40 GeV some 30 percent will decay in the D3-D4 and/or D4-D5 region. Vees can also be detected off-line by reconstructing vertices which do not occur near the interaction point in the target, e.g., vertices in the drift spaces. It is unknown whether an on-line trigger processor can be realized to perform this function. Finally, although the overall acceptance of a vee trigger may be of the order of 10 percent of all K_S^o and $\Lambda(\bar{\Lambda})$, such events are extremely useful and interesting.

Although the maximum transverse momentum of the decay products from charmed particles is large, the large average multiplicity results in an average transverse momentum per particle which is not much higher than the normal hadronic value (about 0.3-0.4 GeV). However, a selective trigger based on high transverse momentum, or a large longitudinal momentum of one or more particles might be useful. The hadrometer could provide this information for both charged and neutral particles.

The above considerations lead us to specify that the

following information be available in approximately one microsecond for use by the next level of trigger-processors:

1. D_i cell bits
2. Cerenkov cell bits
3. SLIC large pulse height bits defined by discriminator thresholds (say one high, one low)
4. Hadrometer large pulse height bits.

From this information, multiplicity, change of multiplicity, particle identification, neutral kaon or neutron detection, and large transverse or longitudinal momenta can, in principle,be determined and used by a trigger processor to enhance charmed pair production.

Although hadronic decays of charmed particles dominate the decay process, leptonic final states need not be ignored. Much of the above can be used to construct leptonic triggers also, since the SLIC can detect electrons. In addition, there will be muon counters buried in iron shielding behind the hadrometer.

Primakoff production of the η_c is a very important process to be found and measured. Here the cross section is several orders of magnitude below that of charmed pairs. The highest luminosities and a more highly selective trigger will be required, although a preliminary search may well be carried out with a "no-recoil" trigger. The η_c, with $I^G J^P = 0^+0^-$ and an expected mass value near 3 GeV, will have many multiparticle decay modes. It is produced singly with all

the energy of the beam ($\gamma\gamma \rightarrow \eta_c$) and very forward, with no recoil emerging from the target. The recoil detector can be used as a veto, but no missing mass will be available.

Strict two body decays of the η_c are expected to be very small (e.g., $\gamma\gamma$, $\bar{p}p$, $\Lambda\bar{\Lambda}$..., < 1%). Decays like 2π, 2K are excluded by spin and parity. Decays like 3π, 5π... are suppressed by G parity (hadronic decays will dominate over electromagnetic ones). Numerous final states, like 4π, 6π,..., $K\bar{K}\pi$, $K\bar{K}2\pi$,...$\eta 2\pi$, $\eta' 2\pi$... are available, and all will proceed with reasonable branching ratios. Since the cross section for η_c production is so small, one must find a trigger that accepts a significant fraction of the η_c final states. Note that a large fraction of these decay modes involve two charged particles plus several gammas (from π^o decay or direct emission). Thus it will be possible to have a crude trigger for η_c based on 2 and only 2 charged particles and an energy sum of all forward particles equal to that of the incident photons. This will require the following:

1. Charged multiplicity (available from D_i cell bits provided for in the earlier discussion)
2. Energy and angle which can be obtained from the SLIC and hadrometer if fast ADC conversion of the pulse heights can be available for the hit elements in approximately one microsecond. (Whether the high and low pulse height bits,

previously described in the discussion on charmed pairs, can provide a reasonable η_c trigger will have to be studied carefully.)

Fast reconstruction of forward mass can be accomplished if item 2 listed above is available. The forward mass is:

$$M_F^2 = \sum_{ij} \frac{1}{2} P_i P_j \theta_{ij}^{\ 2}$$

$$= \sum_{ij} P_i^x P_j^x (\theta_i^x - \theta_j^x)^2 + \sum_{kl} P_k^y P_l^y (\theta_k^y - \theta_l^y)^2$$

where $P_i^x \simeq P_i^y \simeq 1/2\ P_i$ are the energy deposited by a track in the x or y strips of the hadrometer and/or SLIC. The mass resolution will be dominated by the hadrometer resolution and will be $\sim .15\ M_F$ which is adequate for triggering purposes.

For the η_c, a narrow cut, say $2 < M_F < 4$ GeV added to the charged multiplicity and p_T cuts would lead to a very good η_c trigger. In addition, relaxation of the charged multiplicity requirement might be made, further improving the acceptance of the trigger for η_c.

In addition, a tighter trigger for η_c could be made if fast TDC readout of the drift modules was available. This might allow momentum reconstruction of forward charged tracks on-line in a trigger processor. Thus good mass resolution on the forward mass would be available, resulting in a tighter cut about the η_c mass.

The possibilities that are opened up by having forward track reconstruction available for the trigger are impressive. Accurate mass and $P_\perp$ triggers that are not dependent on poor resolution hadrometers will be very important. Better Cerenkov identification using momentum will be possible. Also possible will be detection of kinks in tracks indicating Λ^o or hyperon decays that will be valuable as triggers. For simple final states, one or two bodies, it will not be difficult to perform fast reconstruction. On the other hand, reconstruction of multiparticle states will require the experience gained from off-line reconstruction work. For this reason we do not expect this type of information to be available for triggers for some time (1-2 years) after the facility starts up.

As higher energy photons become available, pair production of new heavy lepton states may become accessible. Many of the pieces of information made available above and the trigger processors (or modifications of them), will make triggers on heavy leptons possible.

V. Trigger Processor

The trigger processor will take advantage of the present day low prices for large amounts of memory with access times of 30 nsec or faster as well as fast arithmetic logic chips. It will be essentially a hard wired parallel processor possibly in association with a fast sequential instruction processor like that designed by T. Droege for Fermilab Experiment 400.

We will describe here a first look at a detailed conceptual design of this device by looking specifically at how the recoil missing mass trigger will be handled. We fully expect that this design will undergo extensive development as we continue to study and optimize it. For the present it will give some idea of the capabilities of and the techniques to be used in the final system.

In order to select single proton recoils the trigger must reject neutrals (from $n\pi^+$ or $p\pi^o$ states, for example) and charged pions (from $n\pi^+$). In addition the processor must reject events with several tracks at the first interaction ($p\pi^+\pi^-$, etc.) without rejecting good events in which a secondary interacts and produces additional recoil tracks. These excited proton states comprise about 2/3 of all hadronic events so that reasonably good rejection of them is necessary for a clean trigger. On the other hand, the rejection need not attain the levels possible in off-line analysis. Refer to Sections II and VI and Figures 3 and 4 for more detailed discription of the recoil system and its capabilities.

The processor will make frequent use of parallel table lookups to evaluate functions such as the missing mass function of θ, E, and k. On a smaller scale this approach was used previously in Experiment 321 by P. Franzini who suggested it to us. Table IX shows the organization of a memory made up (as an example) of 128 Fairchild 10415A 1024 x1 bit bipolar ECL RAMs.

Table IX

Memory Organization for Table Lookup Functions

Description	Function/#Bits		Organization
Neutral Veto	$NV_i \leftarrow NV\ (A_i, B_i, C_i, D_i)$		15 - 16 x 1
	$i = 1, 15$		
	A_i, B_i, C_i, D_i	1 bit ea.	
	NV_i	1 bit	
	(N_v is same for all i)		
Unit conversion	$TZ \leftarrow Z(Z_{PWC})$		1 - 256 x 4
$Z_{PWC} \rightarrow Z_{timing}$	Z_{PWC}	8 bits	
	TZ	4 bits	
Missing Mass	$MMC \leftarrow MMC\ (\theta, E, K)$		64 - 1024 x 1
Criterion	θ, E	6 bits ea.	
	k	4 bits	
Proton Criterion,	$PC_j \leftarrow PC\ (I_j, \theta)$		16 - 1024 x 1
each scintillator	$j = 1, 4$		
segment function	I_j	8 bits	
of θ.	θ	4 bits	
	PC_j	1 bit	
	(PC is different for each j)		
Proton criterion	$PCS \leftarrow PCS\ (PC_j, E, \theta)$		4 - 1024 x 1
selection as	$j = 1, 4$		
function of energy	PC_j	1 bit ea.	
and θ.	E	6 bits	
	θ	4 bits	
Total	84 - 1024 x 1		84 - 1024 x 1
	15 - 16 x 1	or	15 - 1024 x 1
	1 - 256 x 4		4 - 1024 x 1
			103 - 1024 x 1
		Spare	25 - 1024 x 1
		Total	128 - 1024 x 1

Each of these chips has a 20 nsec access time. The total cost of this memory (as of May 1, 1977) is $2330, about equal to 3 commercial coincidence modules. This memory will, in general, be used for two parameter lookup functions with the answer being a single bit. It will be possible to load the memory in a block transfer from the on-line computer and to read it back for verification and testing. This will allow flexibility in use of the trigger processor and will be essential during debugging. As can be seen from Table IX, even this relatively cheap amount of memory is not nearly filled up by the recoil missing mass trigger requirements.

We now outline an algorithm that at the very least demonstrates that this trigger can be processed easily in the 5-10 μsec that will be available. We start with two operations performed in parallel:

1. Data from the cylindrical PWC's will appear as a list of number pairs corresponding to the last wire address of a cluster and the cluster spread. These numbers will read out from upstream to downstream.
   The cluster address
   $$Z_i = (\text{Cluster})_i - (\text{Spread})_i/2$$
   is computed by dropping the lowest order spread bit and subtracting the remaining 2 bits from the cluster last wire address. At least three such subtractions will be performed in parallel. (This operation may in fact be handled by the arithmetic unit of the PWC system.)

2. Identification of neutral patterns. The scintillator dynode signals will be discriminated and a bit latched for each pulse height that is above a threshold. The bits will be organized in groups of four (A_i, B_i, C_i, D_i). These groups will be used to address 15 sections of memory, each initially containing the 16 bits shown in Table X. A 1 bit is found in memory for the A, B, C, D bit patterns that correspond to a π^o or n interaction in one of the scintillator sections. The 15 groups of ($A_iB_iC_iD_i$) address the memory in parallel and a bit (NV) is set to 1 if any group corresponds to a neutral interaction pattern. This will in most cases be used as a veto to the recoil trigger, since the missing mass only is meaningful for single proton recoils. (There will be about a 10% loss of good triggers from secondary interactions producing neutrals in the recoil system.) The patterns stored in memory will be modified from those in Table X if experience teaches us that a different set of patterns is more appropriate. The total amount of time to cycle through the 15 sectors is ~ 15 x 20 nsec ≈ 300 nsec. This veto will therefore be available ahead of the more complicated processing of tracks (described below) that will go on simultaneously. (In simpler form this operation may well be first implemented in conventional fast logic or in the matrix logic of a register logic system.)

Table X

Neutral Recoil Veto Patterns

Address				Contents of Memory
A	B	C	D	
0	0	0	0	0
1	0	0	0	0
0	1	0	0	1
1	1	0	0	0
0	0	1	0	1
1	0	1	0	1
0	1	1	0	1
1	1	1	0	0
0	0	0	1	1
1	0	0	1	1
0	1	0	1	1
1	1	0	1	1
0	0	1	1	1
1	0	1	1	1
0	1	1	1	1
1	1	1	1	0

3. As soon as the Z_i are available from operation 1, the processor will start to determine PWC track parameters. In an ideal situation of a single proton track there will be 3 Z_i with $Z_3 - Z_2 = Z_2 - Z_1$. (As described in Section VI, the concentric wires of the three PWC's at one Z location are tied together into one amplifier.) In many cases the problem will be complicated by one or more of three effects: a) secondary particle interaction that results in recoil tracks that cross the primary recoil; b) multiparticle recoils at the primary vertex ($P\pi^+\pi^-$, for example) that are in most cases to be rejected for M_x calculations; c) δ rays which may add a cluster anywhere in the inner chamber. To deal with this the processor will be wired to perform a three-nested do loop which we describe below in fractured Fortran. In this, L is the number of clusters and is read in from the PWC electronics. The δ's are parameters which may be varied from the on-line computer.

```
DO  1  I = 1, L-2
DO  1  J = I+1, L-1
θA = Z(J) - Z(I)
DO  1  K = J+1, L
θB = Z(K) - Z(J)

IF (|θA - θB| > δ1) GO TO 1        (no track)
STORE I,K and increment track count N
```

V(N) = Z(I) - $\theta_A/2$ Vertex, since target to inner ring ≈ 1/2 ring to ring distance.

IF(N = 1) STORE V(1) and GO TO 1

IF(|V(N) - V(1)| > δ_2) GO TO 1

SET "more than 1 track at first vertex" bit and exit loops.

1 Continue

IF (NO TRACK). . . .

$\theta = \theta_A + \theta_B$

4. The next step is to find the A,B,C,D scintillator segments that correspond to the wire chamber track. This is done by finding a ϕ sector i with end to end timing information corresponding to a location sufficiently close to Z(K), the outer chamber coordinate. The difference between pulse times at each end of the scintillators in the inner ring (A_i) will be digitized by 15 4 bit TDC's, T(I). This measures the Z location of the track in ϕ segment i to ± ~ 6 cm. The outer chamber coordinate, Z(K), is converted to time units (TZ) by an 8 bit to 4 bit lookup. The memory will be loaded with data based on calibration studies of the end to end timing of the inner scintillator segments. Then the following search is performed:

DO 2 M = 1,15

IF (|TZ - T(M)| < δ_3) GO TO 3

2 CONTINUE

GO TO "NO MATCH"

3 STORE M

The appropriate energy is

$$E = A(M) + B(M) + C(M) + D(M)$$

The following two operations are performed simultaneously.

5. Look up E vs θ in memory (see Table IX). If the location has a 1 then M_x is greater than a threshold or is in a range selected at the time the memory was loaded from the on-line computer. There will be up to 16 different E vs θ tables in memory corresponding to different tagging system bins of photon energy K and the appropriate table will be used. The tagging bins are latches set by the overlap of the hodoscopes in front of the tagging shower counters. This information is available immediately and is transmitted as a 16 bit word to the processor.

6. Determining whether the track is a $\pi^{\pm}$ or p is a two step process. The threshold for protons at sufficiently high energy E in each sector is a function of θ. This is determined first by four parallel lookups $I_j(M)$ vs θ (where $I_1 = A, I_2 = B$, etc) which set four bits (PC_j) which indicate pulses above proton threshold. Another lookup of PC_j vs E for 16 values of θ will provide a bit if the event corresponds to an acceptable proton pattern.

Typically, at the end of these operations, a NIM level will be set if the M_x criterion (above 2.5 GeV, for example) is met, the proton bit is set, and neither the neutral veto bit

nor the "greater than one track at the first vertex" bit is set.

We can now estimate how long these operations will take:

Read in (including operation 1) faster than	1000 nsec
Operation 2 is parallel to operation 3	0 nsec
Operation 3: Simple case of single proton, no other hits, is 1 full cycle of do loop and will take ~ 350 nsec. The average case of 5 clusters with 1-2 tracks takes ~ 8½ short cycles (150 nsec each) and ~ 1½ full cycles: Average	1800 nsec
Worst case, which may happen 3% of the time is a $p\pi^+\pi^-$ recoil from a secondary interaction which crosses the primary proton recoil, needs about 55 short cycles and 2 long cycles. Total worst case: 9000 nsec	
Operation 4: Average of 7 cycles, 20 nsec each, of a sequential processor pulse one table lookup.	370 nsec
Operation 7: Two level lookup.	60 nsec
Average total	3.2 μsec
Worst case:	10.4 μsec

The average time is safely below the specified requirement of 10 μsec.

Other triggers can be handled in a similar way. Most of the triggers involving the forward spectrometer are, in fact, less complicated than the recoil trigger we have just described.

VI. Recoil System

A. Cylindrical Wire Chambers

The trajectory of the recoil proton will be measured by three concentric equispaced cylindrical proportional chambers (see Figures 3 and 4) with both anode and cathode readout. Their mass must be as low as possible to minimize both energy loss and multiple scattering. Rapid readout of the chambers is necessary for the fast missing mass trigger. In addition to the recoil proton, background tracks from various sources will be present, and must be properly handled. A design for the chambers within the framework of these constraints is presented below.

The readout HV cathodes, which measure the polar angle, θ, are made from foils consisting of 5 mil Al wire flattened to 1 mil and epoxied onto a mylar sheet at 1 mm spacing (such foils are available from Argonne National Lab). The foils are formed in cylinders so that each cathode wire becomes a circle in a plane perpendicular to the chamber axis. The non-readout cathodes are simply aluminized mylar foils. Two possible constructions are under consideration. The first requires that the foils be free-standing and held under tension by end rings separated by support rods (indicated in Fig. 3). Separate rings are needed for the anode wires, the inner cathode and the outer cathode in each chamber, so a complicated mechanical structure must be built at both ends. However, this type of chamber could have a low mass of .050 - .060 gm/cm^2. In the second

approach, the cathode foils are glued to ¼" NOMEX honeycomb to form rigid cylinders. The ends of the chamber can be much simpler, construction details in general are easier and cheaper, but the mass is ~ .105 gm/cm^2. This is not an intolerably high mass, so the second method seems preferable. An additional constraint, which renders the first method less attractive, is that the downstream end of the inner chamber must be low mass since it intercepts part of the forward spectrometer acceptance. However, we are presently designing and building a 34 cm. radius prototype of the free-standing chamber in order to understand better the mechanical problems involved.

The gap between cathodes is ½" and the anode wire spacing will be as large as possible, up to 5 mm (larger than this makes the time resolution unacceptable). Any adverse effects on the induced cathode pulse due to wide anode wire spacing will be investigated in a small flat test chamber. Because the anode wires are 2 m long, they must be supported at three or four locations along their length. For this purpose, foam rings ¼" square in cross-section will be cemented to the inner cathode foil.

An integral part of each chamber will be two rigid beams on either side of the 22.5° bottom access opening along the full length. These beams will slide or roll on their own sets of rails along the z direction so that each chamber can easily be installed or removed for repair.

At lower values of the t acceptance the contribution to the missing mass error from angular resolution in θ is dominated by multiple scattering in the target and chambers. However, at larger t, the measurement error in the chambers is the controlling factor. In order that this not dominate the total missing mass error, θ must be measured to roughly $\pm$ 6 mr.

The measurement error is

$$\delta\theta = \frac{Wg \sin^2 \theta}{\sqrt{3}\, d}$$

where d is the radial distance between the first and third chambers, W is the cathode wire spacing and g is a factor, certainly less than $\sqrt{2}$, which accounts for the degradation in resolution due to the spatial width (~1 cm) of the induced pulse on the cathode. For the worst case, ($g = 1.4$, $\theta = 70^{\circ}$) we require $W \simeq 3$ mm for $d = 30$ cm and $\delta\theta = 6$ mr. Thus the cathode wires (1 mm spacing on the foils) can be tied together in groups of three, giving 667 channels per chamber. Since the hits in each chamber are well separated in z ($\theta = 70^{\circ}$ is the largest angle of interest), independent cathode readout for three chambers would be redundant. Therefore, corresponding channels in the 3 chambers will be summed into the same amplifier. Reading out from the upstream end, the first hit then will be from the first chamber, the second hit from the second chamber and the third hit from the third chamber. In this way only 667 channels are needed for the θ measurement.

The azimuthal angle ϕ, of course, does not enter the missing mass calculation. However, for off-line reconstruction of events, and to correct for edge effects in the liquid scintillator cells, a measurement of ϕ to $\pm 1^{\circ}$ will be useful. This means anode wires can be tied together in $\sim 2^{\circ}$ bins, giving a total of 169 ϕ channels. Only one chamber's anode plane need be read out.

As discussed below,an additional 32 channels will be used to sort out background tracks. Therefore, a total of 667 + 169 + 32 = 868 readout channels are required.

The electronics will be based on a system already built and working for cathode plane readout of a small (64 wires) chamber tested with cosmic rays. In this prototype setup it is assumed that each event has only one cluster of cathode wires.to be located. Output from the amplifiers (8 channels/card) and discriminators (8 channels/unit) is fed to two 64 bit priority encoders followed by an arithmetic unit, which calculates and stores the position and width (3 - 5 channels with 3 mm wire grouping) of the cluster within 150 ns of the passage of the particle. Design of a scheme to handle several clusters is underway. It is anticipated that the positions and width of all clusters in the cathode plane can be found and stored in 0.5 - 1.0 μsec. From this information it is a straightforward task for the trigger processor to compute θ, assuming that the first three clusters belong to the recoil proton (see background discussion below).

In the system envisaged, the amplifier cards are positioned as close as possible to the chamber mother-boards in the bottom access space (recall that cathode channels at the same z from the three chambers are summed before the amplifiers - the amplifier cards therefore plug into a grandmother-board which performs the sum). Connections from amplifier to discriminator units, which sit in NIM-like bins (30 units/bin) near the chambers, are made by twisted pairs. Output from the discriminators is strobed by the scintillator trigger into the priority encoder-arithmetic box. This is also located on the experimental floor, so only cluster positions and widths are sent to the counting room; a huge bundle of cabling is thereby eliminated. The anode readout will probably be handled in a parallel, but identical, manner. Cost of the system up to the input of the trigger processor is ~ $30./channel.

Extra tracks in the chambers are possible from four sources: δ rays, low energy pair production and interactions of the secondary hadrons in the target and extra particles from the primary interactions (for example, $p\pi^+\pi^-$ target disassociation).

A crude calculation indicates that in a five prong event, ~ 2 δ rays escape the target. These typically have energy (after escape) of < 0.5 MeV and angle $\theta < 45^{\circ}$, and so will unlikely reach beyond the first chamber. Furthermore, the z distribution of escaping δ rays increases with distance from the primary interaction vertex as the secondaries spread toward the edge of the target. Thus extra clusters

in the cathode readout from δ rays are most probably downstream of the three primary clusters from the proton recoil and cause no confusion in the trigger processor.

The background from low energy pairs is an accidentals problem. At the highest beam rates contemplated, there are $\sim 5.10^6$ photons/sec in the lower part of the bremsstrahlung spectrum, which yield ~ 0.1 pair in the target in the ~ 100 ns resolving time of the chambers. A very rough estimate shows that a conservative upper limit of 10% of these have an electron of low enough energy to scatter at large enough angle to enter the chambers. Thus this background is < 1% and can be ignored.

The most serious background is a second recoil particle from an interaction of one of the secondary particles in the target, which, for a five prong event, occurs with a probability of 0.5. Perhaps 20% of these overlap in z in the chambers, causing confusion in the θ calculation in the trigger processor, unless it is intelligent enough to extract two θ angles from two overlapping sets of three clusters. If we have a dumb trigger processor, ~ 10% of the events are lost. In the remaining two-recoil events there is a θ-ϕ matching ambiguity. This can be resolved for most cases by the trigger processor using end to end timing on the inner fifteen scintillation counters. Another possibility is to provide ~ 10° (to the anode wires) stereo readout on the unused cathode of one chamber. About 32 channels on the inner chamber or 60 channels on the middle

chamber would suffice. We expect to build this option into the chambers. It will be useful for dealing with events where the target nucleon breaks up ($p\pi^+\pi^-$, etc.)

All the above assumes noiseless chambers. In the real world the trigger processor will have to be able to recognize and ignore at least some low level of extra clusters from noise. A useful suppression criterion may be the width of the signal clusters.

B. Liquid Scintillator Range Detector

After passing through the cylindrical wire chambers, the recoil particle enters a liquid scintillator range detector. This detector has 15 separate segments in the azimuthal angle ϕ. Each segment subtends approximately 22.5°. The total coverage is over 90% of the full 360°. Every segment in ϕ has four compartments (labelled A_i, B_i, C_i, D_i in Fig. 4) which provide up to four dE/dx samples along the path of the particle. Altogether there are 60 compartments in the liquid scintillator, each having photomultiplier tubes at both ends to ensure efficient light collection. Each tube has one ADC. The innermost 30 tubes have a TDC channel as well for end to end timing which gives $\delta z \simeq \pm 3''$. The liquid scintillator detector is used for a number of on-line and off-line functions.

The total light from a stopping proton in the liquid scintillator measures its kinetic energy. The recoil detector, as seen in Figures 3 and 4, is designed to do this simply and quickly. (The kinetic energy can be

determined from a number of dE/dx measurements as well, but this is a more difficult procedure, as it depends on the recoil angle θ and may require a longer, off-line calculation.) The proton recoil energy, the angle θ and the beam energy k can be used to evaluate the missing mass in the forward arm of the spectrometer. The calculation is quite simple and will be done by the trigger processor (see Section V).

Because the recoil angle θ determines the maximum thickness of liquid scintillator, it also affects the total energy range acceptance, the energy loss per compartment and the probability of a nuclear interaction before the proton stops. These numbers are summarized in Table XI for θ angles of 90°, 45° and 30° (see also Fig. 7 in Section II). But because the signal is read out from both ends of a ϕ segment, to a first approximation the total scintillator signal will be independent of the interaction position along the z axis and the recoil angle θ. After a valid stopping particle trigger has been indicated, the 8 photomultiplier ADC's for one segment are summed to give the total energy deposited in the liquid. This may have to be corrected slightly (<15%) for the attenuation differences to the opposite ends of the 2.4 m compartments.

The aim is a kinetic energy resolution in the neighborhood of $\frac{\Delta T}{T} \simeq \pm 8\%$ to $\pm 12\%$. As discussed in an earlier section, this range of $\Delta T/T$ provides an acceptable M_x error at masses of 2 to 6 GeV/c^2 and beam energies of 50 to 150 GeV/c.

The $\Delta T/T$ resolution of the recoil detector will be verified with tests on a prototype of one of the segments which is currently under construction.

The missing mass calculation is only valid if there is a single quasi-elastic proton recoil. There are several handles on identifying such events. These include absence of a $\pi^{\pm}$, π^{o} or neutron and counting recoil tracks from the primary vertex. Table XI shows a 0.53 probability that a photon will convert in 57 cm of liquid scintillator. A π^{o} will then have a probability of 0.72 for converting at least one of its two photons. A π^{o} signal would be indicated by one of the following no-yes combinations

$$\bar{A}_i \cdot B_i$$
$$\bar{A}_i \cdot \bar{B}_i \cdot C_i$$
$$\bar{A}_i \cdot \bar{B}_i \cdot \bar{C}_i \cdot D_i$$

This same signal may indicate a neutron interaction, in compartments B_i or C_i or D_i. The probability for a neutron interaction varies as a function of angle from 0.38 to 0.49 for $30^{o} < \theta < 90^{o}$. This signal can be used to reject most events that do not have elastic proton recoils.

For similar reasons, it is desirable to have a pion/proton identification trigger available from the dE/dx information in compartments A_i, B_i, C_i and D_i. This may be difficult in the high level trigger because it depends on the angle θ and on how good the ΔE measurement is.

Table XI

Recoil Liquid Scintillator Range Detector

	θ Recoil Angle		
	90°	45°	30°
1. Maximum scintillator thickness (cm)	40 cm	57 cm	80 cm
2. Acceptance from 2 m. target	100%	$\gtrsim$ 75%	$\gtrsim$ 38%
3. Probability of nuclear interaction	.38	.49	.61
4. Probability of photon conversion	.41	.53	.65
5. ΔE loss for minimum ionizing particle	72 MeV	102 MeV	144 MeV
6. ΔE loss for stopping protons	$\leq$ 250 MeV	$\leq$ 300 MeV	$\leq$ 375 MeV
7. ΔE loss for stopping pions	$\leq$ 120 MeV	$\leq$ 160 MeV	$\leq$ 200 MeV

If more than one charged particle enters the liquid scintillator tank, it is very unlikely that more than one will enter the same ϕ segment (the probability for 2 uncorrelated particles in the same $\Delta\theta = 22.5^{\circ}$ is 6%). Thus the number of inner scintillator tracks (A_i) with pulses above a discriminator threshold, measures the charged multiplicity entering the liquid scintillator. This information is redundant to that available from the PWC θ readout when there is no secondary interaction.

If all of the liquid scintillator compartments A_i, B_i, C_i, D_i in one segment register a minimum ionizing particle and there is no evidence for other than single-proton recoil, the event can be interpreted as a probable high t recoil proton. For a minimum ionizing particle the signal ratios are

$$\frac{B_i}{A_i} \simeq 2, \quad \frac{C_i}{A_i} \simeq 3, \quad \frac{B_i}{D_i} \simeq 3$$

for thickness A_i, B_i, C_i, D_i = 6, 12, 18, 4 cm respectively. These ratios are a test for high t recoil which is independent of the recoil angle θ. Higher mass diffractive states are apparently produced with a flatter t slope. Therefore a signal indicating a high $|t|$ recoil may be a useful additional way of enhancing higher mass states in the trigger.

Off-line it will be possible to use careful calibration

and mapping to increase the level of sophistication in the use of the recoil information. For example, a careful off-line analysis of the four dE/dx samples for an exiting (high $|t|$) proton should enable one to extend the measurement of the energy range. This will be determined by the precise $\Delta T/T$ values of the resolution function. If a stopping proton interacts with and transfers energy to a neutron in the liquid scintillator, the dE/dx measurement is not valid. Furthermore, if the proton stops but a neutron carries some kinetic energy out of the liquid scintillator, the proton range measurement E is not valid. The added check for a consistent set of dE/dx in A_i, B_i, C_i, D_i for a stopping proton hypothesis will help identify a "clean" data sample in the off-line analysis.

The large cylindrical container enclosing the cylindrical proportional chambers will have an inside radius of 57 cm, outside radius 97 cm and a length of 240 cm. The volume enclosed is about 4.52 m^3 (1000 gallons) and the weight of this volume of liquid NE 235 A scintillator is 3900 kg (4.3 Tons). The construction material for the container will be steel, which will be coated with teflon and/or NE #561 scotchlight white epoxy paint on all the inside walls in contact with the liquid scintillator. The large cylindrical container will come in three separate sections (labelled I, II and III in Fig. 3). The three sections will bolt rigidly together when in place on the experimental floor and a set

of wheels on rails will provide movement for the whole unit along and perpendicular to the beam axis. As seen in Figure 3 a missing wedge on the underside provides access, support and readout space for the cylindrical chambers.

The inside (r = 57 cm.) surface of the container must have a minimum amount of material to maximize the acceptance for the low end of the proton energy spectrum. The present thought is to use a 1/16" stainless steel plate, but if this proves unacceptable from a structural standpoint, an alternate solution is to place thick acrylic scintillator slabs in the space between the third PWC and the inside steel surface. This would improve the acceptance for low energy protons, and allow for a thicker container wall. The hydrostatic pressure on the inside surface of Sections I or II has the maximum value of 1.4 lbs./sq. in.

The 60 compartments will be separated from each other by thin walls designed only for light isolation. These inner walls will only support themselves and not provide any structural rigidity for the container. They will be thin so that a stopping particle can scatter across and leave energy in the adjoining compartments. Appropriate small holes will allow for the scintillator to flow between the compartments when the containers are being filled or emptied.

The end faces of the cylindrical vessel will have plexiglass windows, to contain the fluid and transmit the light to green wavelength shifter bars (as shown in Figure

13). The shifter bars will be viewed by light guides and 2" photomultiplier tubes. The plexiglass ports will have to be individually cut and then glued to an opaque barrier between the compartments. Considerable care will be taken to seal these ends so that they do not leak. The purpose of the green shifter bars is twofold. First they are used to ensure a reasonably uniform light collection efficiency over the whole end face of each compartment. If the output pulse is to be used in the trigger, there will be time to evaluate only the most simple types of corrections. Secondly, on the downstream end of the range detector there is a maximum of 40 cm. between the scintillator and the first magnet face. The shifter bars bend the output light signal through 90° and the photomultiplier tubes can be kept away from the magnet and its fringe field.

The dynamic range of signals from the various compartments is shown in Table XII. The attenuation length of NE 235 A is about 1.7 m. Thus equal signals at 0.1 meter from one end and 2.3 meters from the other end will have a pulse height ratio of about 4 for the two phototubes. Combining the dynamic range requirements with the attenuation factor of 4 suggests that we use ADC's with a range of 1 : 1000, or 10 bits. At present this range of 10^3 seems a rather conservative estimate. Resolution studies with the scale model later this year may reduce it.

LIQUID SCINTILLATOR LIGHT COLLECTION

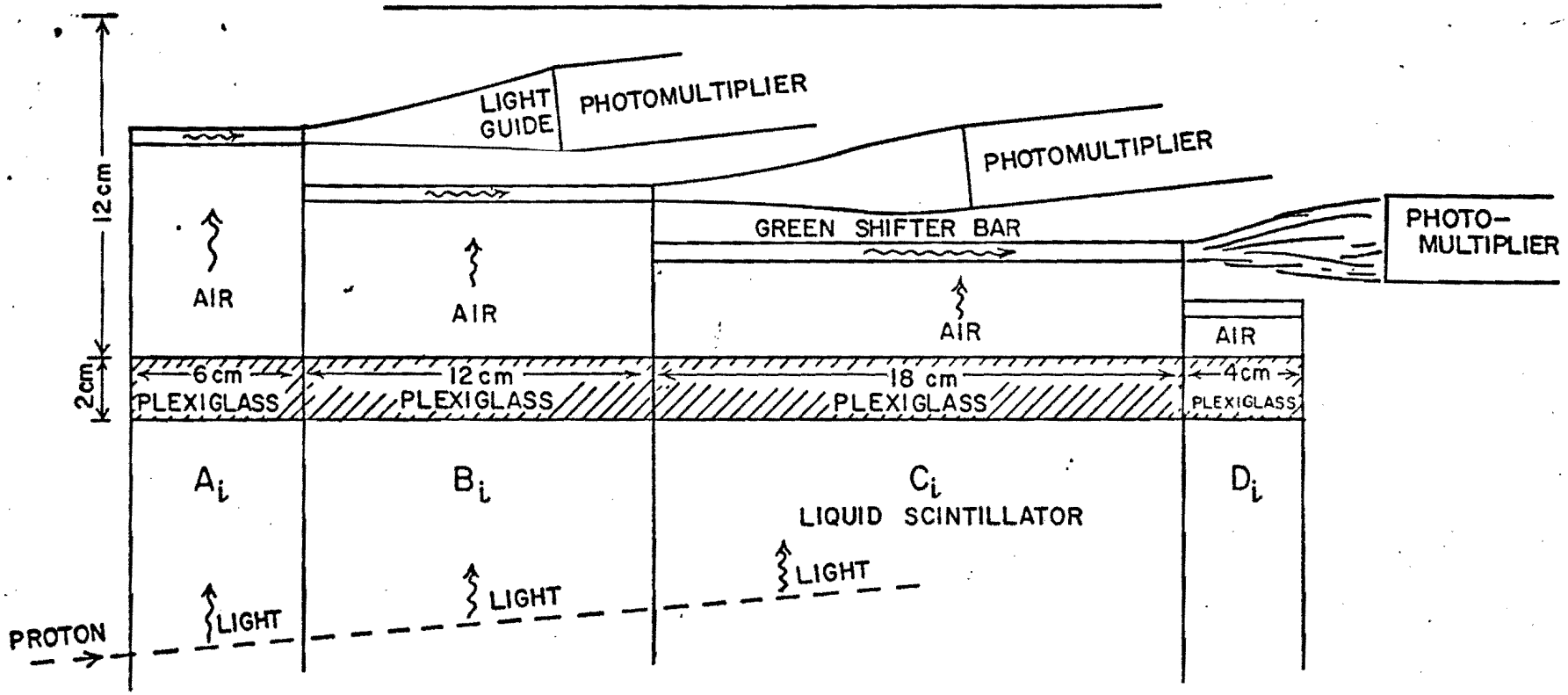

Figure 13

Table XII

Dynamic Range Requirements of Recoil Liquid Scintillator Compartments

Compartment	Thickness	$\theta = 90^{\circ}$ Min. Ioniz.	$\theta = 90^{\circ}$ Max.	$\theta = 30^{\circ}$ Maximum	Sensitivity Required	Dynamic Range
A	6 cm	12 MeV	80 MeV	125 MeV	1/2 MeV	250
B	12	24	120	175	1	200
C	18	36	150	230	2	100
D	4	8	46	100	1/2	200

The absolute calibration of the phototubes will be done with real experimental data during the run. Compartment A tubes can be calibrated with protons that traverse it and just barely enter into the next compartment B. Knowing the θ angle from the PWC's one can calculate the exact range of the proton traversing A (to ± 2 mm). The range then specifies the energy, which then calibrates the photomultiplier tubes. Compartments B and C will be calibrated in a similar fashion. Compartment D will be calibrated using minimum ionizing particles passing through A, B, C and D.

VII. Liquid Hydrogen Target

The liquid hydrogen target system will accommodate target flasks of various lengths. It will be possible to exchange these in a few days turn around time. This will allow experiments to optimize the length for the particular physics being pursued. For example, to maximize rates a 2 m target will be used. To reduce the interaction of secondaries a short 1/2 meter flask would be possible. The flasks will be of thin wall construction to offer the minimum possible mass to low energy recoil protons and will be supported from only one end. Initially, the target flask will have a diameter of 2 inches and a length of 2 meters. Figure 14 shows a cross section of the target with the various dimensions. A breakdown of the material comprising the target is as follows:

	Thickness	Mass
A) Flask (Mylar) $\rho = 1.39\ g/cm^3$	0.005"	.0177 g/cm^2
B) Foam Vacuum Jacket (Rohacell) $= 0.053\ g/cm^3$	0.5"	.0673 gm/cm^2
C) Outer Vacuum Jacket Skin (Mylar) $\rho = 1.39\ g/cm^3$	0.005"	.0177 gm/cm^2
Total		.103 gm/cm^2

This compares with .36 gm/cm^2 for 2" liquid H_2.

The volume of the 2m flask is about 4 liters. The hydrogen gas will be condensed and refrigerated by a 10 watt Air Products helium refrigerator. The time required for filling from warm will be about 25 hours. The time to empty the target into the reservoir is about 12 minutes while the refill is about 60 minutes.

The target system will be mounted on a rail system to allow it to be withdrawn from the recoil detector. Pump cart compressor and controls will be located on top of the shielding adjacent to the rails with flexible tubes connected to the refrigerator.

HYDROGEN TARGET FLASK

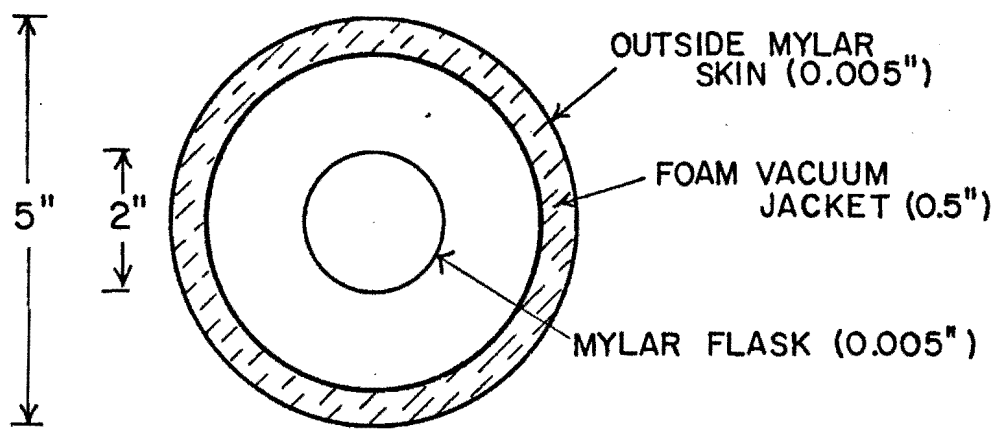

Figure 14

VIII. Forward Detectors

A. Drift Chambers

Charged particles will be tracked in the forward spectrometer by 32 planes of drift chambers. The general characteristics of these chambers are summarized in Table VIII (Sec. II F). The motivation for our choice of wire orientation and chamber location was discussed in earlier sections of this report. We will now discuss some of the mechanical and electrical details of the chambers.

The chamber construction will be guided by the results of a prototype and testing program which will begin soon. We envisage a technique similar to that of R. Thun et al.[6] Field shaping wires will be 127 μm diameter hard copper wire and sense wires will be 25 μm diameter gold plated tungsten. Figure 15 shows the structure planned for the cells.

Sense (anode) wires will be at ground potential and nearby field wire potentials chosen at negative voltages which give nearly cylindrical equipotential patterns around each sense wire. All wires will be mounted on G-10 frames which will be mounted in groups inside a gas tight aluminum box. This box simultaneously provides a rigid surveyable mounting structure and shields against noise. In addition, each chamber will be isolated from its neighbor by a ground plane which will be a plane of aluminum wires in order to minimize material in the spectrometer. Figure 16 indicates the preliminary design for construction of a single plane.

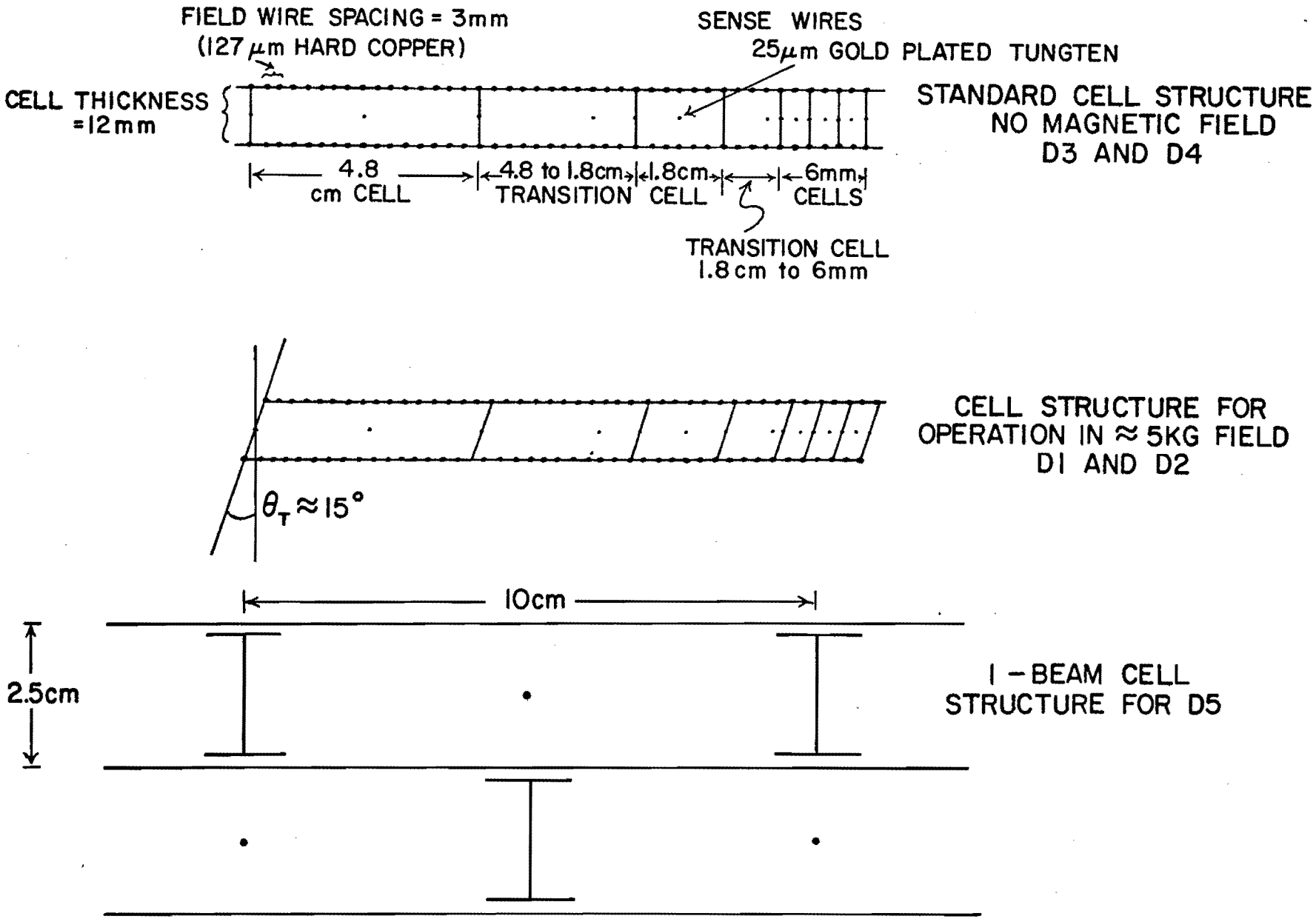

CELL STRUCTURE

Figure 15

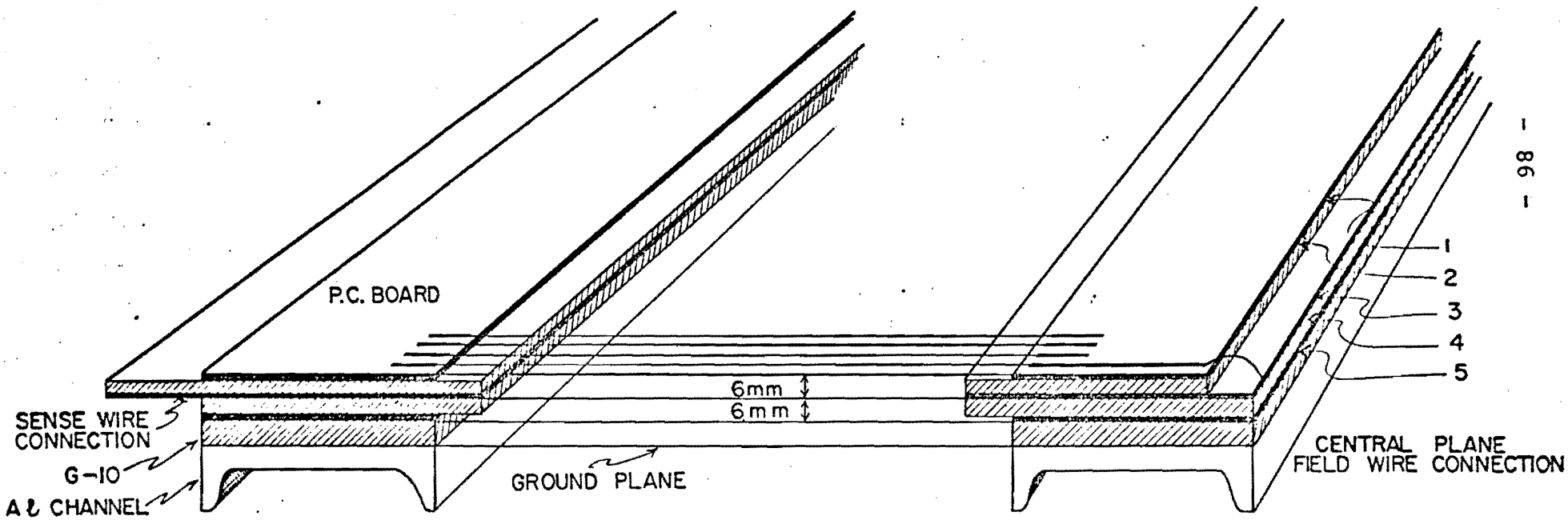

1,3,5 - P.C. BOARDS FOR FIELD & SENSE WIRE CONNECTIONS

1,2,3 - LAMINATED WITH EPOXY

4, 5 - LAMINATED WITH EPOXY

ENTIRE ASSEMBLY BOLTED TOGETHER

CROSS SECTION OF SINGLE DRIFT PLANE

Figure 16

The guiding principles for this design have been serviceability (it should be possible to easily access all wires should it be necessary to replace a wire for any reason) and the ability to mass produce the final design.

We have seen earlier that the physics we want to do places rather severe requirements on our ability to resolve closely spaced tracks inthe chambers. There are two possible competing philosophies which may be adopted to meet these requirements: 1) Large cells may be used which then have multiple track readout capability, and 2) Smaller cells may be chosen with the capability to read only one coordinate. In the first instance the pulse width which may be obtained in a drift chamber limits the inherent pulse pair resolution to 50-100 ns (2.5 mm - 5 mm). In addition, the electronics is complicated by either having more than one TDC per wire or by a multiplexing scheme to route pulses to a smaller number of TDC's. In the second case one has more wires to deal with but the electronics is much simpler. The smallest drift space which is practical is 2-3 mm which matches the pulse pair resolution described above. Our choice is to simplify the electronics and keep cell sizes relatively smaller.

As described earlier four cell sizes (.6 cm, 1.8 cm, 4.8 cm, and 10 cm) will be used with the size increasing away from the beam. The distribution of cells is shown in Table VIII.

It should be noted that the overall cost of the system is dominated by the cost of the readout electronics. It may be that the most cost effective technique is to minimize the cell size. For example, we are considering the possibility that it may be less expensive to make chambers with only 6 mm cells (3 mm drift spaces) and thereby have only TDC's with a smaller number of bits. There are also advantages involving the field shaping wires in the magnet (M1) for small drift spaces since compensation for the B field will probably not be necessary.

Our experience has been that Argon (90%) - CO_2 (10%) is a satisfactory gas for drift chamber use. However, the drift velocity in Ar - CO_2 is more strongly dependent on electric field than in some other hydrocarbon mixtures. This may be a disadvantage in an experiment where most of the cell sizes are small and one is more often than not in the region close to the sense wire where fields vary rapidly. For this reason we will investigate this variable during the prototype and test stage.

It is now well known that it is possible to operate large drift chambers in high, uniform magnetic fields by skewing the $\vec{E}$ field to compensate for the average Lorentz force on the drifting electrons. For small drift spaces this compensation is not necessary. For larger drift spaces (1.8 cm and 4.8 cm cells) it is our intention to arrange the voltage divider networks for the field shaping wires so that the

$\vec{E}$ field skew angle ($\theta_T \approx \sin^{-1} (\frac{vB}{E}) = 14°$ for E = 1000v/cm and B = 5 Kg) is easily variable within limits so that there is some flexibility in choosing the magnetic field in M1. This option may be most important as the Energy Doubler/Saver becomes operational.

It is desirable from the standpoint of avoiding noise problems to have the amplifier-discriminator shielded well and as close to the chamber as possible. Therefore, small packaging is necessary so that even for 6 mm cell sizes it is possible to place the amplifier-discriminator directly on the chamber. In addition, little space is available for electronics on the chambers inside the magnet before reduction of solid angle becomes an important question.

However, placing the amplifier-discriminator directly on the chamber may not be desirable from the serviceability point of view for the chambers inthe first magnet. An additional requirement for the amplifier-discriminator is set by the desire that the discriminator output be available to a preprocessor. For example, such information may be used in a multiplicity trigger.

Electronics for drift chambers is a continously developing field. We outline here the requirements that the electronics for this system of drift chambers will have to meet. Average drift velocities on the order of 5.0 cm/μs are expected. Thus, the drift times for .6 mm, 1.8 cm, and 4.8 cm

cells are expected to be 60 ns, 180 ns, and 480 ns. We are striving to reach a spatial resolution of from ± 100 μm to ± 150 μm which implies measuring drift times to an accuracy of ± 2 ns. We therefore, desire a digitizing system with a least bit accuracy of ~ 2 ns. For a strictly digital system this requires a 500 MHz clock. Analogue systems readily obtain this accuracy but there is an additional burden to calibrate and monitor independently each TDC channel. A hybrid technique like that of T. Droege eliminates this problem. We note that for the drift times mentioned above we require TDC's with 5 bits, 7 bits, and 8 bits, respectively in order to achieve the desired accuracy.

We will use Droege high voltage power supplies like those presently in common use for MWPCs and drift chambers elsewhere at Fermilab. Each chamber will be provided with a separate voltage divider for each cell size in order to provide field shaping. Because there are only four separate cell sizes, we need only 4 distinct voltages. However, it is extremely desirable when debugging chamber problems to have a limited number of chambers sharing one supply. Chamber problems are then localized more efficiently. For these reasons we will use 18 dual modules. There are then nine supplies at each of 4 voltages. With 32 chambers we then have at most 4 chambers on any one supply.

B. Cerenkov Counters

We will use two segmented Cerenkov counters for particle identification. The first one will be a 3.25 meter long nitrogen gas filled counter and the second will be a 7 meter long nitrogen helium mixed gas counter. The basic properties of these counters are shown in Table XIII. Also Figs. 17 and 18 show the excitation characteristics of these counters. In addition we will be able to use other gases like CO_2, C_8H_8 (propane), and Fr_{12}, as the experimental situation requires it.

In order to handle the large multiplicity expected in the final states that will be studied, each of these Cerenkov counters will have a 20 mirror segmentation arrangement. These spherical mirrors will be slump-molded out of thin Plexiglas in order to reduce the amount of material in the path of the particles. The focused Cerenkov light will be reflected into Winston cones whose dimensions are shown in Fig. 19. Finally, the light is detected by RCA 8854 5" phototubes which have a high photoelectron efficiency (~18%). An ADC will be attached to every phototube in order to measure pulse height. This procedure may help extend the range of separation of pions and kaons.

Using threshold information alone, the counter will separate pions from either kaons or protons for momenta between 5.5 and 36 GeV. All three particles can be separated from each other for the more restricted range of 21-36 GeV.

TABLE XIII

Upstream Cerenkov Counter (C_1)

Gas	100% N_2
Length of Counter	3.25 m
Transverse Dimensions Upstream	1.4 x 0.64 m
Transverse Dimensions Downstream	2.5 x 1.14 m
Index of Refraction (n-1) at STP($\lambda \approx 3500\mathring{A}$)	3.089×10^{-4}
Cerenkov Angle ($\gamma \to \infty$)	25 mrad
Threshold for Pions	5.5 GeV/c
Threshold for Kaons	20 GeV/c
Threshold for Protons	38 GeV/c
Number of Reflections (N_R)	2
Total Number of Photoelectrons ($\gamma \to \infty$) N_{pe} per cm = $170 \sin^2\theta_c x(.70)^{N_R}$	16

Downstream Cerenkov Counter (C_2)

Gas	21.8% N_2 & 78.2% He by volume
Length of Counter	7 m
Transverse Dimension Upstream	2.1 x 1.25 m
Transverse Dimension Downstream	4.3 x 2.5 m
Index of Refraction (n-1) at STP(λ-3500$\mathring{A}$)	0.950×10^{-4}
Cerenkov Angle ($\gamma \to \infty$)	14 mrad
Threshold for Pions	11 GeV/c
Threshold for Kaons	36 GeV/c
Threshold for Protons	69 GeV/c
Number of Reflections (N_R)	1
Total Number of Photoelectrons ($\gamma \to \infty$) N_{pe} per cm = $170 \sin^2\theta_c x(.70)^{N_R}$	15

PROPERTIES OF THE
UPSTREAM CERENKOV COUNTERS (C_1)

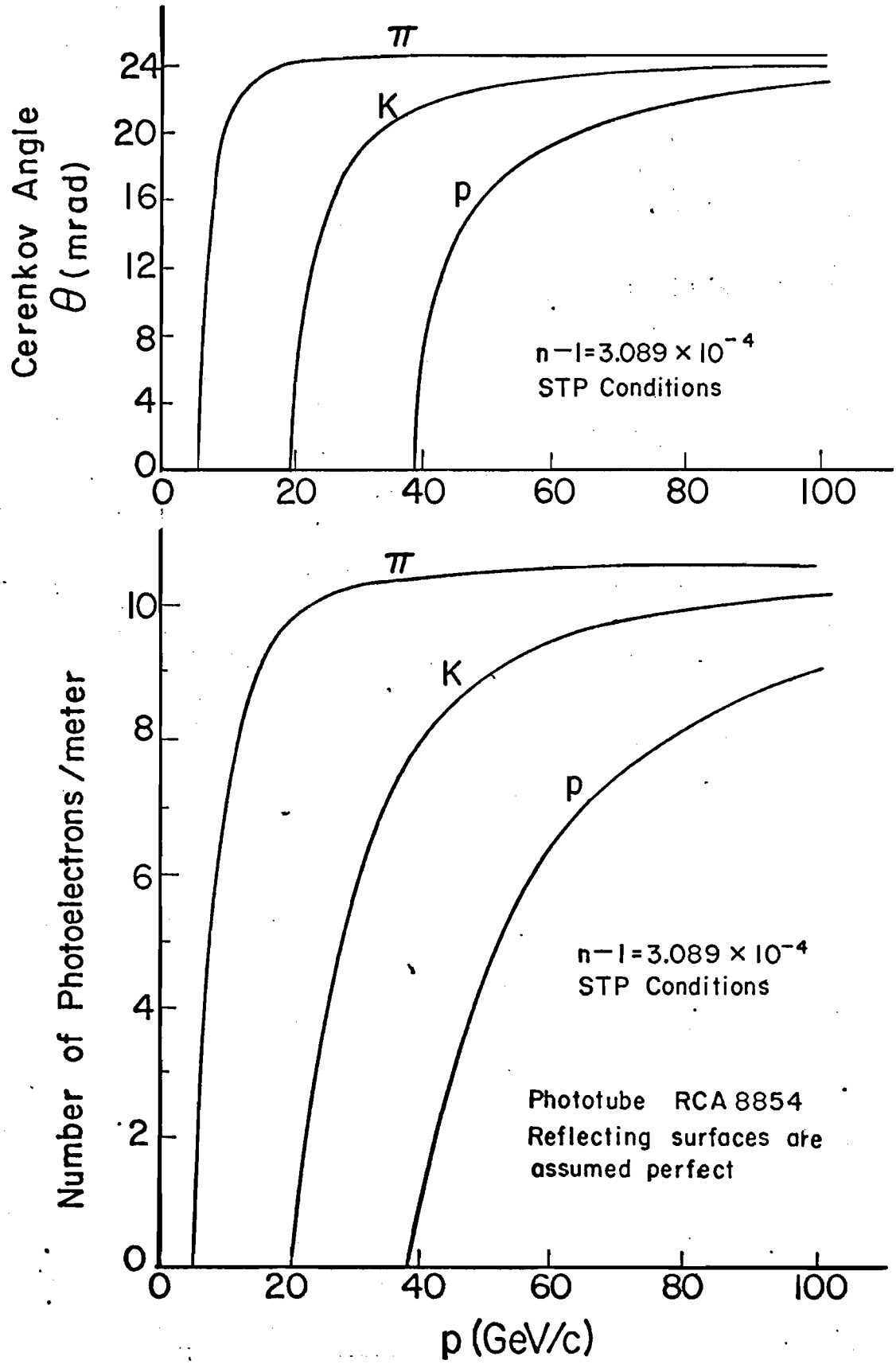

Figure 17

PROPERTIES OF THE DOWNSTREAM CERENKOV COUNTERS (C_2)

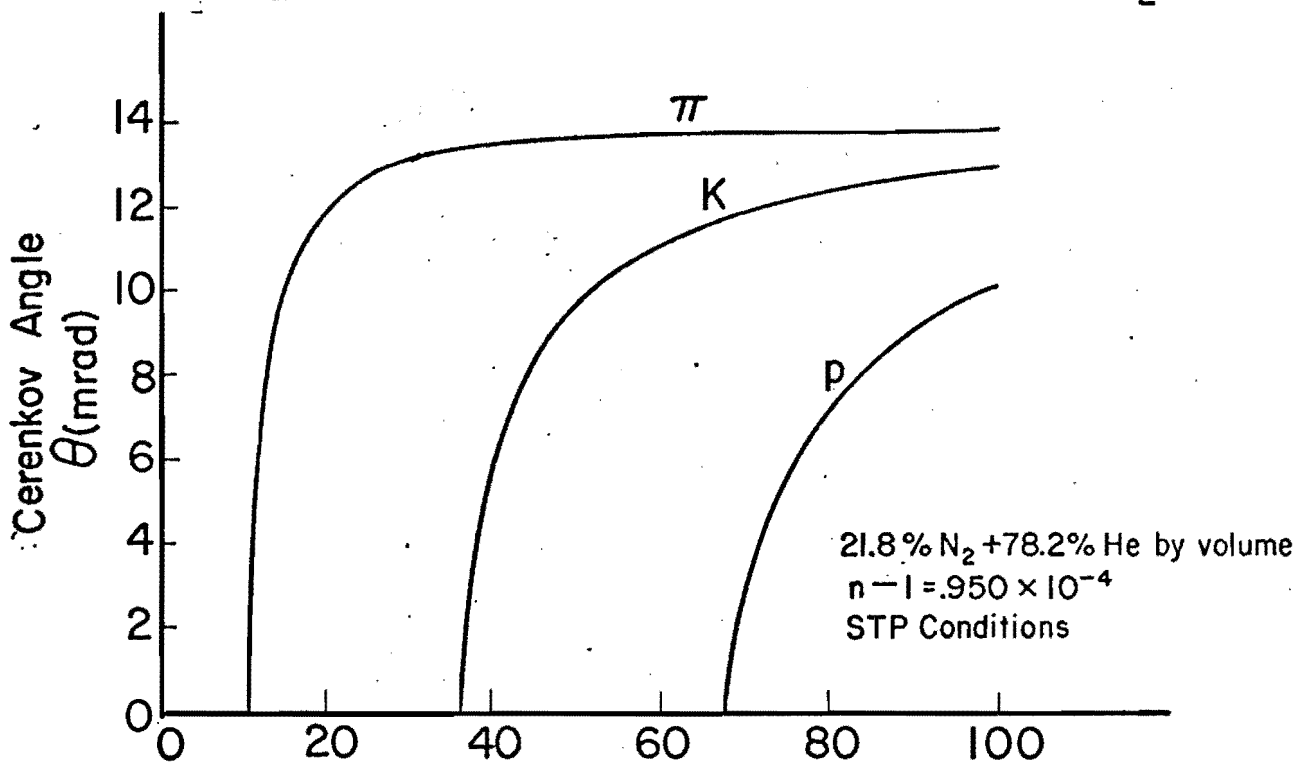

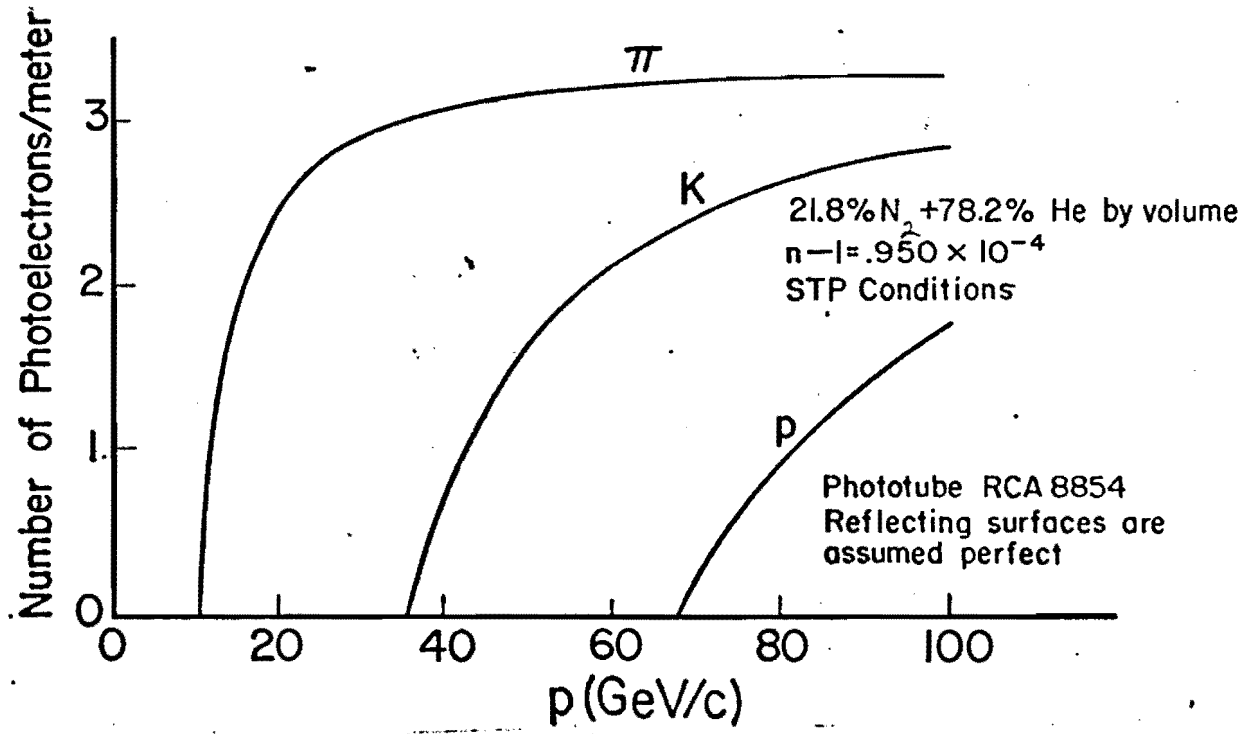

Figure 18

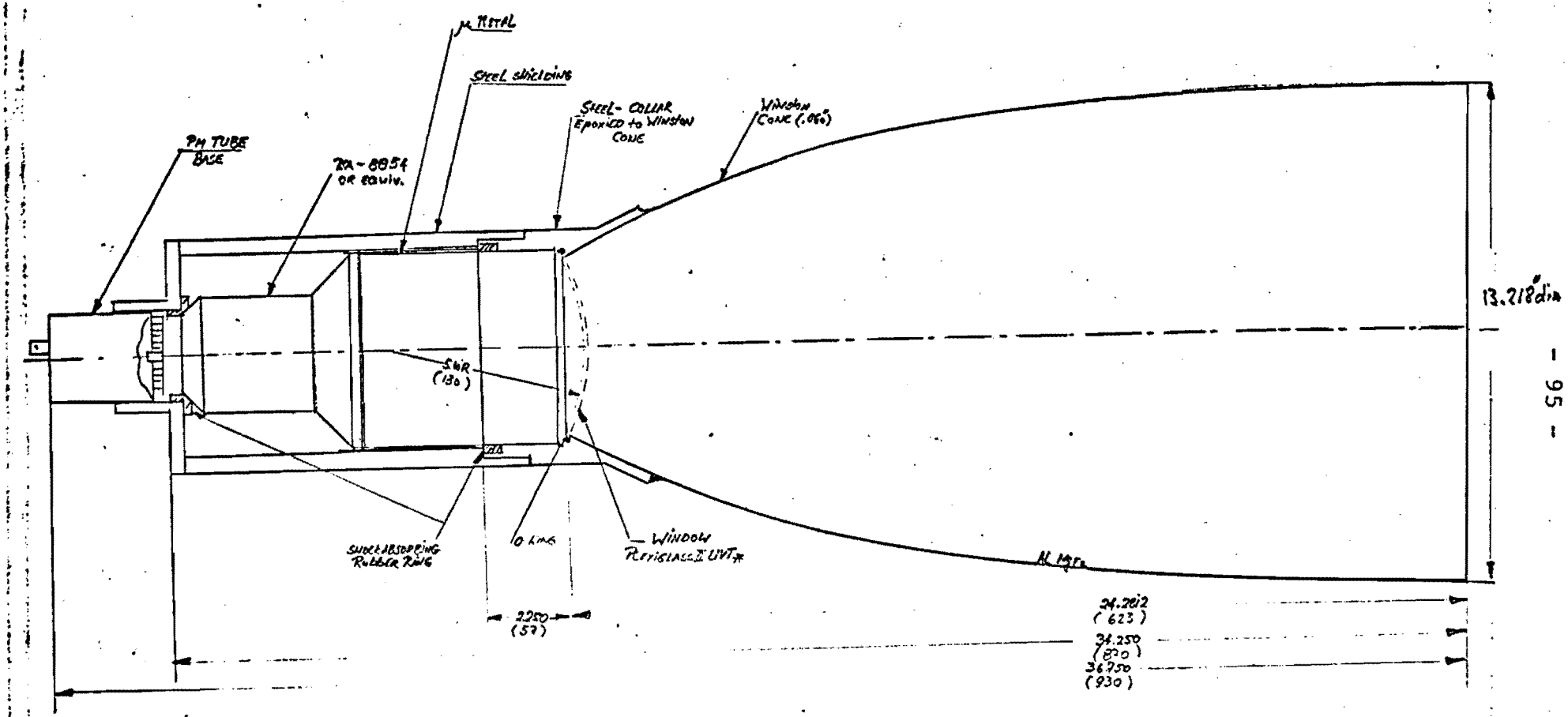

Figure 19

Winston Cone, PM-TUBE, TUBE BASE ASS'y

$y = 0.0295x^2$; SIN 20°

* UVT = ULTRA VIOLET TRANSMITTING

The counters, however, are sufficiently long that about 15 photoelectrons can be recorded from the passage of a single particle. By recording the number of photoelectrons the upper limits on the range of particle distributions can be increased by 50%.

Both Cerenkov counter vessels are manufactured from 1/4" thick 6061 T6 aluminum plate welded into frustum-shaped containers, reinforced with externally welded ribs. Both ends of each vessel will have a full sized flanged opening, to allow the use of thinner material along the path of the beam. Two access ports in each vessel (24 x 48") are provided to permit entry for mirror alignment. The small vessel (C_1) will be manufactured in two sections joined together with flanges. The large vessel C_2 will be in three sections. After manufacture, both vessels will be purged with helium and tested for leaks. Each vessel will be equipped with its own support and leveling device to permit alignment. Estimated net weight for the large counter is 4500 lbs. and for the small counter, 1800 lbs.

After closing the counters, they will be purged with dry nitrogen. The nitrogen-helium mixture for the large vessel and nitrogen for the small vessel will be introduced into the top of the counter. Displaced gas is vented through the bottom until the desired purity or mixture is obtained (Fig. 20). A low range differential switch will provide regulation.

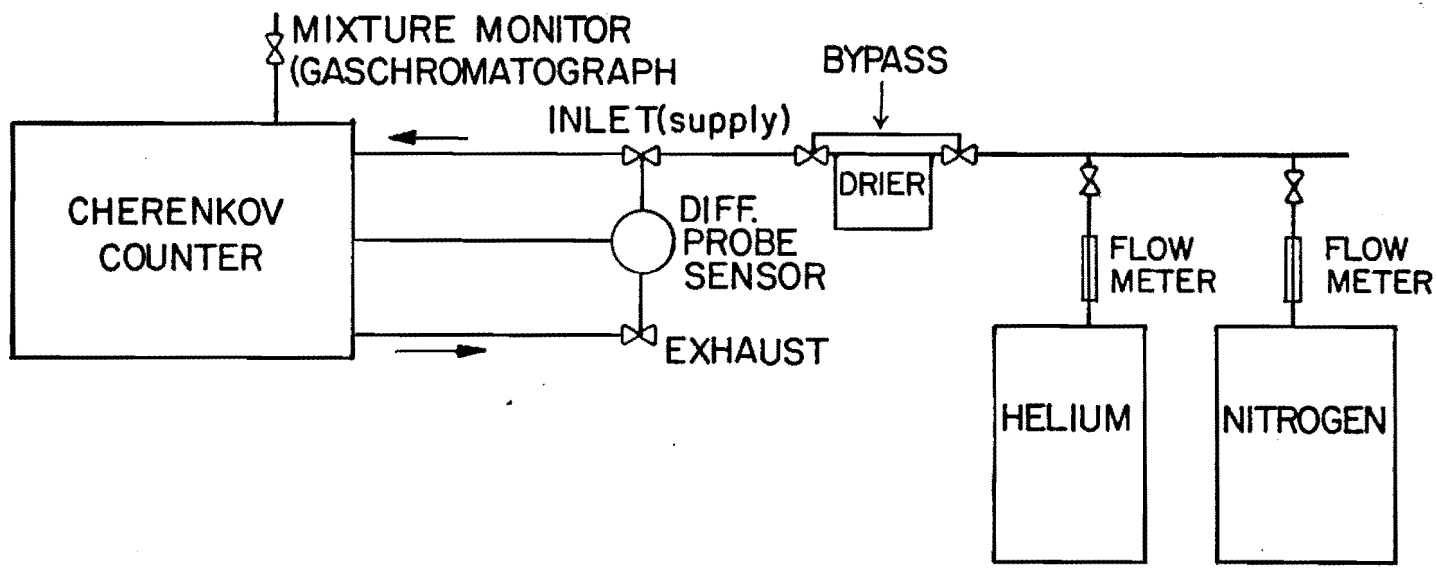
MIXTURE MONITOR
(GASCHROMATOGRAPH
BYPASS
INLET(supply)
CHERENKOV
COUNTER
DRIER
DIFF.
PROBE
SENSOR
FLOW
METER
FLOW
METER
EXHAUST
HELIUM
NITROGEN

Figure 20

The mirror planes in both counters will have 20 segments of various sizes but constant focal length (78"). To minimize labor costs and material expenses 1/4" block acrylic sheet is being considered. The surfaces of acrylic are already of sufficient optical quality; the exiting light ray should deviate from its expected direction by no more than 5 milliradians.[7] The construction of the mirrors will proceed as follows: oversized sheets will be slumped into a female aluminum mold to produce a spherical shape.[7] A cover will prevent deposition of dust and permits uniform heating of mold and acrylic sheet. The cover also will prevent local deviations in the plastic sheet. A fluorocarbon release agent will be applied to the mold prior to shaping to prevent sticking of the plastic to the mold surface. Acceptable mirrors then will be attached to their mounts and aluminized. If necessary the mirrors will be reinforced with a hexcell structure.

The collection cones will be fabricated in one of two ways: A) Spinning aluminum sheet over a steel mandrel of desired shape; and B) By blowing acrylic tubing inside a heated mandrel of correct size.[8] While option A entails a minimal expense in manufacturing aluminum cones, the polishing process is very time consuming and laborious. Option B on the other hand, presents a greater expense for both material and mandrel. If metal cones are used, prior to aluminizing, cones will be dipped and baked with a lacquer

coating to increase reflectivity. If acrylic cones are used, the aluminizing will be the same process as for the spherical reflectors.

To prevent leaking of helium-gas into the photomultiplier tube (RCA 8854) we plan to install a 3/16" thick UV-transmitting window slumped to an inside spherical radius which will mate with the spherical face of the tube. The separation of about 1/16" between tube-face and plastic window can be continuously flushed with nitrogen gas to keep helium away from the phototube window. (Nitrogen gas is essentially transparent over the wavelength range 1875Å to 8000Å.[9]) To increase sensitivity to UV photons the plastic window will be coated with an organic wavelength shifter, P-terphenyl (PTP) or diphenyl stilbene. This process converts photons in the 1700 to 3600Å range to a range centered around 3805Å.[10]

C. Segmented Liquid Scintillator Shower Counter (SLIC)

As shown in Fig. 21, the SLIC is a multilayered lead-liquid scintillator shower counter. Position resolution is obtained by segmenting the liquid layers into a number of teflon coated light pipe channels. Every third channel, progressing longitudinally through the detector, will be oriented in the same direction.

The periphery of the detector is composed of Lucite windows and thin wave bar strips optically coupled to phototubes. The strips are oriented longitudinally and have a

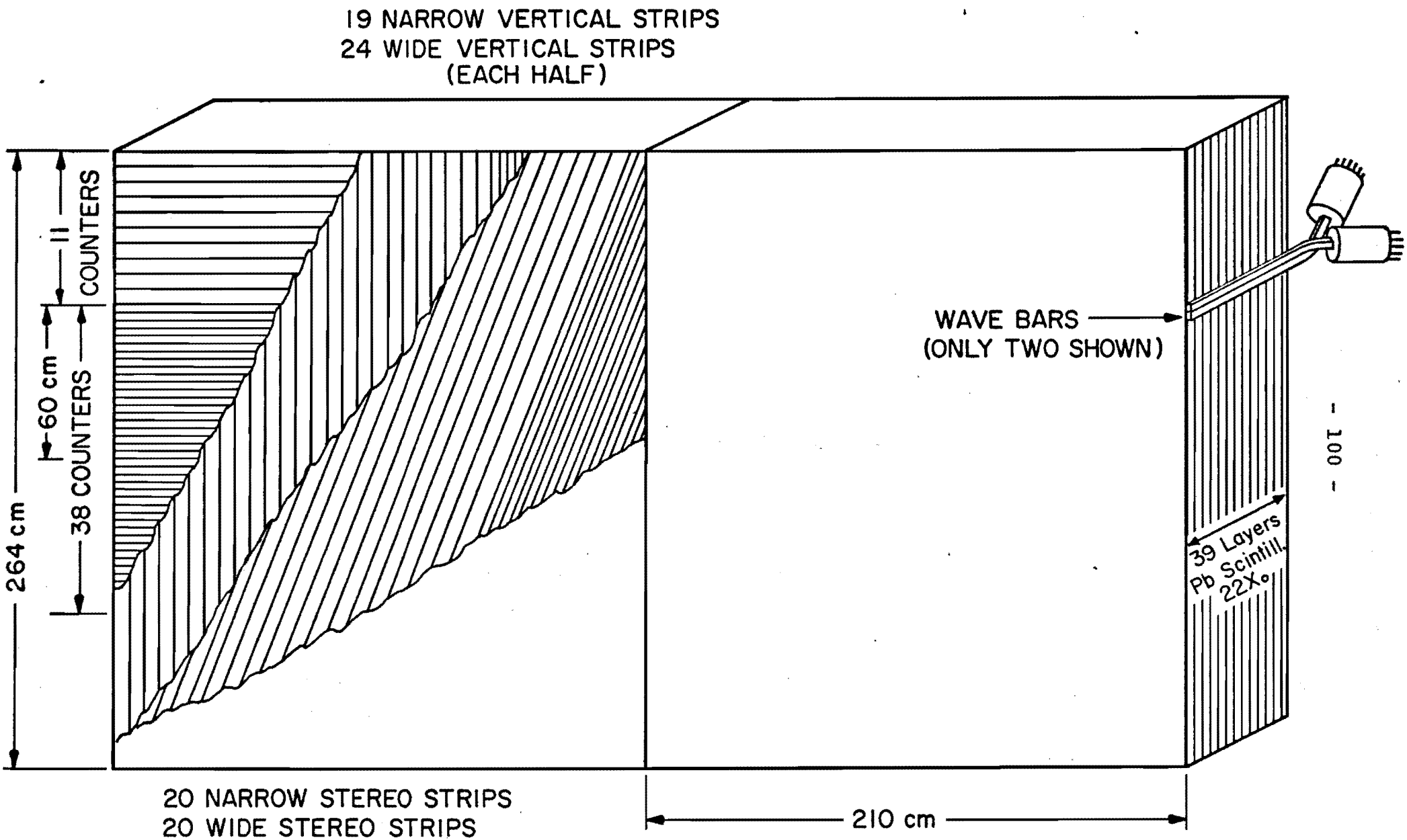
19 NARROW VERTICAL STRIPS
24 WIDE VERTICAL STRIPS
(EACH HALF)
11 COUNTERS
60 cm
38 COUNTERS
264 cm
WAVE BARS
(ONLY TWO SHOWN)
39 Layers
Pb Scintill.
22X₀
20 NARROW STEREO STRIPS
20 WIDE STEREO STRIPS
210 cm

Figure 21

width which is a multiple of the light channel widths. For a single shower, the position of the shower is determined from the location of the photomultipliers which view light from the top, giving the x coordinate, and from the side, giving the y coordinate. In fact, from the distribution of pulse heights on the neighboring counters, the position can be determined much better than the width of the channels. Our experience with lead glass indicates that with 2.5" channels one can always do better than ± .6" and will usually have a resolution of ± 0.2". This corresponds to $\delta\theta \simeq .3$ mrad.

The third view, at 20° with respect to the vertical and taken from the bottom of the detector, is to remove ambiguities for cases of multiple showers. These ambiguities are not as serious as for the case of wire chambers since they only arise in the case of showers of nearly equal energy. We believe, however, that this degree of redundancy will be very useful for resolving complex patterns. In addition, at least at lower beam intensities, this may enable us to eliminate separate lead glass pair counters for the fast trigger (see Section IV A). This in turn will improve our ability to have a running calibration of the SLIC using the high rate of pairs.

We plan to have segmentation of 1.25" (3.18 cm) in the region near the beam and 2.5" toward the periphery. The regions are shown in Fig. 21. The total number of counters is 278.

A nice feature of this type of counter is the great variety of possible configurations which are economically feasible. The scintillator and segmenting materials are relatively cheap so thatthe counter can be made with many layers improving resolution.

The wave bar light collection scheme also allows for great flexibility in design. One has the choice of taking one or more views of the shower light between each lead layer. This choice involves compromises between various desirable counter performance characteristics. For example, taking three views between each lead layer would improve the ability to separate complicated patterns since each view would have the full energy resolution. But then either the counter would need to be deeper resulting in more overlap of close showers, or the liquid layers would have to be thin leading to worse light attenuation, or one would have fewer layers of lead leading to worse overall resolution.

Another example of flexibility results from the fact that the wave bars are not glued to the scintillator channels. This means that if in the future it is desirable to change the readout cell size of the SLIC, it will be possible to move wave bars of differing widths (always multiples of scintillator channels) to different regions of the SLIC. This change could be made without changing the basic liquid scintillator and lead structure.

Since this detector is a new development, some of the

important input design information is not yet available. In particular, we can only estimate the total amount of light, the number of photoelectrons which will actually be produced per GeV, and the effective attenuation properties of easily fabricated liquid channels. Experimental studies of these quantities are underway using a prototype but are not yet complete. The design presented here is therefore based on estimates of these properties obtained from the literature combined with our limited experience.

We believe that we can achieve attenuation lengths of greater than the 2.4 meters length of the longest channels of the detector. Mirrors at the far ends of each channel will improve this further. Combined with the self-calibrating properties of this detector this should be quite adequate. The main disadvantage of the long channels is the somewhat sloppy threshold for triggering on pulse height that will result.

A total length of 22 radiation lengths should be adequate since this is longer than the lead glass blocks used at similar energies in Experiment 25A where $\frac{\delta E}{E} \approx \pm \frac{13\%}{\sqrt{E}}$ was obtained. But we note that the light attenuation effect of the glass in that case tended to cancel the effect of fluctuations in shower loss out the back of the counters. The same will be true in this case with the wave bars if the tubes are downstream. If the tubes are placed upstream, which is advantageous for geometrical reasons, the counter

may need to be somewhat deeper. The 22 radiation lengths are divided into 39 layers of .56 radiation lengths each. If the light collection is adequate, this will lead to a resolution which is improved by $\sqrt{.56}$ compared with standard $1X_o$ detectors and might be as good as $\frac{\delta E}{E} \simeq \pm \frac{8}{\sqrt{E}}\%$. Finer sampling could be achieved at the cost of either worse attenuation (thinner layers) or a longer detector. The latter case would lead to more overlap of close showers. We believe that the 39 layer choice with 1/2" liquid layers is a good compromise.

The detector will contain about 16 tons of lead. To make manageable modules we will build it in two roughly square modules. The lead will be in sheets laminated between .040" layers of aluminum. This ensures that the surfaces are flat and provides mechanical support for the lead. While the lamination adds to the cost of the lead, it will make possible a very simple mechanical construction.

D. Hadrometer

The hadrometer is a steel/scintillator hadron calorimeter segmented both vertically and horizontally. It is designed for use with the segmented electromagnetic shower counter (SLIC) for measurement of hadron energy and angle. In particular, it will provide the only information on the energy and angle of neutral hadron components in the disintegration of charmed states. It also provides the capability of a fast trigger based on a rough mass calculation from angles and energies of several hadrons. Calorimeters of this type have also been effective in resolving ambiguities in the off-line pattern recognition.

A sketch of the hadrometer is shown in Figure 22a and a summary of the specifications are shown in Table XIV. The hadrometer consists of inter-spaced layers of steel and acrylic scintillator. The counter is divided into four sections, two located right and two left of the beam line. Each part consists of a stack of 32 steel plates each one inch thick. The modules composing the scintillator segments are made up of 16 strips of acrylic scintillator each 0.5 inch thick and four inches wide. Acrylic wave shifter bars collect the light from the scintillator strips and connect to the RCA 6342A phototubes by means of a folded lucite light pipe. (See scintillator module details in Figure 22b.) Some tests will be performed to acertain the exact combination of scintillator thickness, wrapping, gluing and light filtering techniques to insure that the response across the module is uniform. On

Table XIV

Hadrometer Specifications

Total Thickness:	Fe	8 collision length
	Scintillator	1 collision length
Sample Interval:	1" Fe, 0.5" Scintillator	
Total Samples:	32	
Phototubes:	RCA 6342A	
Energy Resolution:	$\frac{\delta E}{E} \simeq \pm \frac{.65}{\sqrt{E}}$	
Position Resolution:	± 2 inches	

	Vertical	Horizontal
Size:	295 cm	490 cm
Angular Acceptance:		
Magnets at same polarity		
P = 5 GeV (charged)	± 81 mr	± 87 mr
P = 20 GeV (charged)	± 81 mr	± 123 mr
Magnets at opposite polarity and neutrals	± 81 mr	± 135 mr
Segmentation:	56 modules	56 modules

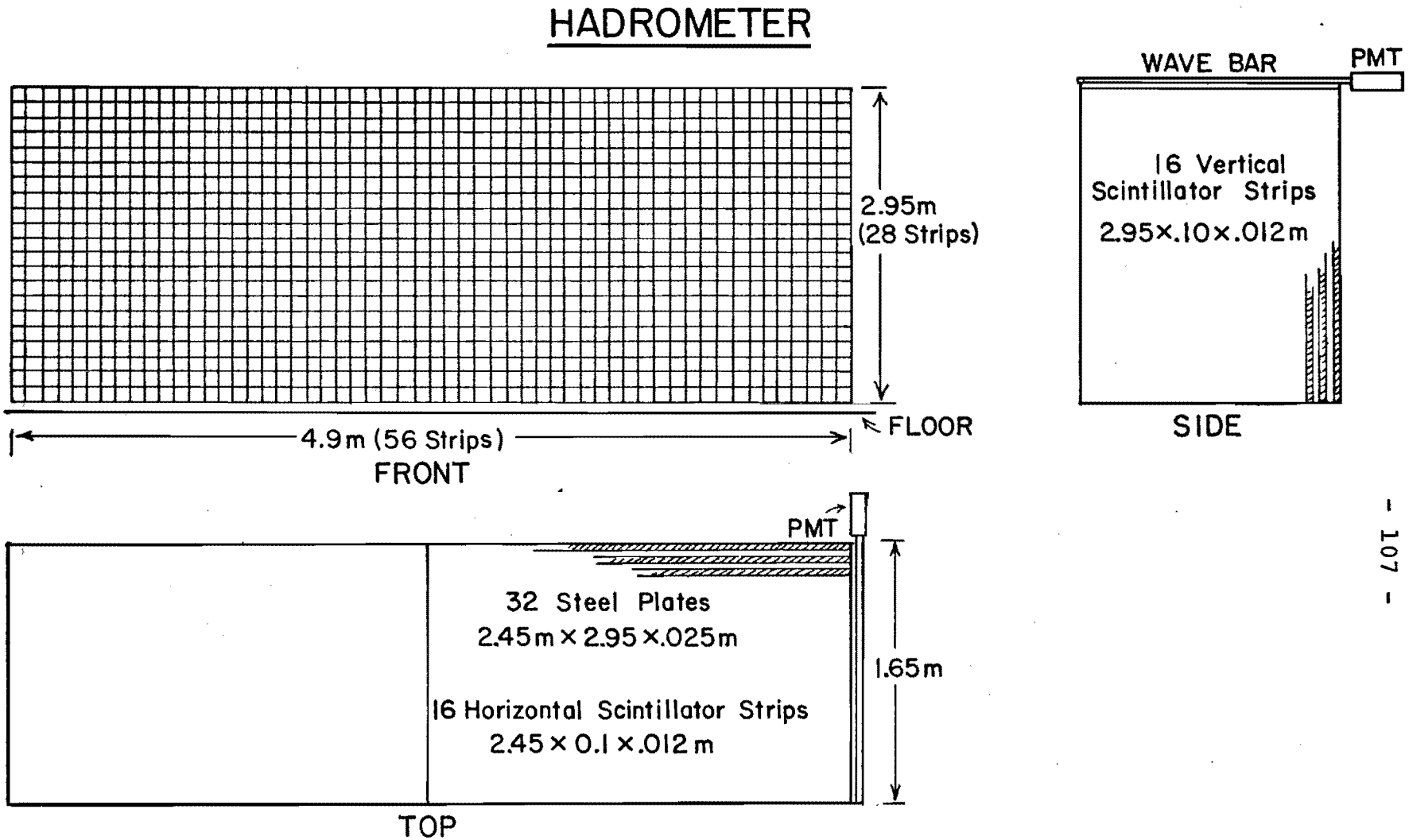
HADROMETER
2.95m
(28 Strips)
4.9m (56 Strips)
FRONT
FLOOR
WAVE BAR
PMT
16 Vertical
Scintillator Strips
2.95×.10×.012m
SIDE
PMT
32 Steel Plates
2.45m × 2.95 ×.025m
16 Horizontal Scintillator Strips
2.45 × 0.1 ×.012 m
1.65m
TOP

Figure 22a

TYPICAL VERTICAL SCINTILLATOR MODULE

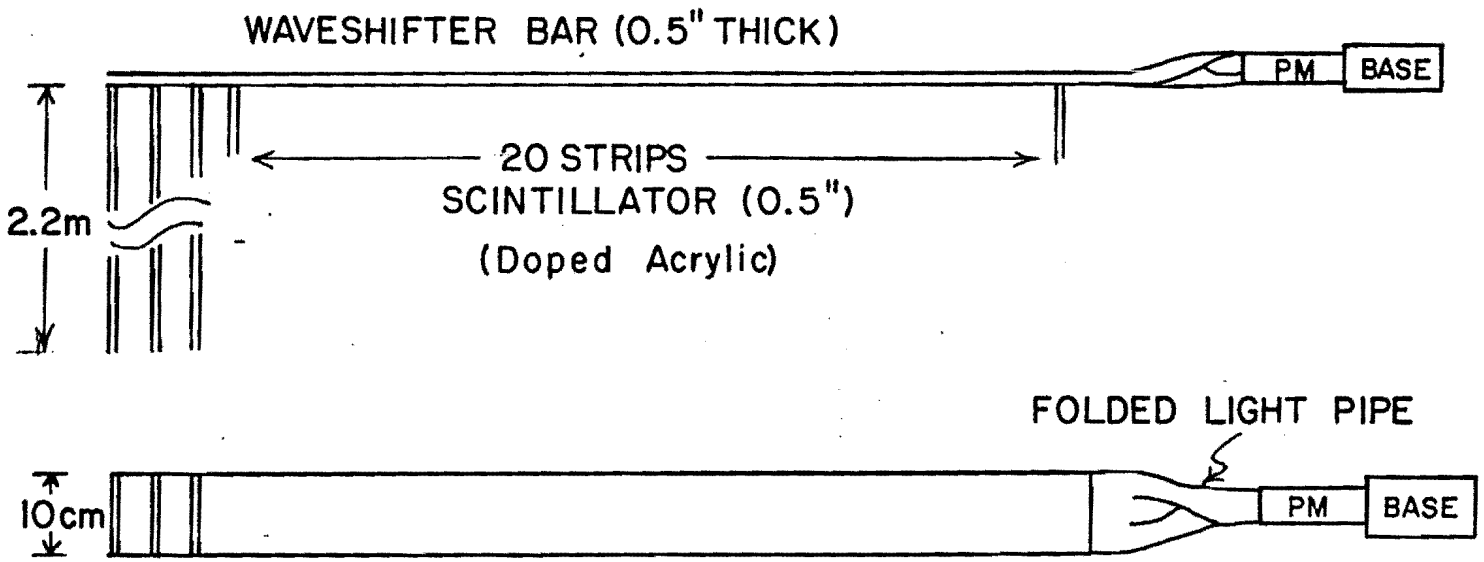

Figure 22b

the basis of previous work,[11] it is likely that the uniformity can be maintained within a few percent.

The dynode signals of all 112 tubes are routed to ADC's for transfer to storage. Signals are also used as input to processors capable of making event selections on the basis of kinematics.

The gains of the modules are balanced using pulse heights from muons through all parts of the counter. Energy calibration is determined from low energy beams transported down the tagged photon line. The calibration will be monitored and maintained by a laser/fiber optics system like that used on the E-25 lead glass.

The hadron energy resolution of the hadrometer in conjunction with the SLIC is expected to be:

$$\frac{\delta E}{E} \simeq \pm \frac{.65}{\sqrt{E}}$$

The position of the incident hadron is determined from energy shared by adjacent strips that cover the shower. Although the counter width could in principle give a position of ± 1 inch, the position resolution is dominated by the jitter in transverse deposition of energy. The final position resolution will be about ± 2 inches. At 15 meters this gives an angular resolution of about ± 4 mrad.

Following a meter of steel behind the hadrometer sixteen 12 inch wide by 1/4 inch thick counters with high gain tubes will identify spectrometer tracks that are muons.

IX. Online Computer Configuration

A. Hardware Requirements

Our choice of computer hardware is motivated by the particular experimental data acquisition problems. The event rate contemplated, assuming the fast trigger logic, is 100 to 200 events per beam-second. Our estimate of the number of 16 bit words per event is 400 words (average). We plan for 1 or 2 beam-seconds every 7 clock seconds.

To handle this data rate, we need to buffer to disk and to core. The best buffering rate to disk actually achieved is 40,000 words/beam-second with disks currently in use on the PDP/11. This will handle the low rate limit. To handle the high rate limit, which will more likely be the average, we will need 32K of core buffers for the one second spill case. We will require 64K of core buffers for the two second spill case. These core requirements are over and above that required for the monitor and data acquisition program.

This core buffer will require CAMAC transfers into the region above 32K. Thus a Jorway 411 branch driver which handles memory addresses greater than 32K will be required. Manipulation of this data by the CPU will be necessary, and a KT-11 memory management unit will be required to access the data above 32K.

At even 1 beam-second per 7 clock-seconds, one 2400 foot tape will be filled in 68 minutes at the 100 event per second rate, assuming a 1600 BPI tape drive. A two second spill is anticipated and an average rate nearer the 200 per second figure is also more likely. Two 1600 BPI tape drives will be required to handle this efficiently if the time due to tape

changing is not to be a significant fraction of the running time.

The offline analysis of large volumes of taped data is costly. Thus it is important to analyze, compress, and filter the data as much as possible before writing it to tape. This sort of processing should be done in a high-level language and as fast as possible. The high-level language is required to maintain flexibility and ease of understanding of the processing programs by facility users. The speed is required to reduce the number of data tapes to as few as possible. These considerations dictate the use of the fast in-line Fortran available under RSX-11M, the use of an 11/55 CPU with its faster processing capability, and the use of the hardware floating point option.

Complete analysis of a portion of the data is required to be certain that the physics goals are being met. The results are needed quickly in order to respond to current problems. We require a BISON-NET link to the central computing facility for this purpose.

The RSX-11M software provides much of what typical large experiments eventually build into less advanced monitor softwares, such as sophisticated overlay schemes, checkpoint capability, and multi-tasking features. To start with these features already developed will speed up the programming for the facility considerably. This system will require 2 RK05 disks to handle the monitor, the buffering, and the fast Fortran disk storage requirements.

Our estimate for the core requirements for the monitor and

data acquisition programs, exclusive of the core buffering is obtained by simply adding the size of the on-line programs under RT-11 to the size of the RSX-11M monitor. The first size is 26K (28K total size for program and monitor less 2K for size of the monitor). The second size is between 12K and 16K, depending on various capabilities included in the monitor. The core estimate is thus 38K to 42K.

The total core requirements are 70K to 74K for the one second spill case and 102K to 106K for the two second spill case.

In addition to the above general hardware requirements, we require certain peripherals. The standard ones are: a Versatec Printer/Plotter, 2 Floppy Disks, a Bison Interrupt/Gate Control Box, and a 613 Tektronix Storage Scope with hard-copy interface.

Also we will require a second 613 storage scope and two "dumb" CRT terminals. Note that we will <u>not</u> need a DECwriter. We plan to rely on the Versatec line printer for hardcopy printed output. We plan to set up two separate console stations. Each will have a graphics channel (the 613) and a totally separate command channel (the CRT terminal). We plan to use one console station for the immediate monitoring and control of the experiment. The second console station will be used for the review of past experimental status using the data-base continually generated by the data runs being taken. Our further use of these separate console stations is discussed in the software plans stated below.

We need to monitor the beam line controls for such informa-

tion as target parameters, magnet settings, etc. We also need to monitor the experiment's high voltages. To accomplish these things, we will need a set of 036 modules for interfacing with the beam line controls system and a Peripheral Node Module for transfer of graphics information from the control system. For the voltage monitoring, we need a computer-controlled digital voltmeter.

The online computer configuration is summarized in Table XV.

TABLE XV

Online Computer Requirements

1. PDP 11/55 CPU
2. Floating Point Processor Hardware
3. Memory Management Unit (KT-11)
4. MOS Memory, 74K for 1 second spill, 106K for 2 second spill
5. Two 1600 BPI 9 track Magnetic Tape Drives
6. Jorway 411 CAMAC branch driver
7. Versatec Line Printer
8. Two Floppy Disk Drives
9. Two RK05 Cartridge Disk Drives
10. Bison Interrupt Gate/Control Module and DR-11C
11. Two 613 Storage Scopes with Hardcopy Unit
12. Two "Dumb" CRT Terminals
13. BISON-NET Link
14. Two Beam Line Interface 035 Modules and 1 Peripheral Node Module
15. A Computer-Controlled Digital Voltmeter

B. Online Software

Within the RSX-11M framework, we plan to develop a set of data acquisition routines. These will be tailored to the special needs of the facility for handling high data rates. This set of routines will use software currently being developed within the Computer Department for fast CAMAC data acquisition and disk buffering under RSX-11M.

To solve the experimental control and data monitoring needs, we will use the package called "MULTI". It has already been quite successfully used by a number of Fermilab experiments (E-110, E-379, etc.). The experimenter will use MULTI to do such things as begin and end runs, to monitor high voltages, positions of centroids on pulse height histograms, etc. This sort of monitoring, control, and alarms typeout will be done at the first graphics/command console.

MULTI gives the experimenter the capability to set up from the keyboard various histogramming and display processes for data items. These may be set to be done conditionally depending on the value of other data items. For example, a pulse height in one scintillator may be histogrammed whenever a bit in a latch has fired.

MULTI further gives the experimenter convenient places to attach special subroutines. In these subroutines, one can process the data in ways difficult or inefficient to do via the general keyboard capability. The output from these special subroutines is then available to the general keyboard processor for histogramming and display.

In addition to data acquisition and monitoring of current data, we require a capability to review past runs to compare rates and other characteristics with the present run. We plan to use the second graphics/command console for this review. The advantage of a second console is that the review activity may proceed, even while the experimenter is handling an alarm or equipment problem that may have arisen at the other console. Further, when two experimenters are present, both may easily conduct investigations of the data. It will also be used for the preparation of configuration files, specifying the run parameters for subsequent runs. The data acquisition, control, and monitoring system will continually generate files in the style of a data-base. The information in these files will characterize the last several events, the last several beam spills, and the last several runs. The experimenter will use this second console to compare and look for problems and trends.

At present, our plan is to implement a dual console version of MULTI. At the second console, the experimenter can examine the data-base through the use of the same commands that are used at the first console to control and monitor the experiment.

The data acquisition routines are already being developed for RSX-11M by members of the Computing Department in connection with other projects. The adaption of MULTI to RSX-11M is also currently being developed for similar reasons. Completion of the MULTI in RSX project is predicted for June, 1977. Thus, much of the software is well along towards implementation for this facility.

X. Track Reconstruction

It has been indicated in previous discussions of the drift chambers that a great deal of thought has been given to the problems of tracking multiparticle events in the forward spectrometer and that the chamber number, positions, and wire orientations have been chosen to ease the pains of tracking.

We will not reiterate here all the reasons for our choice of geometry. Instead, we will discuss approaches to tracking the proposed chamber system that will be developed for the Central Laboratory Computing Facility programs.

The forward chamber system is pictured schematically in Figure 23. For tracking purposes D1 and D2 are considered together as a single module (D1-2) with four chambers having each wire orientation (x, u, and v). D3 and D4 both have three chambers with each wire orientation. D5 has only two planes of x chambers. Note that except for the two D5 chambers, the system is identical in the x, u, and v planes.

We now describe a tracking algorithm which demonstrates the flexibility of the system. Common to any tracking technique is the necessity to convert TDC counts to position coordinates, each wire hit generates two such coordinates equidistant to but on opposite sides of the hit wire. The techniques for performing this conversion are straight forward and need not be elaborated here.

The algorithm begins by independently finding track segments in the three modules (D1-2, D3, D4). We believe that it is very important for computing speed that the coordinate data be presented to the tracking program in an ordered form. Increasing address should correspond to increasing coordinate. This may be accomplished in the hardware or (less desireably) at some earlier point in the

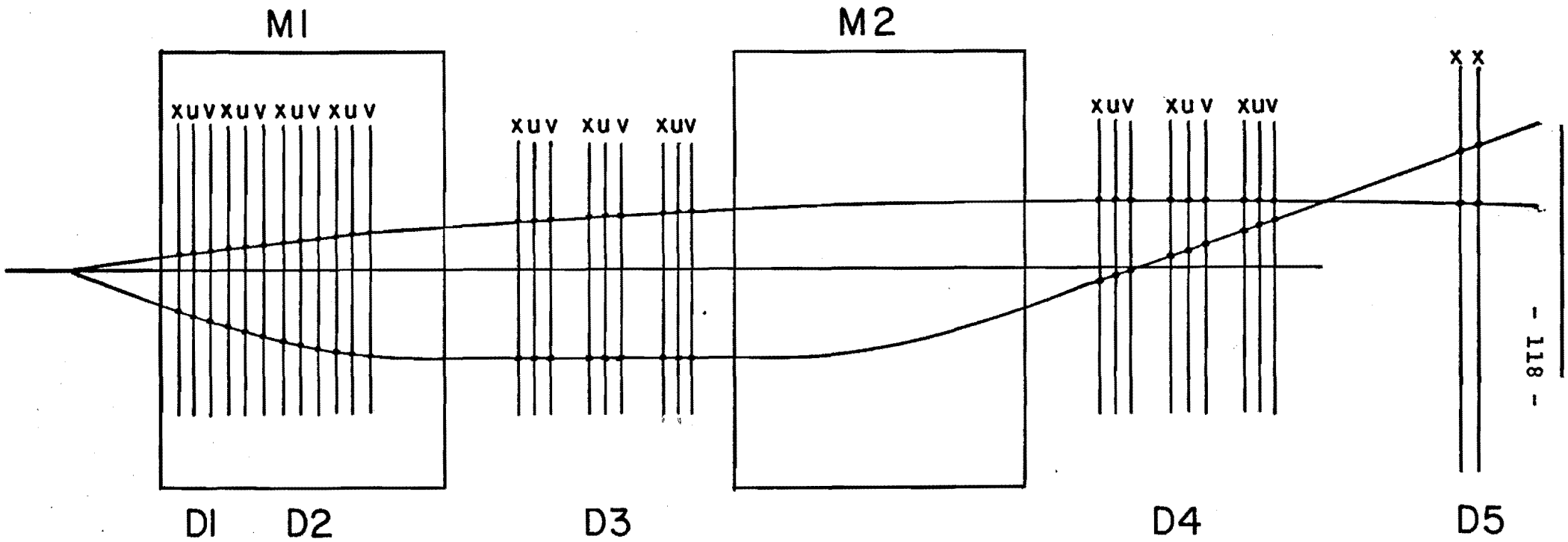

Figure 23

analysis programs.

Tracking Algorithm:

1. Find all 3 hit lines in D3 and D4 in each view. Let ξ_i be one of x, u, or v. A line is found when: $\frac{1}{2}(\xi_1 + \xi_3) - \xi_2 < \delta\xi$, where $\delta\xi$ is a cut whose size is related to the spatial resolution and which is determined experimentally. As soon as a coordinate is used in a line, eliminate that coordinate and its left-right ambiguous pair from the search. Note that the ordering of the data will speed up this process considerably. Reasonable tracks will have a specified range of angles relative to the beam line. This fact will be used to limit the number of ξ_3 coordinates which are paired with a given ξ_1. The outer limits for this pairing can be established and the data ordering insures that only those coordinates within these limits will be searched. Similarly in checking ξ_2 for the third hit on a line one searches until a match is found or until a coordinate is found which exceeds the predicted value. Again the data ordering insured that the correct coordinate has not been missed. All these techniques limit the combinatorial growth of computing time expected with a straight forward brute force approach.

2. After all three point lines are found, define all two point lines possible from unused hits in each view of D3 and D4. The set of two point lines can be limited by considering only reasonable angles.

3. Correlate the three views eliminating "ghost" lines. Consider only lines which have three hits in at least one view.

4. Project x view of "real" lines in D4 into D5. Use D5 information to refine x slope if at least one out of two D5

chambers gives a match.

5. Proceed to tracking D1-2. Each view has four chambers which are equally spaced. We may use the property that the two line segments defined by ξ_1, ξ_2, and ξ_3, ξ_4 must meet within a calculable distance on a line halfway between the second and third chamber. Given the bend angle implied by the two line segments, one can calculate how the lines should intersect if they indeed form a single track. A lower momentum cut will limit the set of line segments for which this test is attempted. Also, a proximity requirement can be imposed for the two line segments. After 4 point circles are found the corresponding coordinates are eliminated from the search. Finally, all three point circles which can be formed from unused hits and which have reasonable momenta are tabulated.

6. Correlate the three views in D1-2. This can be done by requiring that the same momentum can be obtained in each view or from purely geometrical considerations. Ghost tracks are, thereby, eliminated. A track candidate should have a four point circle in at least one view.

7. At this point we have established track segments inside M1 and in the drift space before and after M2. It is possible to calculate intercepts and slopes in any plane, and it should, therefore, now be an easy task to match track segments. This can be done by seeking common slopes and intercepts in the vertical plane. It can also be accomplished in the horizontal plane by looking for a match at the magnet centers.

8. After at least two tracks are found, a vertex can be established. This vertex can be used to relax the hit requirements

in the first magnet. For example, if a track projects to the vertex properly it need not be required to have four hits in any view.

9. Similarly, we can use the information from one module to track another. For example, two point line segments are perfectly acceptable if they intersect track segments from other modules properly at the magnet centers.

Finally, it should be noted that the above discussion can not possibly do justice to the hundreds of man hours of programming effort which will ultimately go into tracking. We have tried to make the point that the system is sufficiently redundant that efficient multiparticle tracking is possible. Further, we think that the system is designed so that computing time is efficiently used and that the combinational problems encountered in tracking events are well under control.

XI. Beam

To a large degree the range of photon physics that will be feasible is determined by the fluxes available in the beam. Here we look at the question of how much tagged photon flux can be reliably anticipated in the next generation of experiments based on present experience with the beam. The real limit on flux is the rate at which one can tag photons. Using techniques based on some developed during summer 1975 we will be able to tag as many as 6×10^6 γ/ second. Modest improvements to the electron beam and reasonable assumptions about 1978 proton beam parameters (6×10^{12}, 450 GeV, 480 seconds/hour) will make it possible for us to obtain this photon flux with 150 GeV e^-. Figure 24 shows the photon spectrum expected. Also shown is the e^- spectrum. Details of how we will obtain these fluxes are given below. Figure 25 is a schematic drawing of the Tagged Photon Beam and may be helpful as a road map in the discussion that follows.

During August of 1975, the beam was operated at $\sim$ 100 GeV with 3×10^{12} 400 GeV protons on target and produced about 2.2×10^7 electrons. With 450 GeV protons and 6×10^{12} p/sec, we can expect 6×10^7 electrons/sec. at 100 GeV. This flux is more than adequate for much of the physics to be done on this spectrometer. However, experiments dealing with low cross section states (η_c, heavy leptons) will need all the flux they can get. The electron flux is presently limited by the relatively smaller vertical acceptance. This vertical acceptance can be recovered in one of two ways. In a Technical Memo, TM-633, Morrison and Murphy suggested increasing the vertical acceptance by installing the lead convertor (that converts photons from the primary target to electrons) inside a

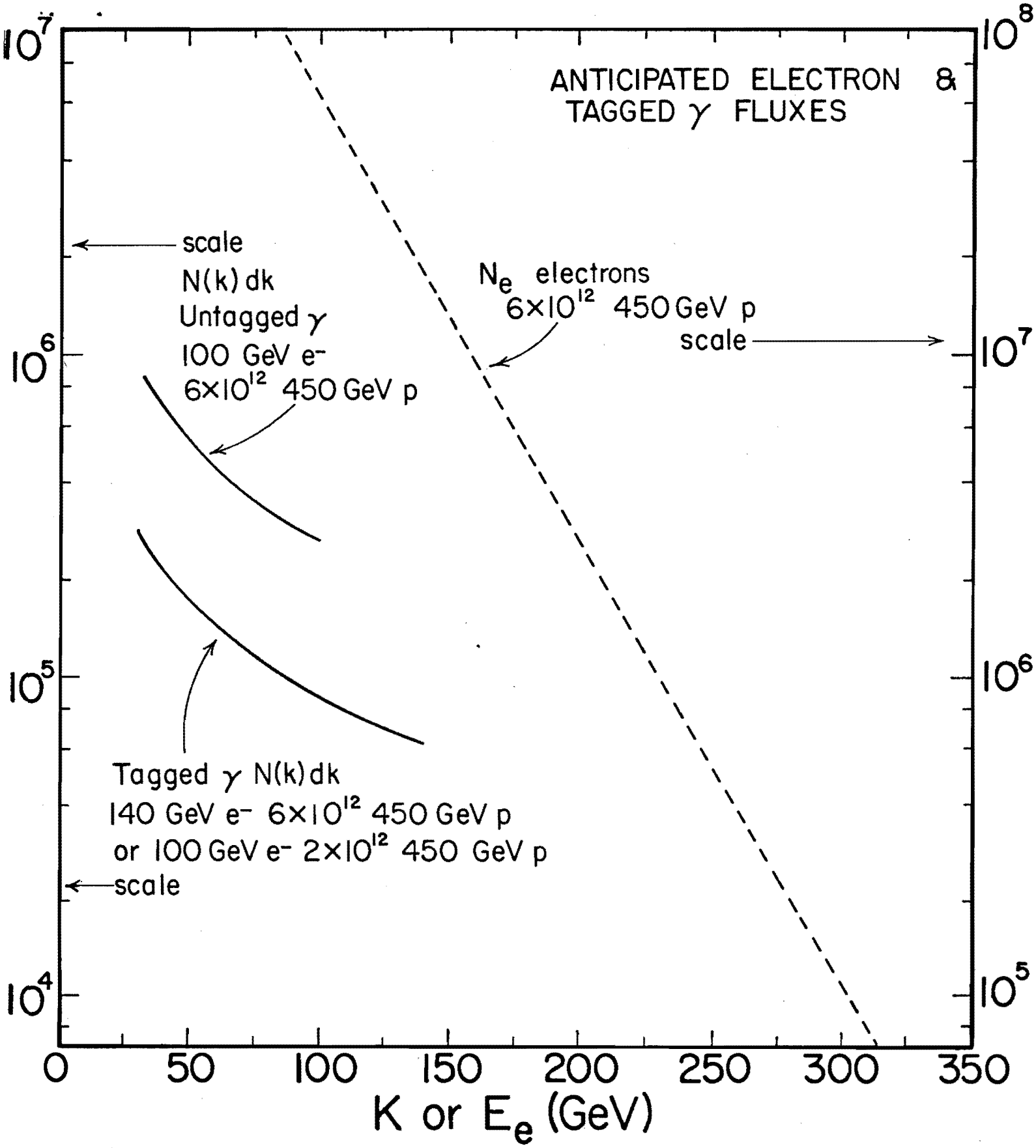
ANTICIPATED ELECTRON & TAGGED γ FLUXES
scale
N(k) dk
Untagged γ
100 GeV e⁻
6×10¹² 450 GeV p
N_e electrons
6×10¹² 450 GeV p
scale
Tagged γ N(k) dk
140 GeV e⁻ 6×10¹² 450 GeV p
or 100 GeV e⁻ 2×10¹² 450 GeV p
scale
10⁷
10⁶
10⁵
10⁴
10⁸
10⁷
10⁶
10⁵
0
50
100
150
200
250
300
350
K or E_e (GeV)

Figure 24

SCHEMATIC DRAWING OF TAGGED PHOTON BEAM

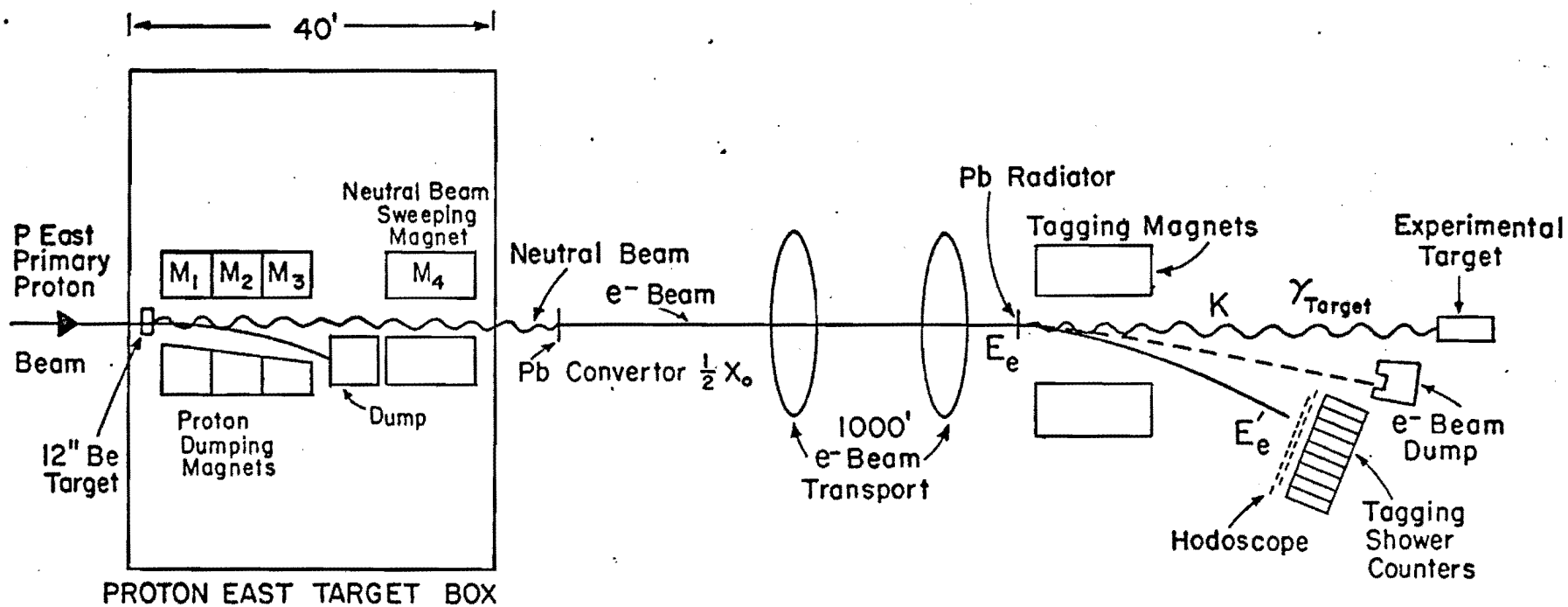

Figure 25

dipole. As can be seen in Figure 26, the lead is at a shallow angle (α) relative to the beam axis. Thus the more positive the photon production angle the more magnetic field will be traversed by the resulting electron. The net effect is a vertical focussing of the electrons plus a small mean bend which is corrected by a following magnet. There is no horizontal defocussing. To get the most significant increase in vertical acceptance using this approach the lead convertor would be placed in the third dumping magnet (M3) inside the target box with the sweeping magnet (M4) acting as the correction magnet. This would increase the vertical acceptance from $\sim$1 mr to $\sim$5mr with negligible effect on other beam parameters. Using measurements of the electron beam flux as a function of production angle, we estimate this larger vertical acceptance will increase the flux at 100 - 150 GeV by $\sim$ 3.5. This would give $\sim 2 \times 10^8$ 100 GeV or 6×10^7 140 GeV electrons (see Figure 25). Another approach (suggested by B. Cox) is to add a third quadrupole to the first doublet and thereby achieve a more symmetric acceptance. A careful transport study of using a triplet will have to be made before deciding whether to use a Morrison element or a triplet to increase the beam acceptance.

Using a 20% radiator and ignoring tagging for the moment

$$N_\gamma(k)dk > N_e \times .2 \times f(k) \times \frac{1}{k} dk =$$

$$\frac{2.6\ 10^7}{k} dk \quad 100 \text{ GeV}$$

$$\frac{8.7\ 10^6}{k} dk \quad 140 \text{ GeV}$$

The factor $f(k) = .65$ comes from thick target and QED corrections to the simple $\frac{dk}{k}$ form. Integrating from 20 GeV to k_{max} we will get 4.2×10^7 photons for the 100 GeV setting and 1.8×10^7 with 150 GeV electrons, untagged. This high rate is useful for physics

SCHEMATIC DRAWING OF VERTICAL FOCUSING OF ELECTRON BEAM IN TARGET BOX

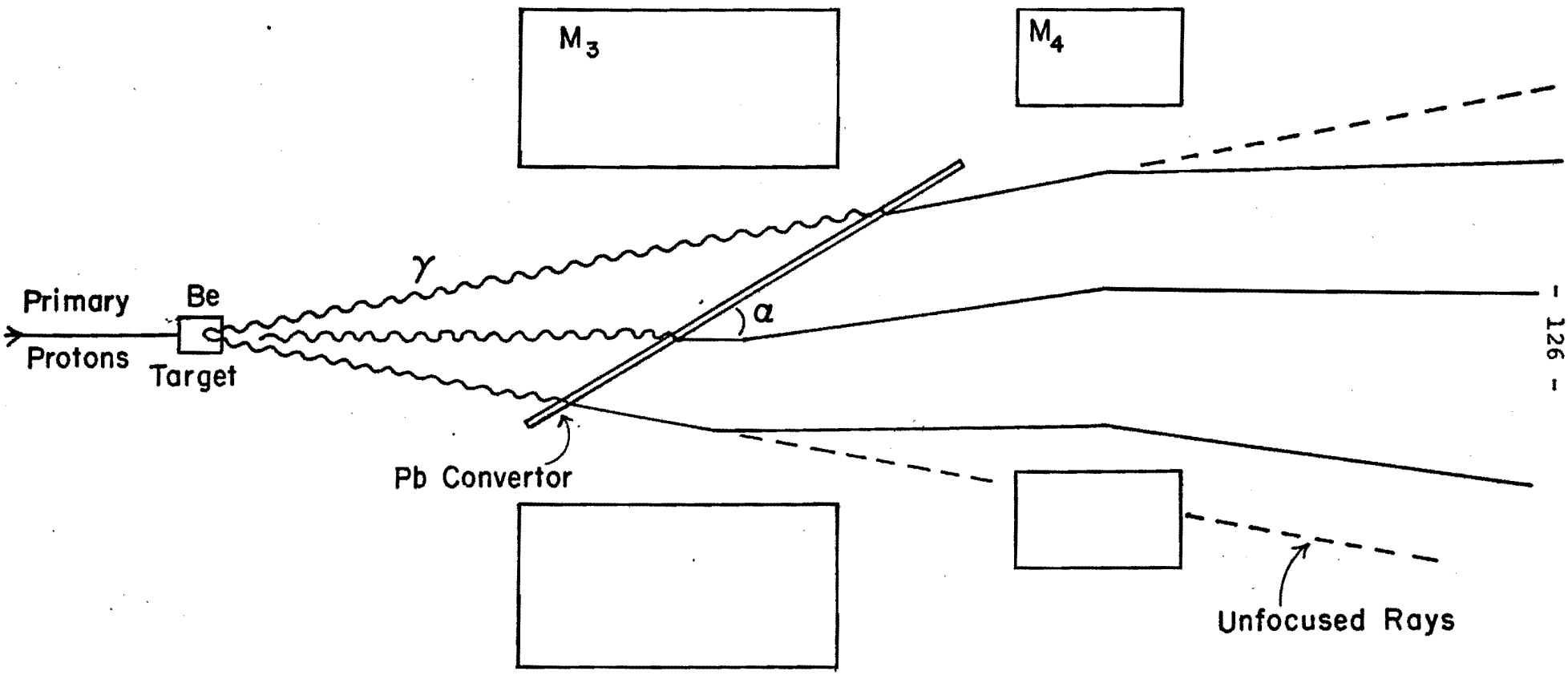

Figure 26

when one chooses not to take advantage of the energy constraint and missing mass capability allowed by the tagging system.

If tagging is required, the real limit on flux is the rate at which one can tag the photons. With electron fluxes approaching those noted above, a large fraction of RF buckets will be populated with more than one electron. The likelihood of more than one radiated photon of significant energy per electron is also high when using a thick radiator. Thus, it is necessary to cope with more than one electron and more than one photon to tag the energy of the interacting photon. The saving grace is the very low interaction probability of photons which means that it is extremely unlikely ($< 10^{-3}$) for more than one γ to interact hadronically per bucket. The energy of all non-hadronically interacting photons in the beam (Σk_{NI}) will be measured by a central counter (C) which will measure photons that have not converted and by the central horizontal strip of the SLIC which will measure e^+e^- pairs with $p > 1.5$ GeV that have been swept out of 0° in the bend plane.

Extra scintillation counters near the beam in the tagging array will pick up higher energy electrons that radiated lower energy photons. Combined with the shower counters of the tagging system, these will determine the number of electrons (N) in the bucket and their total energy after radiating ($\Sigma E'$). Thus, one can determine the interacted photon's energy:

$$k_I = NE_{beam} - \Sigma E' - \Sigma k_{NI}.$$

A specific scheme has been worked out along these lines which allows tagging radiated photons with a resolution of $\frac{\delta k_I}{k_I} \sim 5\%$

from up to 6×10^7 100 GeV e^- in a 20% radiator (6×10^6 tagged photons). The only changes to the tagging system are eleven scintillation counters which would be added to the present tagging hodoscopes on the high e^- energy end. The tagging magnets would be run at maximum current (the present 300 GeV setting) in order a: to spread out the electrons so that there is a sufficient spatial resolution to measure E' of the higher energy electron well enough to get $\delta k_I \sim 5.5$ GeV; and b: to keep the counting rate < 2MHz in the hodoscopes and < 0.3 MHz in the shower tagging counters.

The C counter will require special consideration. The pulse height of this counter, like the tagging counters, will be digitized for any RF bucket with an interaction that satisfies the experimental trigger. The problem is to get the pulse height information from only the relevant bucket without contamination from the preceding or following buckets. The pulse can be clipped to 15 ns and the ADC gate set short enough to ignore the following bucket. The energy at the preceding bucket can also be digitized (with appropriate delaying). Using calibration data one will then be able to subtract the energy that leaked from the previous bucket. The problem is by no means trivial, but techniques like these are similar to those used in correcting for shower leakage from a neighboring shower counter.

We have described above what might be called a second generation tagging system which, with minor modifications based on previous experience, will push the tagging rate a factor of ~ 6 beyond that already attained. When 1,000 GeV protons are available in P-East, the choice will be whether to use the extra energy to do physics in the 200 - 300 GeV range or to continue in the 100 - 150 GeV range with substantially increased intensity. If the latter choice

is made, the tagging system will have to be modified to cope with the higher rates. Perhaps this will be done by adding more magnets which will spread the electrons and photons out vertically and horizontally to keep rates manageable in each of a greater number of counters.

The electron beam can also be used to transport pions into the Tagged Photon Laboratory[12]. R. Rubinstein notes that although spot sizes will be somewhat larger the intensities are potentially only a factor of ~ 3 below the P-West pion beam.

XII. Schedule

Rough time estimates for various components in the facility have been made (Table XVI). The primary purpose of these estimates is to detect the critical time elements in the assembly of the facility. Work has already begun on prototype components. This work puts the whole program in an excellent starting position. These efforts are being made in good faith and with the conviction that the facility is too important not to proceed as indicated. Nevertheless, formal approval of the facility will be required to permit component acquisition in sufficient quantity to mount an experiment. The importance of this approval for those groups seeking extraordinary funding for their contributions can not be overemphasized.

One other most critical element is the final specification of the exact magnet apertures to be used. If existing magnets are to be made available, this task is easier. It is directly related to the formal approval. If new magnets are to be built, an added constraint arises. Unless existing copper coil supplies can be utilized, coil winding will be hindered. One possibility is to do design work now and begin copper procurement before the new fiscal year.

Many of the major final component commitments can be delayed until next fiscal year, but only if bid packages and decisions have been made in advance of October 1, 1977. For example, if an ADC system of the type now being discussed in PREP is ordered for other purposes and debugged earlier, our time estimates remain reasonable. Similarly, most photomultipliers, metals, and plastics can be purchased after October 1, 1977.

The net effect of the schedule is to suggest that the facility could begin set up in the Tagged Photon Laboratory in April. First

beam testing of the assembled apparatus would be useful as early as June, 1978.

Table XVI Time Schedule

TAGGED PHOTON FACILITY

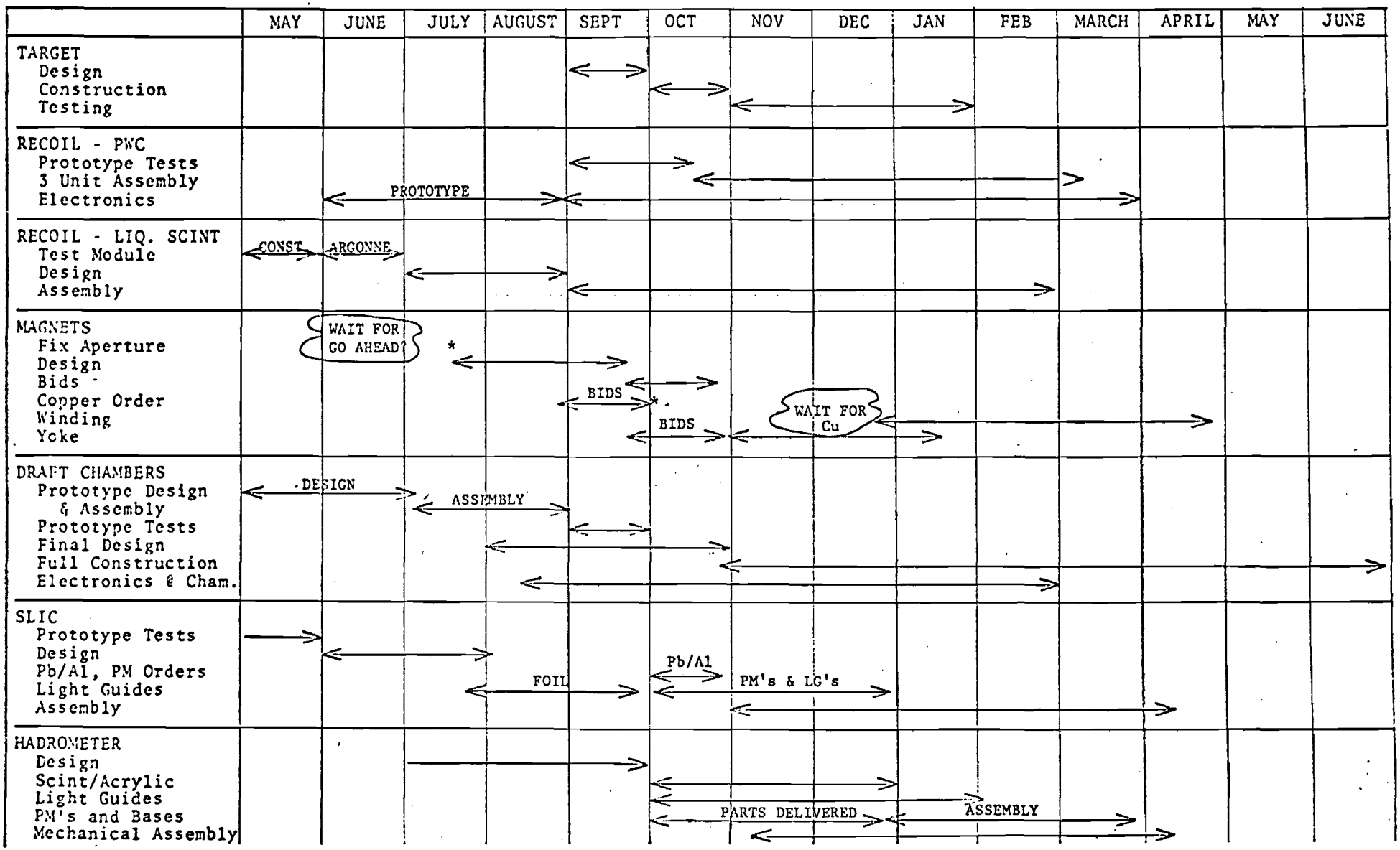

Table XVI (continued)

TAGGED PHOTON FACILITY

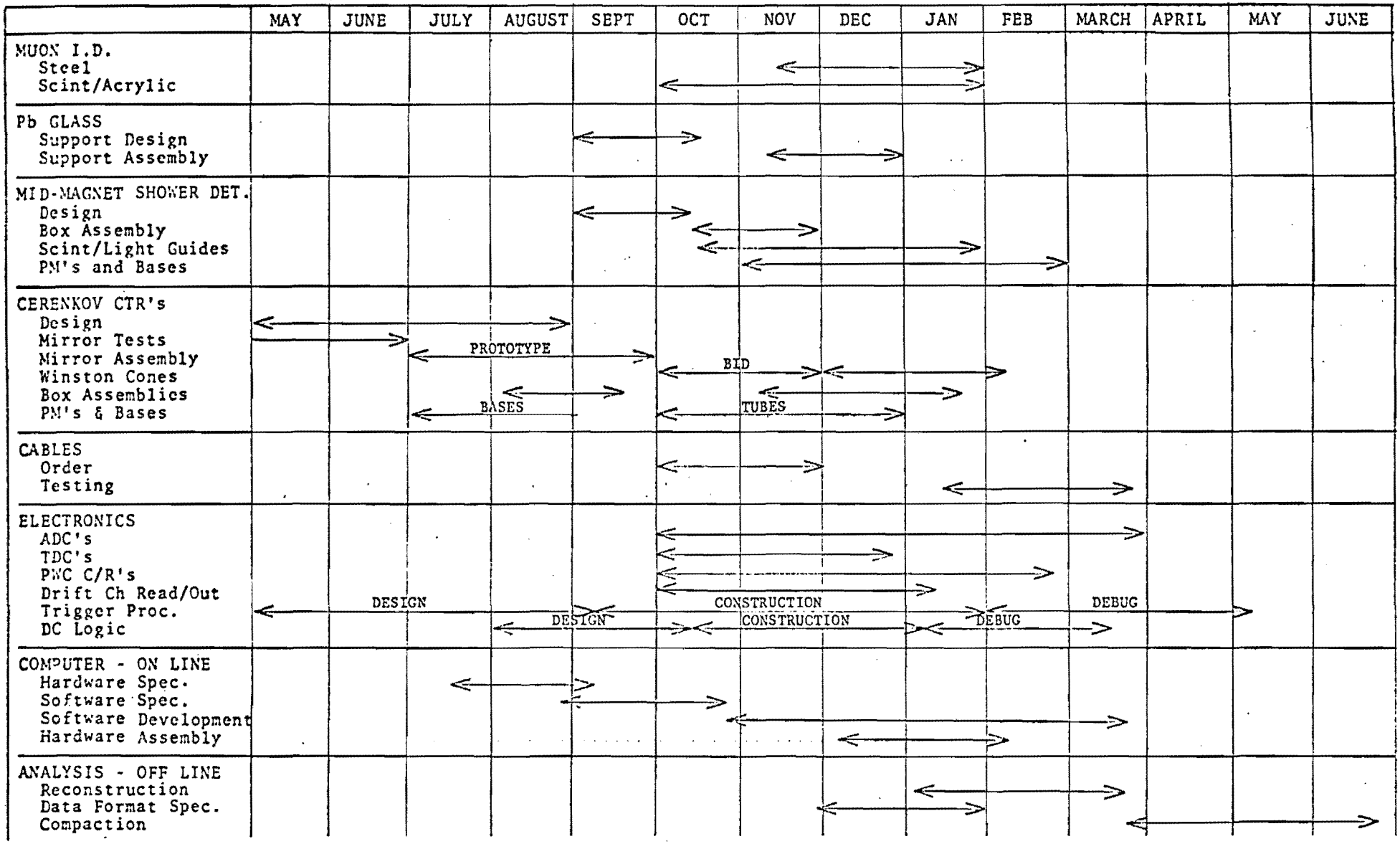

XIII. Cost Estimates

The new equipment costs of the Tagged Photon Facility will be borne approximately equally by Fermilab and the out-of-laboratory collaborators of P-516. A detailed breakdown is given in Table XVII. In the table, the items with an asterisk might well be delayed until after the startup of the facility. This would delay a portion of the Fermilab expenditure. However, such an action would be severe from the point of view of starting with a complete facility.

XIV. Acknowledgements

We would like to acknowledge the encouragement and support we have received from J. Peoples, E. L. Goldwasser, and R. R. Wilson at Fermilab. We have had valuable conversations with J. Franzini and P. Franzini, and with T. Droege. We would also like to thank B. Perington for her editorial and typing assistance. We have had important technical support from L. Bird (Carleton Univ., collaborated in design and testing of recoil wire chamber system), A. Kiang (U. Toronto, recoil system), and G. Schultz (U. Colorado, Cerenkov counters). We thank also R. Carnegie for his encouragement and support at Carleton University in Ottawa.

Table XVII

Tagged Photon Facility

Estimated Costs of New Facility

May 1, 1977

	Fermilab		Others
	Exist'g	New	
A. Beam Improvements*			
1. Slanted Target in Magnet } either one	20K	20K*	
2. New Quadrupoles in Target Box } either one			
B. Tagging System Improvements*			
1. 20 Scintillation Counter Hodoscope		5K*	
C. Hydrogen Target			
1. Mechanical Assembly: flask, vacuum, transfer lines, etc.		15K	
2. 10-12 watt, ½ ℓ/hr refrigerator, dewars	35K		
D. Recoil System (Canadian Collaborators, P-516)			
1. Cylindrical PWC (1,200 wires)			
a. Fabrication of Mechanical Assembly			60K
b. Electronics at Chamber			36K
2. Range Liquid Scintillation System			
a. Fabrication of Mechanical Assembly			20K
b. 120 Photomultipliers, bases, guides			30K
c. Liquid Scintillator			10K
d. Laser Calibration System			6K
E. Magnets			
1. Moving 2 SCM105's from Argonne and Assembly		14K	
2. Power Supplies (2 ½-MW Transrexes or equivalent)	32K		
3. Additional LCW Cooling		20K	
F. Calorimeters			
1. Segmented Liquid Ionization Counter (UC, SB)			
a. Fabrication (including Pb plates, teflon foil, liquid).			90K
b. Phototubes, Light Guides (278 elements)			35K
2. Hadrometer*			
a. Steel Plates		50K*	
b. Fabrication of Mechanical Assembly		5K*	
c. Acrylic Detectors with Phototube Assemblies		69K*	
3. Muon Identifier			
a. Steel Absorber	20K		
b. Acrylic Detectors with Phototube Assemblies (16 elements)		7K	

*These items might be delayed or simplified at the beginning of the facility (164K total).

TAGGED PHOTON FACILITY

page two of two

	Fermilab		Others
	Exist'g	New	
4. Shower Counters (Univ. of California, Santa Barbara)			
a. Between Magnets		18K	
b. Pb Glass			2K
G. Gas Cerenkov Counters (U of Colorado)			
1. Metal Enclosures (C1, C2)			25K
2. Photomultiplier Assemblies (40 elements)			58K
3. Winston Light Funnels			15K
4. Spherical Mirrors and Mounts			15K
H. Trigger Counters (33 elements)			
1. Scintillators and Guides		4K	
2. Photomultiplier Assemblies		8K	
3. Supports		1K	
I. Forward Spectrometer Drift Chambers			
1. Mechanical Assemblies (32 planes)		48K	
2. Electrical Circuits (including TDC's)		108K	
J. Cables			
1. Drift Chamber and PWC Cables		16K	
2. Analog Signal Cables	6K	15K	
3. High Voltage Cables	6K	16K	
K. Electronics			
1. ADC's (550 channels)		33K	
2. TDC's	4K		
3. Discriminators and Logic Modules	30K		
4. Crates, Bins, Racks for above units	20K		
5. PWC Specialized Units and DC Logic		10K	
6. Trigger Processor (Recoil)		20K	
7. Trigger Processor (Forward Spectrometer)*		15K*	
8. Miscellaneous Spectrometer Electronics		5K	
L. Computer			
1. Bison System (standard)	96K		
2. Additional Facility Equipment	38K		
TOTALS	307K	522K	402K

*These items might be delayed or simplified at the beginning of the facility (164K total).

REFERENCES

1. J. Appel, P. Mantsch, T. Nash, R. J. Morrison and G. Luste, Proposal to Study Photoproduction of Final States of Mass Above 2.5 GeV with a Magnetic Spectrometer in the Tagged Photon Lab, Fermilab Proposal 516.

2. R. F. Schwitters, Proc. 1975 Intern. Symp. on Lepton and Photon Interactions at High Energy, Stanford (1975).

3. A. De Rújula, Howard Georgi, and S. L. Glashow, Phys. Rev. D 12, 147 (1975), A. D. Sukharov, JETP Lett. 21, 258 (1975).

4. Mary K. Gaillard, Benjamin W. Lee, Jonathan L. Rosner, Rev. Mod. Phys 47, 277 (1975).

5. J. Franzini, P. Franzini, et al., (Private Communication).

6. R. Thun et al, Nuclear Instruments and Methods 138, (1976) 437-444.

7. G. B. Bowderr, R. C. Field, R. A. Lewis, C. T. Howard, K. Skarpaas, and P. Baker Nuclear Instruments and Methods 138 (1976).

8. G. Grayer et al, Max Planck Institut fur Physik und Astropysik (Exp. El 40, June 1974).

9. E. L. Garwin and T. Rodes, Nuclear Inst. and Methods 93 (1971).

10. Y. Tomkiewicz and E. L. Garwin, Nuclear Inst. and Methods 114 (1974).

11. P. Mantsch, et al. "A Segmented Hadron Calorimeter for Use as a High Transverse Momentum 'Jet' Trigger", Fermilab Technical Memo TM-721, April 5, 1977.

12. R. Rubinstein, "Use of the NAL Electron Beam for Pion Experiments", NAL TM-476.